

Report 3168  
Aero Report 1158

AD 703669

PARAMETRIC TRADE-OFF ANALYSIS FOR TILTING FREE PROPULSOR  
V/STOL AIRCRAFT IN EQUILIBRIUM TRANSITION

# NAVAL SHIP RESEARCH AND DEVELOPMENT CENTER

Washington, D.C. 20007



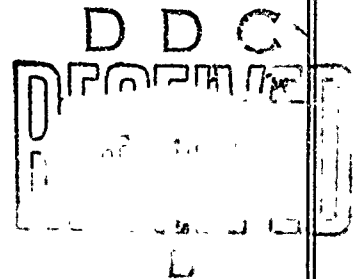
## PARAMETRIC TRADE-OFF ANALYSIS FOR TILTING FREE PROPULSOR V/STOL AIRCRAFT IN EQUILIBRIUM TRANSITION

by

Robert J. Englar and Douglas G. Kirkpatrick

This document has been approved for public release  
and sale; its distribution is unlimited.

DEPARTMENT OF AERODYNAMICS  
RESEARCH AND DEVELOPMENT REPORT



July 1969

Report 3168  
Aero Report 1158

97

The Naval Ship Research and Development Center is a U.S. Navy center for laboratory effort directed at achieving improved sea and air vehicles. It was formed in March 1967 by merging the David Taylor Model Basin at Carderock, Maryland and the Marine Engineering Laboratory at Annapolis, Maryland. The Mine Defense Laboratory, Panama City, Florida became part of the Center in November 1967.

Naval Ship Research and Development Center  
Washington, D.C. 20007

ACCESSION for	
OFSTI	WAVE SECTION <input type="checkbox"/>
BDC	BUWF SECTION <input type="checkbox"/>
WAVE SECTION	<input type="checkbox"/>
CHECK BUWF AVAILABILITY CODES	
BDC	AVAIL. SEC. OF SPECIAL
2	

**BLANK PAGE**

DEPARTMENT OF THE NAVY  
NAVAL SHIP RESEARCH AND DEVELOPMENT CENTER  
WASHINGTON, D. C. 20007

PARAMETRIC TRADE-OFF ANALYSIS FOR TILTING FREE PROPULSOR  
V/STOL AIRCRAFT IN EQUILIBRIUM TRANSITION

by

Robert J. Englar and Douglas G. Kirkpatrick

This document has been approved for public release  
and sale; its distribution is unlimited.

July 1969

Report 3168  
Aero Report 1158

## TABLE OF CONTENTS

	Page
SUMMARY . . . . .	1
INTRODUCTION . . . . .	1
METHOD OF ANALYSIS . . . . .	2
APPLICATION TO TRADE-OFF ANALYSIS . . . . .	10
TILT-WING AIRCRAFT ANALYSIS . . . . .	12
PARAMETRIC VARIATIONS . . . . .	14
Disc Loading . . . . .	14
Wing Loading . . . . .	15
Aspect Ratio . . . . .	15
Flight Path Angle . . . . .	16
Thrust Offset Angle . . . . .	16
Number of Engines . . . . .	17
Spanwise Engine Location . . . . .	17
Taper Ratio . . . . .	18
TILT-ROTOR AIRCRAFT ANALYSIS . . . . .	18
PARAMETRIC VARIATIONS . . . . .	21
Disc Loading . . . . .	21
Wing Loading . . . . .	21
Aspect Ratio . . . . .	22
Flight Path Angle . . . . .	22
Wing Incidence . . . . .	23
Taper Ratio . . . . .	23
Engine Location, Number of Engines, Thrust Offset Angle . .	23
COMPARISON OF TILT-WING AND TILT-ROTOR CONFIGURATIONS . . . . .	23
TILT-WING CHARACTERISTICS . . . . .	24
TILT-ROTOR CHARACTERISTICS . . . . .	24
CONCLUSIONS . . . . .	25
TILT-WING AIRCRAFT . . . . .	25
TILT-ROTOR AIRCRAFT . . . . .	25
APPENDIX - DERIVATIVES USED IN NEWTON SOLUTION OF EQUILIBRIUM FORCE SUMMATIONS (EQUATIONS [1] AND [2]) . . . . .	27
REFERENCES . . . . .	32

TABLE OF CONTENTS (Continued)

	Page
LIST OF TABLES	
Table 1 - Ideal Hover Quantities . . . . .	34
LIST OF FIGURES	
Figure 1 - Velocity, Force, and Pressure Geometries . . . . .	35
Figure 2 - Airfoil Characteristics . . . . .	37
Figure 3 - Dynamic Pressure Distributions . . . . .	39
Figure 4 - Experimental and Calculated Data for Canadair CL-84 . . . . .	40
Figure 5 - Design Limitations Based on Fuselage-Propulsor Interference (Gross Weight = 10,000 Pounds) . . . . .	41
Figure 6 - Design Limitations Based on Fuselage-Propulsor Interference (Gross Weight = 30,000 Pounds) . . . . .	42
Figure 7 - Design Limitations Based on Fuselage-Propulsor Interference (Gross Weight = 100,000 Pounds) . . . . .	43
Figure 8 - Effects of Airfoil Variation on Tilt-Wing Configuration . . . . .	44
Figure 9 - Transition Data for Baseline Tilt-Wing Configuration . . . . .	45
Figure 10 - Effects of Variation in Disc Loading on Baseline Tilt-Wing Configuration . . . . .	47
Figure 11 - Effects of Low Disc Loadings on Wing Stall for Lightly Immersed Tilting Wings $X/R_p = 0.0$ . . . . .	54
Figure 12 - Effects of Variation in Wing Loading on Baseline Tilt-Wing Configuration . . . . .	55
Figure 13 - Effects of Variation in Aspect Ratio on Baseline Tilt-Wing Configuration . . . . .	60
Figure 14 - Effects of Variation in Flight Path Angle on Baseline Tilt-Wing Configuration . . . . .	61
Figure 15 - Effects of Variation in Thrust Offset Angle on Baseline Tilt-Wing Configuration . . . . .	62
Figure 16 - Effects of Variation in Number of Engines on Baseline Tilt-Wing Configuration . . . . .	63
Figure 17 - Effects of Variation in Spanwise Engine Location on Baseline Tilt-Wing Configuration . . . . .	64
Figure 18 - Effects of Reduced Wing Immersion and High Wing Loadings on Baseline Tilt-Wing Configuration . . . . .	65
Figure 19 - Effects of Variation in Taper Ratio on Baseline Tilt-Wing Configuration . . . . .	66

TABLE OF CONTENTS (Concluded)

	Page
LIST OF FIGURES (Concluded)	
Figure 20 - Effects of Airfoil Variation on Tilt-Rotor Configuration . . . . .	67
Figure 21 - Effects of Fuselage Rotation on Tilt-Rotor Configuration . . . . .	68
Figure 22 - Transition Data for Baseline Tilt-Rotor Configuration	69
Figure 23 - Effects of Variation in Disc Loading on Baseline Tilt-Rotor Configuration . . . . .	71
Figure 24 - Effects of Variation in Wing Loading on Baseline Tilt-Rotor Configuration . . . . .	76
Figure 25 - Effects of Variation in Aspect Ratio on Baseline Tilt-Rotor Configuration . . . . .	82
Figure 26 - Effects of Variation in Flight Path Angle on Baseline Tilt-Rotor Configuration . . . . .	83
Figure 27 - Effects of Variation in Wing Incidence on Baseline Tilt-Rotor Configuration . . . . .	84
Figure 28 - Effects of Variation in Taper Ratio on Baseline Tilt-Rotor Configuration . . . . .	85

### SYMBOLS

AR	total wing aspect ratio
AR <sub>eff</sub>	effective aspect ratio of wing endplated by slipstream
AR <sub>s</sub>	effective aspect ratio of wing immersed in slipstream
C <sub>D<sub>B</sub></sub>	basic drag coefficient for cylindrical bodies
C <sub>D<sub>F</sub></sub>	induced drag coefficient of fuselage at angle of attack
C <sub>D<sub>q</sub></sub>	total drag coefficient of wing immersed in free stream
C <sub>D<sub>s</sub></sub>	total drag coefficient of wing immersed in slipstream
C <sub>D<sub>N</sub></sub>	total drag coefficient of nacelle
C <sub>D<sub>1</sub></sub>	total drag coefficient of wing immersed in slipstream at ( $\alpha_s - 0.1^\circ$ )
C <sub>D<sub>o<sub>N</sub></sub></sub>	profile drag coefficient of nacelle
C <sub>D<sub>o<sub>q</sub></sub></sub>	profile drag coefficient of wing immersed in free stream
C <sub>D<sub>o<sub>s</sub></sub></sub>	profile drag coefficient of wing immersed in slipstream
C <sub>L<sub>N</sub></sub>	lift coefficient of nacelle immersed in slipstream
C <sub>L<sub>q</sub></sub>	lift coefficient of wing immersed in free stream
C <sub>L<sub>F</sub></sub>	lift coefficient of fuselage at angle of attack
C <sub>L<sub>s</sub></sub>	lift coefficient of wing immersed in slipstream
C <sub>L<sub>1</sub></sub>	lift coefficient of wing immersed in slipstream at ( $\alpha_s - 0.1^\circ$ )
DL	disc loading in hover, $\text{lbs/ft}^2 \left( \frac{W}{N_p S_p} \right)$
D <sub>BT</sub>	total drag on body tail combination, lb.
D <sub>BT<sub>p</sub></sub>	profile drag on body-tail combination, lbs

SYMBOLS (Continued)

$D_{Fi}$	induced drag on fuselage at angle of attack, lbs.
$D_N$	total drag on nacelles
$d_n$	nacelle diameter, ft.
$d_F$	fuselage diameter ft.
$D_q$	drag on wing portion immersed in free stream, lbs
$D_s$	drag on wing portion immersed in slipstream, lbs
$e$	aircraft efficiency factor
$f$	equivalent parasite area of body-tail combination
$F$	force parallel to flight path, lbs
$F_h$	force parallel to flight path, lbs
$f_R$	fuselage rotation factor
$F_v$	force perpendicular to flight path, lbs
$F_{wh}$	resultant wing force parallel to flight path, lbs
$F_{wv}$	resultant wing force perpendicular to flight path, lbs.
$i_w$	wing incidence relative to fuselage center line, deg
$L_{BT}$	lift on body-tail combination, lb.
$L_N$	lift on nacelle immersed in slipstream, lbs.
$l_F$	fuselage length, ft.
$l_n$	nacelle length, ft.
$L_q$	lift on wing immersed in free stream, lbs
$L_s$	lift on wing immersed in slipstream, lbs
$N_p$	number of propulsors per aircraft
$c$	free-stream dynamic pressure, lb/ft <sup>2</sup>
$c_s$	dynamic pressure in slipstream at the wing, lb/ft <sup>2</sup>
$c_{sH}$	dynamic pressure in slipstream in hover, lb/ft <sup>2</sup> $\left( \frac{W}{N_p S_p} \right)$

SYMBOLS (Continued)

$R_1$	summation of forces perpendicular to flight path, lbs.
$R_2$	summation of forces parallel to flight path, lbs.
$R_p$	propulsor blade radius, ft.
$r$	velocity ratio, $V/V_s$
$S$	total wing area, $ft^2$
$S_F$	fuselage area $=d_F \times l_F$ , $ft.^2$
$S_I$	area of wing immersed in fully contracted slipstream, $ft^2$
$S_{I_c}$	corrected $S_I$
$S_N$	nacelle area $=d_N \times l_N$ , $ft.^2$
$S_p$	area of one propulsor disc, $ft^2$
$S_q$	area of wing immersed in free stream, $ft^2$
$T$	total thrust required for equilibrium, lb
$t_c$	clearance between fuselage and rotor tip, ft.
$T_p$	thrust required per propulsor, lb
$THP_H$	total ideal thrust horsepower required in hover
$THP$	total thrust horsepower required
$V$	free-stream velocity, ft/sec
$V_I$	induced velocity at plane of propulsor disc, ft/sec
$V_p$	resultant velocity at the prop, ft/sec
$V_{PH}$	resultant velocity at the prop in hover, ft/sec
$V_s$	velocity in the slipstream at the wing, ft/sec
$V_{sH}$	slipstream velocity at the wing in hover, ft/sec
$W$	gross weight during transition, lb.
$w_F$	fuselage width, ft
$X$	distance from engine center line to wing tip, ft.
$X/R_p$	engine location parameter

SYMBOLS (Concluded)

$\alpha_o$	wing angle of attack relative to free stream, deg
$\alpha_s$	wing angle of attack relative to slipstream, deg
$\alpha_l$	$\alpha_s - 0.1^\circ$
$\alpha_N$	nacelle angle of attack relative to $q_s$
$\alpha_{OL}$	zero lift $\alpha$
$\alpha_{st}$	stall angle of attack for positive lift, deg
$\alpha_{st_N}$	stall angle of attack for negative lift, deg
$\beta$	local slipstream resultant angle relative to flight path, deg
$\gamma$	flight path angle relative to horizon, deg
$\delta$	fuselage rotation angle relative to flight path, deg
$\zeta$	angle between induced and slipstream velocity vectors, deg
$\theta$	propulsor tilt angle relative to fuselage center line, deg
$\lambda$	wing taper ratio
$\rho$	local air density, slugs/ft <sup>3</sup>
$\psi$	angle between thrust and resultant velocity vector ( $V_p$ ) at prop, deg
$\psi$	thrust offset angle relative to wing chord, deg (positive if thrust axis is below wing chord, negative if above)

## SUMMARY

An analysis for tilting free propulsor Vertical/Short Take-Off and Landing (V/STOL) aircraft in equilibrium transition is presented. Families of curves are generated in terms of nondimensional flight parameters so that the effects of aerodynamic interactions and varying geometric configurations may be studied. For known values of the ideal hover quantities, the transition characteristics, including thrust and power requirements, may be determined for specific aircraft designs. Suggestions are presented as to those characteristics which should be incorporated into the design of a tilting free propulsor V/STOL aircraft. A comparison is then made between a tilt-wing and tilt-rotor aircraft, each employing the favorable characteristics prescribed by the tradeoff study.

## INTRODUCTION

Present V/STOL technology has led to a large number of design proposals, ranging in concept from high disc loading aircraft, such as fan-in-wing or lift jet, to the lower disc loading configurations, including tilt wing (wing and rotors tilt simultaneously) and tilt rotor (rotor alone tilts) designs. Reference 1 indicated that the tilt wing and/or tilt rotor concepts are more desirable than the very high disc loading designs with regard to low downwash and installed power requirements as well as higher maneuverability and hover efficiencies. A means is provided by the design study of Reference 2 to analyze tilt-wing and tilt-rotor concepts during equilibrium transition in which all inertia forces are considered zero. By using that methodology, it is the purpose of this report to provide comparative curves of transition characteristics and power requirements for various disc loadings (10 psf to 100 psf), wing loadings (10 psf to 100 psf), aspect ratios (4 to 12) and other descriptive parameters. These nondimensional curves are referenced to the ideal hover mode characteristics (i.e., values calculated for a gross weight supported by rotors of a given disc area, with no regard for download on the wing or fuselage). This allows the determination of relative quantities

throughout the entire transition once the easily calculated ideal hover values are known. The equilibrium case of transition was chosen because it was expected to show closer agreement with wind-tunnel tests (usually conducted in a constrained mode involving no accelerations) and because it was noted that under the assumption of an infinite transitioning time, the dynamic case degenerated to the equilibrium mode, Reference 2. A relative comparison between dynamic and equilibrium transitions is provided in Reference 3:

- (1) For a given airspeed in an accelerating transition from hover to cruise, greater power at a lower wing tilt angle would be required relative to a similar equilibrium airspeed.
- (2) In deceleration to hover, less power at a higher tilt angle would be necessary relative to equilibrium at a certain airspeed.

Thus the equilibrium case is useful in providing some indications as to the limits of certain characteristics of the dynamics transition.

In addition to predicting forces in transition, the generated curves are intended to aid in determining feasibility of certain designs. Analysis of the curves may suggest limiting values as well as the most desirable parameter combination for a particular configuration. This in turn will allow the merits of the tilt wing and tilt rotor designs to be compared.

#### METHOD OF ANALYSIS

The methodology of this analysis was developed in conjunction with a tilt rigid rotor design concept study (Reference 2) and then extended to encompass a wide range of parameters and transition details. For a given geometric configuration, this computerized technique was employed to predict local flow angles, free-stream and slipstream velocities, relative wing angles of attack, resultant wing and body forces, and thrust and power required to maintain a non-accelerated condition at specific propulsor tilt angles throughout the tilt range from cruise to hover.

The entire analysis considered within this report was confined to the equilibrium transition, excluding all inertial forces or, more precisely, any time dependency. Thus, each data point on the curves presented was independent of the preceding points and no propulsor tilting schedule was required. The effects of varying the following parameters were considered: disc loading, wing loading, aspect ratio, taper ratio, spanwise engine location, number of engines, wing incidence (tilt rotor only), and thrust off-set angle (thrust axis relative to mean airfoil section chord). In addition, fuselage rotation about the pitch axis, various flight path slopes, and airfoil variations (including various flaps and spoilers) were studied. The variation in flow over the wing due to slipstream induced velocity was incorporated in the analysis, as was the change in resulting effective aspect ratio calculated from Reference 4.

Analysis was limited to tilt-wing and tilt-rotor V/STOL aircraft. A different transitioning technique was employed for each of these two designs, since a large drag force was found necessary to decrease the aircraft's velocity as the propulsors rotated towards the hover position. Tilting of the wing rotated the lift vector rearward and provided sufficient drag to slow the tilt wing design to a near-zero forward velocity, but the fixed wing tilt-rotor vehicle lacked this velocity reduction capability. As an alternative, it was necessary to pitch the tilt rotor's fuselage upward in a maneuver similar to a helicopter's flare upon landing. This resulted in the same effect for the fixed wing as a partial wing rotation for the tilt wing, and the resultant drag significantly reduced the tilt rotor's forward velocity. The question of the degree of fuselage rotation then became another parameter to be considered. For both aircraft designs, properties of the airfoil sections used and characteristics of the flow around the wing thus became important factors.

By means of summing the forces perpendicular and parallel to the assumed flight path slope, the slipstream dynamic pressure ( $q_s$ ) and thrust ( $T_p$ ) required for equilibrium were determined at each rotation angle ( $\theta$ ). A complicated interrelation of thrust, free-stream and

slipstream dynamic pressures, and dependent terms made necessary a means of solution of the force summation equations in terms of the independent variables  $q_s$  and  $T_p$  (see Figure 1).

$$\begin{aligned}
 R_1 &= \Sigma F_v = N_p T_p \sin(\theta + \delta) + L_q + L_s \cos \beta + L_N \cos \beta \\
 &\quad - D_N \sin \beta - D_s \sin \beta + L_{BT} - W \cos \gamma \\
 &= N_p T_p \sin(\theta + \delta) + C_{L_q} q S_q + C_{L_s} q S_I \cos \beta + C_{L_N} q S_N \cos \beta \\
 &\quad - C_{D_N} q S_N \sin \beta - C_{D_s} q S_I \sin \beta + C_{L_F} q S_F - W \cos \gamma \quad [1]
 \end{aligned}$$

$$\begin{aligned}
 R_2 &= \Sigma F_h = N_p T_p \cos(\theta + \delta) - L_s \sin \beta - L_N \sin \beta - D_{BT} \\
 &\quad - D_q - D_s \cos \beta - D_N \cos \beta - W \sin \gamma \\
 &= N_p T_p \cos(\theta + \delta) - C_{L_s} q S_I \sin \beta - C_{L_N} q S_N \sin \beta \\
 &\quad - \left( C_{D_F} q S_F + f_F q \right) - C_{D_q} q S_q - C_{D_s} q S_I \cos \beta \\
 &\quad - C_{D_N} q S_N \cos \beta - W \sin \gamma \quad [2]
 \end{aligned}$$

Note that the variables in Figure 1 were related to the independent variables  $T_p$  and  $q_s$  as follows:

$$\beta = \sin^{-1} \left[ \frac{T_p \sin(\theta + \delta)}{S_p q_s} \right] = \tan^{-1} \left[ \frac{T_p \sin(\theta + \delta)}{S_p q + T_p \cos(\theta + \delta)} \right] \quad [3]$$

$$\alpha_s = i_w + \delta - \beta \quad [4]$$

$$\alpha_q = i_w + \delta \quad (\text{Tilt Rotor}) \quad [5a]$$

$$\alpha_q = \alpha_s + \beta = i_w + \delta = \theta + \psi + \delta \quad (\text{Tilt Wing}) \quad [5b]$$

$$q = q_s \cos \beta - \frac{T_p}{S_p} \cos (\theta + \delta) \quad [6]$$

Equations [1] and [2] were solved simultaneously for  $T_p$  and  $q_s$  in conjunction with Equations [3] through [6] using a Modified Newton-Raphson numerical technique. (See Reference 2 (Appendix A), Reference 5 and Appendix of this report.) The lift and profile drag coefficients corresponding to free stream ( $C_{L_q}$ ,  $C_{D_{oq}}$ ) and slipstream ( $C_{L_s}$ ,  $C_{D_{os}}$ ) wing angles of attack were obtained from the curves of Figure 2 by an interpolation subroutine. Since these curves were required for angles of attack from  $-90^\circ$  to  $+90^\circ$ , they were not readily available. The required curves could be calculated from the theory of Reference 6, while References 7, 8, and 9 provided empirical curves and showed the effects of flap and spoiler employment.

A method from Reference 4 for predicting lift and drag on cylindrical bodies was extended so that the forces on both the fuselage and nacelles could be determined. The nacelles were considered to be totally immersed in the slipstream, thus experiencing the dynamic pressure  $q_s$  at an angle of attack  $\alpha_N$ , where

$$\alpha_N = \theta + \delta - \beta \quad [7]$$

The nacelle lift and drag coefficients were then defined as

$$\begin{aligned} C_{L_N} &= C_{D_B} \sin^2 \alpha_N \cos \alpha_N \\ C_{D_N} &= C_{D_B} \sin^3 \alpha_N + \tau_{D_{oN}} \end{aligned} \quad [8]$$

with values of the basic cylindrical drag coefficient ( $C_{D_B}$ ) and nacelle profile drag coefficient ( $C_{D_{oN}}$ ) taken to be 1.0 and 0.045, respectively. The lift and drag forces per nacelle then became

$$L_N = C_{L_N} q_s S_N \quad [9]$$

$$D_N = C_{D_N} q_s S_N \quad [10]$$

with the corresponding area a product of nacelle diameter and length,

$$S_N = d_N \ell_N \quad [11]$$

The lift and drag of the fuselage-empennage combination were calculated in a similar way, and were associated with the free-stream dynamic pressure  $q$  at an angle  $\delta$ .

$$C_{L_F} = C_{D_B} \sin^2 \delta \cos \delta \quad [12]$$

$$C_{D_F} = C_{D_B} \sin^3 \delta \quad [13]$$

$$L_{BT} = C_{L_F} q S_F \quad [14]$$

$$D_{BT} = D_{F_i} + D_{BT_p} = C_{D_F} q S_F + f_F q \quad [15]$$

where  $S_F = d_F \ell_F$  and the profile drag term was based on an empirical equivalent parasite area,  $f_F$ , similar to Reference 6.

A major part of the analysis involved the effects of the slipstream flow field over the wing on the corresponding velocities, pressures, and forces of Figure 1. The free-stream dynamic pressure ( $q$ ) was altered in Equation [6] by the thrust loading  $\left(\frac{T_p}{S_p}\right)$  so that an effective dynamic pressure ( $q_s$ ) was produced in the slipstream and experienced by the immersed wing area ( $S_I$ ). This appears in Figure 1 as the vector addition of free-stream velocity ( $V$ ) and twice the propulsor induced velocity ( $V_I$ ) to produce the velocity in the slipstream ( $V_S$ ). These velocities were defined as:

$$V = \sqrt{\frac{2q}{\rho}} \quad [16]$$

$$V_s = \sqrt{\frac{2q_s}{\rho}} \quad [17]$$

$$V_I = \frac{1}{2} \left\{ \left[ V_s^2 - v^2 \sin^2 (\theta + \delta) \right]^{\frac{1}{2}} - v \cos (\theta + \delta) \right\} \quad [18]$$

Consideration of separate free-stream and slipstream flow regions involved the assumption that the actual dynamic pressure distribution across the wing (Figure 3) could be represented by approximately constant values of  $q$  and  $q_s$  in uniform flow fields. The higher velocity slipstream produced an effective aspect ratio due to an endplating effect on the free-stream-immersed wing portion, and the total wing drag coefficient in the free stream then became

$$C_{D_q} = C_{D_{o_q}} + \frac{C_{L_q}^2}{\pi AR_{eff}} \quad [19]$$

Reference 4 was used to determine  $AR_{eff}$  employing the related wing span ( $b_q$ ) as shown in Figure 3. The remaining wing span ( $b_s$ ) was used to define the aspect ratio in the slipstream ( $AR_s$ ) so that the total slipstream drag coefficient could be calculated for the wing as

$$C_{D_s} = C_{D_{o_s}} + \frac{C_{L_s}^2}{\pi AR_s e} \quad [20]$$

with an assumed aircraft efficiency factor ( $e$ ) of 0.9. This immersed wing section ( $S_I$ ) was always considered to have the wing tips within the boundary of the slipstream so that the induced drag coefficient could be defined as in Equation [20]. Both the slipstream and freestream immersed areas were altered accordingly for variations in aspect ratio, taper ratio, propulsor radius and spanwise engine location.

Transition power requirements as a function of propulsor tilt angle were calculated based on the total propulsor thrust and associated flow velocity at the propulsor plane ( $V_p$ ) necessary to maintain the unaccelerated condition:

$$\text{THP} = \frac{N_T \cos \phi V_P}{550} \quad [21]$$

$$= \frac{N_T}{550} [V \cos (\theta + \delta) + V_I]$$

where

$$V_p = \frac{V_s}{2} \left\{ 1 + r^2 \left[ 1 + 2 \sin^2 (\theta + \delta) \right] + 2 r \cos (\theta + \delta) \left[ 1 - r^2 \sin^2 (\theta + \delta) \right]^{\frac{1}{2}} \right\}^{\frac{1}{2}} \quad [22]$$

$$r = \frac{V}{V_s}$$

$$\phi = \cos^{-1} \left[ \frac{V_p^2 + V_I^2 - V^2}{2V_p V_I} \right] \quad [23]$$

In order to avoid involving the tradeoff study with the complexity of rotor design and blade characteristics, the propulsor was assumed to be simply an impulse disc of a given area able to produce the required equilibrium thrust, and the rotor drag, rotor normal force, tip losses, and slipstream swirl were neglected. This led to the assumption of a propulsive efficiency of 1.0, and caused Equation [21] to yield thrust horsepower only; therefore, the predicted power requirements of this report are underestimated.

Use of the dimensionless ratios required that disc loading, wing loading, and certain other quantities be calculated using input physical characteristics of the aircraft in hover as follows ( $V=0$ ,  $T=W$ ,  $\phi=0$ ):

$$\text{disc loading} = \frac{W}{N_p S_p} \quad [24]$$

$$\text{wing loading} = \frac{W}{S} \quad [25]$$

$$q_{sH} = \frac{W}{N_p S_p} \quad [26]$$

$$V_{sH} = \left( \frac{2q_{sH}}{\rho} \right)^{\frac{1}{2}} \quad [27]$$

$$V_{PH} = \frac{V_{SH}}{2} \quad [28]$$

$$THP_H = \frac{W V_{PH}}{550} \quad [29]$$

Equations [24] through [29] are ideal hover quantities based only on the thrust necessary to support in equilibrium the gross weight of the aircraft, and do not include slipstream download effects on the wing or fuselage, rotor losses or rotor profile power. For convenience in obtaining absolute quantities from values of the nondimensional ratios, Table 1 presents values of  $V_{SH}$  and  $THP_H$  for given disc loadings (noting that disc loading and  $q_{SH}$  are equivalent in hover) and a gross weight of 30,000 pounds.

Assumptions made in this analysis should be noted so that limitations on the results may be realized. Since the major purpose of the program was prediction of equilibrium forces as a function of tilt angle in transition, the aircraft was considered to have sufficient tail forces and rotor control moments to keep it trimmed during propulsor tilting. Yaw, roll, and side force terms were eliminated by considering only longitudinal motions in the vertical plane. The wing area  $S_I$  was assumed to be continually immersed in a uniform, nonrotating slipstream (i.e. no swirl effects considered). In addition, the entire transition was considered to occur at a constant aircraft gross weight and density altitude (sea level), inferring that dynamic pressures  $q$  and  $q_s$  were indicative of velocities  $V$  and  $V_s$ . Fuselage drag calculations assumed a retracted landing gear.

Data for a sample case are shown in Figure 4, where the predicted transition is compared to flight test data from the Canadair CL-84 tilt wing, twin-engined V/STOL aircraft. Curve A was based on an assumed dynamic pressure distribution as given in Figure 3. However, Reference 1 denoted the difficulty experienced in determining the proper relationships between the freestream and slipstream flows, and referred to

the ability of the propulsor slipstream to influence flow from the surrounding freestream. This effectively increased the diameter of the higher velocity slipstream, and added to its lift-producing capabilities. To approximate this factor an increase of 30% in the slipstream immersed wing area (i.e.  $S_{IC} = 1.3 S_I$ , curve B) gave better agreement with the experimental data towards the cruise portion of the curve  $\left(\frac{v}{v_{s_H}} \geq 1.1\right)$ . The comparison in this figure is actually between the experimental curve occurring over a finite time interval and the equilibrium curves A and B occurring over an infinite time. Past exploratory work supported the assertion of Reference 2 that the dynamic transition degenerated into the equilibrium case in the limit as transition time became infinite. Curve B, with the increased slipstream immersed area, is felt to be a closer approximation of that limit since agreement with the flight data is very good in both hover and cruise (the two near-equilibrium portions of the experimental curve).

#### APPLICATION TO TRADE-OFF ANALYSIS

The original equilibrium transition analysis (Reference 2) was enlarged so that many families of curves could be generated to provide a rapid survey of various parameter effects, availing itself for vehicle trade-off study purposes. By nondimensionalizing the curves, an entire spectrum of transition gross weights could be considered for both the tilt wing and tilt rotor configurations. All nondimensional curves were generated using a transition weight of 30,000 pounds, but similar results would be valid for any transition weight if the same disc loading, wing loading, aspect ratio, number of engines, etc., existed. Absolute transition quantities for any given transition weight were obtained from the nondimensional curves and a knowledge of the theoretical hover quantities (Equations [24] through [29]) and the wing stall angle.

It was evident that certain geometric combinations of wing loading, disc loading, aspect ratio, taper ratio, and spanwise engine location were not feasible in that a minimum clearance had to be maintained between rotor and fuselage. Based on an empirical equation for fuselage

width relative to transition gross weight,

$$w_F = 0.26 W_T^{\frac{1}{2}}, \quad [30]$$

the curves in Figures 5, 6, and 7 show design limitations based on clearance that must be maintained between propulsor and fuselage for 10,000, 30,000 and 100,000 pound aircraft, respectively. These limiting values were adhered to when determining which configurations to use in curve generation and should be kept in mind as a guide for proposed designs.

The families of curves, though intended to be as general as possible, must of necessity be limited to a particular airfoil section and its corresponding aerodynamic data. Effort was made to choose wing airfoils which were complimentary to the type of V/STOL being analyzed, and it is felt that those airfoils used do clearly show the trends displayed by a particular configuration. Since the curves presented cannot cover all possible parameter combinations, including choice of wing sections, there may be other cases which the reader may want to examine.

Figures 8 through 28 present the curves generated to illustrate general equilibrium transition trends and the effects of parameter variation. These were analyzed in two separate groups due to the distinct transition techniques found necessary for tilt wing and tilt rotor aircraft. Both configurations transitioned along a horizontal flight path, with the approach angle being one of the parameters under consideration. The differing lift requirements of the two V/STOL types determined both the choice of airfoil sections and the initial wing incidence settings.

In producing the characteristic curves, initial effort was made to determine appropriate airfoil sections and body rotation schedules (if any) which would compliment the differing configurations. Emphasis was then placed on recognition of favorable disc loadings with consideration for the dependence of installed power and downwash velocities. A baseline configuration for each V/STOL type was established, keeping physical parameters as similar as possible so that a comparison of tilt wing versus tilt rotor could eventually be made. Parameters were then varied individually and significant trends noted. A final configuration for

each aircraft was proposed as a result and a comparison made between the types.

#### TILT-WING AIRCRAFT ANALYSIS

Simultaneous tilting of both wing and propulsor led to the possibility of flow separation and consequent wing stall, which according to References 3, 11 and 12, could become a serious problem during deceleration or partial power descent, especially on low disc loading aircraft. At wing angles of attack exceeding the normal stall conditions, increased thrust was necessary to augment the induced velocity ( $V_I$ ), thus more effectively turning the incoming flow and reducing the local angle of attack of the immersed wing ( $\alpha_s$ ). Proper airfoil choice should follow the criteria that the stall be postponed as long as possible, although with reasonably high disc loadings, it was found that stall did not often occur on that portion of wing immersed in the slipstream. (The unimmersed wing area always stalled, since its angle of attack was proportional to the tilt angle).

Figure 2(a) presents lift and drag data for the modified NACA 63<sub>3</sub>-418 airfoil with Krüger leading edge flaps and a stall angle of 26°. This airfoil was used effectively on the Canadair CL-84 and should prove favorable on the typical tilt wing configuration because stall is postponed to higher angles of attack than those available with most conventional airfoils. These conventional shapes could, however, provide higher lift coefficients at lower angles of attack [see for example, the flapped NACA 4415 airfoil of Figure 2(b)], but would be undesirable if the stall angle were easily exceeded during wing tilt.

In Figure 8, the NACA 63<sub>3</sub>-418 airfoil and a variation employing simulated spoilers were used on a sample tilt wing aircraft with both disc and wing loadings of 50 lbs/ft<sup>2</sup> and an aspect ratio of 8.0. In both cases, the effects of slipstream turning due to wing downwash were neglected. The ability of this airfoil to postpone stall made it a good choice for illustrative purposes, and it was, therefore, used as the baseline airfoil for the tilt wing configuration. It is interesting to note that the simulated spoilers increased drag, reduced lift, and thus required more thrust and higher velocity to maintain equilibrium. They also required higher angles of attack on the slipstream-immersed wing

at higher tilt angles. Results of variation in airfoil characteristics in Figure 8 served to re-emphasize the heavy dependence of the V/STOL transition upon input airfoil data.

Based on data gathered during the development of preliminary plots, the following physical parameters were chosen as being either complimentary to the tilt wing or necessary to examine certain extremes of parameter values (e.g., use of higher aspect ratio allowed large diameter, low disc loading rotors to be employed without fuselage interference):

gross weight,	$W = 30,000 \text{ lb}$
disc loading,	$DL = 50 \text{ lb/ft}^2$
wing loading,	$W/S = 50 \text{ lb/ft}^2$
aspect ratio,	$AR = 8.0$
flight path angle,	$\gamma = 0^\circ$
taper ratio,	$\lambda = 0.9$
number of propulsors,	$N_p = 2$
engine location parameter,	$X/R_p = 1.0$
thrust offset angle,	$\psi = 3^\circ$
fuselage rotation angle,	$\delta = 0^\circ$
wing incidence,	$i_w = 3^\circ$ (initially, in cruise)
aircraft efficiency factor,	$e = 0.9$
wing stall angle,	$\alpha_{st} = 26^\circ$

These became the characteristics of the baseline tilt wing aircraft, and remained constant throughout the nondimensional curves presented, except when a given parameter was varied and that variation noted on the appropriate plot. Also, the correction factor for the increase in effective slipstream immersed wing area was reduced to 28% (i.e.,  $S_{Ic} = 1.28 S_I$ ) to prevent that area from exceeding the overall wing area in certain cases of large rotor diameter. Fuselage rotation (independent of wing tilting) was found to yield only a small proportion of the drag required for transition to hover, since the main drag terms were produced by the wing at high tilt angles. Therefore, pitching of the fuselage was not employed with the tilt wing aircraft as a means of achieving the hover mode.

Figure 9 presents sample transition data for the baseline tilt wing aircraft, in which variations of velocities, dynamic pressures, flow angles, aerodynamic forces and power with tilt angle may be noted. The hover mode ( $q = 0$ ) was reached at a tilt angle of  $73.5^\circ$ , indicating that the weight was then being supported by a combination lift and thrust vector. The variations in the magnitudes of the forces corresponded directly to the velocities and flow angles of Figure 9(b), in particular  $\alpha_q$  and  $\alpha_s$ .

#### PARAMETRIC VARIATIONS

##### Disc Loading

Reference 10 relates higher disc loadings to increased slipstream velocities and installed power requirements. Using hover quantities as an indication of installed power, this relationship was verified by results from Equations [26] to [29] as presented in Table I. Figure 10 indicates that the same higher power requirement was present throughout the entire transition for larger disc loadings. The associated higher thrust produced greater induced ( $V_I$ ) and slipstream ( $V_s$ ) velocities, thus reducing the angle of attack necessary in the slipstream. In contrast, Figure 11 indicates the inability of a low disc loading to turn the slipstream enough to prevent stall when the wing was not heavily immersed in the slipstream. (This will be further discussed in relation to the spanwise engine location parameter,  $X/R_p$ ). Little variation in equilibrium free-stream dynamic pressure was evident with change in disc loading, except towards hover. There, the higher disc loading designs hovered at lower tilt angles due to greater vertical wing resultant forces ( $F_{w_v}$ ). The above observations would suggest a moderate or "upper moderate" disc loading (on the order of 40 to 60 psf) for tilt wing aircraft. Avoidance of wing stall should determine a minimum disc loading, with the upper limit being established by propulsor downwash velocities and power requirements in hover. (Reference 10 suggests an upper limit of 80 lb/sq. ft. based on installed power requirements and specific fuel consumption.) The final choice would also have to take into consideration range and speed requirements in the cruise mode, which are also functions of disc loading.

Variation in disc loading produced corresponding changes in the hover quantities  $q_{s_H}$ ,  $V_{s_H}$  and  $THP_H$ , which would have made comparisons difficult between curves in Figure 10. To rectify this, the starred quantities  $q_{s_H}^*$ ,  $V_{s_H}^*$ , and  $THP_H^*$  corresponding to a disc loading of 60 lbs/sq. ft. were used as nondimensionalizing values throughout Figure 10, and allowed direct comparison between curves to be made.

#### Wing Loading

An increased aircraft wing loading implied a decreased wing area for a constant weight, and thus, the need for a higher angle of attack to provide the same lift. Higher wing loadings, as shown in Figure 12, thus resulted in greater power requirements due to a reduction of the net vertical wing force produced by smaller wing areas. As a consequence, transition velocity was higher at a given tilt angle, and the conversion to hover was postponed until higher tilt angles were reached. In the near-cruise mode, the higher wing loadings again required greater thrust, velocity and power to maintain equilibrium. As indicated by these trends, a low to moderate wing loading is desirable throughout the entire transition range from cruise to hover.

In the power-velocity curves of Figure 12, it appears that there is some noticeable error near hover where neglect of slipstream turning due to wing downwash effects has probably caused underestimation of required hover power. This may also be due in part to limits placed on the iterative numerical solution near hover (which caused data to be output within a finite number of iterations), and in part to possible overestimation of the slipstream's ability to entrain flow and increase the immersed wing area. It is expected that these curves should actually converge on  $THP/THP_H = 1.0$  as  $V/V_{s_H}$  approaches zero.

#### Aspect Ratio

As the aspect ratio was increased at a constant disc and wing loading, a smaller percentage of the wing was immersed in the propulsor slipstream. Nearer to cruise, this led to reduced wing drag, a lower thrust, and consequently a lower power requirement (Figure 13). At

reduced velocities and higher tilt angles, the larger free-stream wing area ( $S_q$ ) of high aspect ratios led to greater wing drag and higher angle of attack and power requirements. In addition, reduction in the vertical wing force postponed hover to a higher tilt angle. The choice of aspect ratio then fell into two regions, with higher values being more favorable towards cruise and lower values near hover. It is possible that neglect of slipstream turning may again have caused underestimation of power near hover (as in Figure 12) and that the power curves of Figure 13 should more closely approach  $THP/THP_H = 1.0$ . In this case, the emphasis on low aspect ratio near hover would be lessened. Selection of a high aspect ratio must include consideration of structural and mechanical problems involved in tilting a long slender wing.

#### Flight Path Angle

A steeper approach angle ( $\gamma$  more negative) increased the weight component along the flight path, augmenting the required thrust and thus reducing the horsepower. This component contributed to the forward velocity as evidenced by a higher  $q$  in Figure 14. Also, a steeper approach slope required a greater tilt angle to achieve hover ( $q = 0$ ). A positive  $\gamma$  effectively reduced the slipstream angle of attack (reducing the possibility of flow separation and stall), unloaded the wing (reduced  $F_{w_v}$ ) earlier, and transitioned to hover at a lower tilt angle but higher power. This positive flight path angle could be employed in a "pullup" maneuver to reduce aircraft velocity. The final choice of  $\gamma$  would ultimately be determined by mission and landing requirements placed on the aircraft.

#### Thrust Offset Angle

Offsetting the thrust line above ( $\psi$  negative) or below ( $\psi$  positive) the wing chord had the effect of translating the original curves, Figure 15. A positive angle (i.e., wing chord above the thrust axis, Figure 1) caused higher angles of attack and wing drag while bringing the aircraft to hover at a lower tilt angle. Power was less at a given velocity because the wing vertical force was greater and required less thrust for equilibrium.

However, with the avoidance of wing stall being of significant importance, the results of Figure 15 would tend to favor a thrust axis offset several degrees above the wing chord ( $\psi$  negative).

#### Number of Engines

Figure 16 presents data for two- and four-engined tilt wing configurations with the same wing loading, disc loading per propulsor, and  $X/R_p$  at the outer props. To maintain identical disc loadings, the rotor radius on the two-engined design was greater but the total slipstream immersed wing area was less than for the four-engined version. The trends observed were then similar to those for variation in aspect ratio (Figure 13). Four rotors corresponded to low AR and a larger slipstream immersed area thus reducing the required angle of attack and free-stream dynamic pressure. On the other hand, two engines required less thrust and power near cruise, corresponding to the lower immersed area of higher aspect ratios in Figure 13. In both cases, approximated slipstream effects were removed by setting  $S_T$  and  $\lambda$  equal to unity.

#### Spanwise Engine Location

Moving the engines inboard from the wing tip (increasing  $X/R_p$  from 0 to 1) increased the slipstream immersed wing area, requiring a lower free-stream velocity and slipstream angle of attack for the same tilt angle and thereby postponing any existing tendency towards stall in the slipstream. In Figure 17, a hump in the free-stream dynamic pressure occurred for  $X/R_p = 0.0$  (smallest slipstream immersed area since the engine centerline was at the wing tip) where the large non-immersed wing section stalled ( $\alpha_q > \alpha_{st}$ , where  $\alpha_q = \theta$  and  $\alpha_{st} = 26^\circ$ ). As  $X/R_p$  increased to 1.0 the engines were moved inboard and more of the wing became immersed in the slipstream, thereby eliminating the hump. This effectively increased total lift, and reduced thrust, power, angle of attack, and dynamic pressure. These trends were noticed mainly in the region of higher tilt angles. Figure 11 presented regions of stalled flow for  $X/R_p = 0.0$  and various disc loading, wing loading, and tilt angle combinations. A series of plots similar to Figure 18, when cross-plotted with other like plots, gave Figure 11. It is seen that large

non-immersed wing areas on the tilt wing configuration caused stalled flow regions and power requirements greater than those in hover. These effects were even greater for smaller disc loadings. The importance of an inboard engine location immersing as much of the wing as possible in the propulsor slipstream was thus heavily emphasized at higher tilt angles.

#### Taper Ratio

An increase in taper ratio approaching 1.0 made the wing planform more rectangular and, at a constant aspect ratio, disc loading and wing loading, increased the slipstream immersed wing area. It is seen in Figure 19 that these effects were relatively small compared to results of variations in other parameters. Figure 19 does show that increased taper ratio led to trends very similar to a decrease in aspect ratio (Figure 13). Thus, at low tilt angles, lower taper ratios yielded reduced power requirements, but the trend was reversed at higher tilt angles due to the reduced free-stream wing drag of higher taper ratios.

#### TILT-ROTOR AIRCRAFT ANALYSIS

Due to the fixed nature of the wing, the tilt rotor configuration did not encounter the problem of severe wing stall due to flow separation at high wing tilt angles. Thus the high slipstream dynamic pressure necessary to keep the tilt wing from stalling was not required, and low disc loadings could be employed. However, the negative angles of attack experienced by the wing in the slipstream of the tilt rotor led to problems associated with negative lift coefficients (see Figure 2). The equilibrium solution in this negative lift region became difficult to obtain. Greater thrust to overcome the negative wing lift produced higher slipstream velocities, which in turn increased the downward lift vector and required more opposing thrust. This divergent problem could only be resolved after negative stall was exceeded and the negative lift vector was decreased. To avoid this situation, simulated spoilers on the wing underside reduced the undesirable negative region on the NACA 4415 airfoil with 60° split flap (Figure 2).

The NACA 4415 airfoil was chosen to provide reasonably high lift coefficients at the low tilt angle (the incidence angle) of the fixed wing. Figure 20 shows the effects of flaps and the simulated spoilers on the NACA 4415 airfoil. (The stall angle was the negative value

$(\alpha_{st_N})$  from Figure 2, but the absolute value was taken so that the sign of  $\alpha_s$  was apparent in the nondimensional ratio.) A sharp peak in the dynamic pressure curves at tilt angles above  $75^\circ$  and the steep drop immediately following were indicative of an undesirable velocity profile for  $\alpha_s \leq \alpha_{OL}$  which was double-valued and large for most of the transition. Of the three curves, the simulated spoilers produced a smoother  $q$  and  $\alpha_s$  decrease as well as power buildup, but it was questionable that any of these trends were desirable as such.

Comparison with the smooth curves generated for the tilt wing indicated that the problem lay in the fixed wing's inability to produce a sufficient retarding drag force to slow the aircraft during equilibrium transition. A nose-upward rotation of the fuselage created a greatly increased wing drag in addition to drag on the inclined fuselage. This body rotation (through  $\delta$  degrees) was employed as a function of the rotor tilt angle, so that the total rotor rotation ( $\theta + \delta$ ) relative to the flight path was

$$\theta + \delta = \theta + f_R \theta \quad [31]$$

where  $f_R$  was the rotation factor. Figure 21 shows that a total body rotation of  $30^\circ$ , ( $f_R = 0.5$ ), greatly reduced the magnitude and peaks of the dynamic pressure curves as well as the large negative angle of attack (since the wing was at a final effective incidence of  $33^\circ$  relative to the flight path). The penalty to be paid was a peak in the power curve in the mid transition region (due to earlier reduction in lift) and an additional hover power requirement due to the increasing down load on the wing as the fuselage was re-rotated towards the horizontal for the final touchdown.

As a result of the foregoing, the simulated spoilers and  $60^\circ$  split flap on the NACA 4415 airfoil, and a body rotation of  $30^\circ$  were incorporated into the baseline aircraft and its transition technique in the following tradeoff analysis. As with the tilt wing aircraft, preliminary data indicated certain favorable parameters to be employed on the baseline tilt rotor design. The following characteristics

were held constant except when being examined individually:

$$\begin{aligned}W &= 30,000 \text{ lb} \\DL &= 15 \text{ lb/ft}^2 \\W/S &= 80 \text{ lb/ft}^2 \\AR &= 8.0 \\ \gamma &= 0^\circ \\ \lambda &= 0.9 \\ N_p &= 2 \\ X/R_p &= 0.0 \\ \psi &= 0^\circ \\ \delta &= 0.5 \theta \text{ for } \theta \leq 60^\circ \\ \theta_{\delta \text{ max}} &= 60^\circ \\ i_w &= 3^\circ \\ e &= 0.9 \\ \alpha_{st_N} &= -30^\circ\end{aligned}$$

These values were chosen to be as nearly comparable with the tilt wing configuration as possible, so that eventual comparison between the two types could be made.

Typical values of dynamic pressures, power, forces, and flow angles during the tilt rotor transition are given for the baseline aircraft in Figure 22. A smaller disc loading and rotor induced velocity than the tilt wing's caused the velocities  $V$ ,  $V_p$ , and  $V_s$  to be of similar magnitudes and produced a much greater angle ( $\phi$ ) between the thrust axis and the velocity vector at the propulsor ( $V_p$ ). Sudden variations in certain of the forces and flow angles near hover were found to originate at the zero lift angle of attack in the slipstream ( $\alpha_{OL}$ ). This crossover to negative lift was also responsible for the sharp drop-offs in Figures 20 and 21 as well as in many of the following nondimensional curves.

With the employment of fuselage rotation, it was frequently the case that hover did not occur when the rotors were vertical ( $\theta + \delta = 90^\circ$ ).

This was a result of the inclined wing producing a negative lift component perpendicular to the vertical slipstream (i.e., in the forward horizontal direction). Physically, this would require that the thrust vector continue to rotate beyond the vertical to balance the forward lift component. Also, because the computerized force solution was an iterative numerical type, the final equilibrium point did not always occur at exactly  $90^\circ$  tilt angle. In both of the above cases, the curves were incomplete in the near hover region, but based on similar solutions, it was felt that small extrapolations of the data could be made. Finally, it should be noted that power requirements near hover were slightly overestimated, because the slipstream immersed wing areas were based on the rectangular area immersed at low tilt angles rather than the actual circular area covered in hover.

#### PARAMETRIC VARIATIONS

##### Disc Loading

Disc loading variations again involved changes in the denominators  $q_{s_H}$ ,  $V_{s_H}$ , and  $THP_H$ ; therefore, as with the tilt wing, the starred quantities (now corresponding to  $DL = 40 \text{ lb/ft}^2$ ) were used to make the curves of Figures 23 directly comparable. Increasing disc loading implied decreased propulsor area and slipstream immersed wing area, with resulting increases in slipstream dynamic pressure. This led to greater flow deflection angles ( $\beta$ ) and lower  $\alpha_s$ , causing the lift to become negative earlier and increasing requirements on thrust, power, and freestream dynamic pressure at higher tilt angles. According to Reference 10, effort to minimize wing area in the downwash from high disc loadings could lead to excessive wing loadings much higher in value than the associated disc loadings. An upper limit on disc loading of  $20 \text{ lb/ft}^2$  for fixed wing "convertiplanes" was proposed by this reference; the curves of Figure 23 support this emphasis on large diameter, low disc loading rotors.

##### Wing Loading

With wing size, and consequently wing loading, being limited by the clearance which must be maintained between propulsor disc and fuselage, selection of high wing loadings must be considered carefully

to avoid interference. Figure 24 indicates that at low tilt angles increased wing loadings required higher power, slipstream angle of attack, and freestream dynamic pressure to compensate for reduction in wing area. At higher tilt angles, the lower wing loadings experienced increased downloads and associated power requirements. Although this could be partly alleviated by use of additional leading and trailing edge devices to reduce the immersed area, it appeared that higher wing loadings showed more promise near hover, the region of greatest power. In addition they were effective in smoothing out the humps in the dynamic pressure curves. Analysis of Figures 23 and 24 together indicated that the combination of low wing loadings and higher disc loadings should be avoided for the tilt rotor due to high power requirements near hover and double-valued dynamic pressure and velocity curves.

#### Aspect Ratio

For constant disc and wing loadings, an increasing aspect ratio yielded a reduced slipstream immersed wing area and a resulting lower download in hover, but as seen in Figure 25 this effect was not large. A more noticeable variation was found in the power required near the cruise mode where lower aspect ratios experienced higher wing drag and thus required greater thrust and power. It appeared that a high aspect ratio was favorable in both the cruise and hover modes, the upper bound being limited by structural considerations.

#### Flight Path Angle

Figure 26 shows similar trends with variation of flight path angle to those shown in Figure 14 for the tilt wing. A reduction in power definitely seemed to favor the negative  $\gamma$  (descending approach). Reduced thrust required higher  $\alpha_s$  and postponed hover and the occurrence of negative lift components to higher tilt angles, but was also associated with higher dynamic pressures. By comparison, a positive  $\gamma$  (analogous to a "pullup") resulted in approaching hover much earlier in the tilt schedule, as well as larger power requirements. In consideration of the above, a descending transition appears more likely, but the actual decision should depend heavily upon the type of maneuver the particular mission involves.

### Wing Incidence

Increase in the angle of attack of the fixed wing had its greatest effect at low tilt angles where it was useful in producing a higher lift coefficient near cruise. At high tilt angles its effectiveness was decreased. In addition, any advantage obtained could effectively be produced by fuselage rotation. The upper limit on wing incidence would probably be a function of drag generation in cruise. Near the hover mode, very little effect was seen to result from variation in wing incidence (Figure 27).

### Taper Ratio

As with the tilt wing, taper ratio effects (Figure 28) were functions of immersed wing area. A decreased taper ratio was similar to an increase in aspect ratio, yielding lower power and thrust requirements in the near cruise realm due to a decrease in total wing drag. Also related to the decreased  $S_I$  of lower taper ratio was the slight reduction in download on the wing near hover. Whereas the effects of taper ratio change in Figure 28 were small, they did point towards the choice of a taper ratio somewhat less than 1.0.

### Engine Location, Number of Engines, and Thrust Offset Angle

From the standpoints of wing structure and slipstream download on the wing, it was felt that a configuration with two engines, each located at the wing tip was the only reasonable wing-mounted tilt rotor configuration. Variation in the parameters  $X/R_p$  and  $N_p$  was thus not studied, nor was thrust offset angle as the rotor was not fixed relative to the wing chord, and the relative angle between them was the tilt angle ( $\theta$ ) itself.

### COMPARISON OF TILT-WING AND TILT-ROTOR CONFIGURATIONS

The baseline aircraft configurations employed the majority of the favorable transition characteristics recommended by the foregoing observations, and were thus chosen for comparison of the two V/STOL types. Figures 9 and 22 present aerodynamic characteristics for the 30,000-pound tilt wing and tilt rotor aircraft respectively in horizontal equilibrium transition and provide the basis of the following discussion.

In general, use of some type of high lift device was found necessary to meet equilibrium lift requirements, and both aircraft were subjected to a wing stall problem: flow separation at high angle of attack for the tilt wing, and an undesirable negative lift increase up to the negative stall angle for the tilt rotor. The following characteristics were found distinctive for each V/STOL type (comparisons are relative to the contrasting design):

#### TILT-WING CHARACTERISTICS

- Smooth rapid decrease in dynamic pressure and velocity due to rapid wing drag buildup as a result of tilting.
- Greater propulsor induced velocities and resulting slipstream deflection due to higher disc loadings.
- Higher power and thrust requirements through the majority of the transition as a result of higher disc loading and large wing drag.
- Necessity of immersing as much wing area as possible in the slipstream to reduce stall tendencies at higher tilt angles. At low tilt angles, a reduced immersed wing area is desirable.
- No body rotation necessary due to drag of tilted wing.
- Reduced lift and drag on the nacelles due to smaller angle between thrust axis and high energy slipstream.
- Hover occurring at tilt angles less than  $90^\circ$  where a lift and thrust vector resultant equalizes the weight.

#### TILT-ROTOR CHARACTERISTICS

- Slow reduction in dynamic pressure and velocity due to lack of large drag force increase on wing.
- Sudden sharp drop in flows angles and forces at and below the zero lift angle of attack.
- Relative to the tilt wing, lower thrust and power requirements preceding hover due to lower disc loading; higher thrust required near hover due to download on the wing.
- Lower rotor induced velocities and slipstream deflection due to low disc loadings.
- Necessity of fuselage rotation to generate retarding wing and fuselage drag.

- Requirement for a means of reducing the magnitudes of negative lift coefficients below the zero lift angle of attack.
- Larger nacelle net lift and drag terms (regardless of lower slipstream velocities) as a result of a larger nacelle angle of attack caused by less flow deflection.

#### CONCLUSIONS

The effects of various parameters on the equilibrium transition characteristics of tilt wing (tilting wing and rotor) and tilt rotor (rotor alone tilts) V/STOL aircraft have been investigated. Based on the limited number of cases studied, the following characteristics tend to be favorable to transition performance of tilt propulsor configurations:

##### TILT-WING AIRCRAFT

- Airfoil sections employing devices to yield high lift coefficients and to postpone flow separation and stall.
- Moderate disc loading with an upper limit dependent on installed power requirements and downwash velocities, and a lower limit bounding on inability to prevent stall.
- Low to moderate wing loading, maintaining sufficient lift at reduced transition velocities.
- Compromising aspect ratio between high values near cruise and low values near hover based mainly on associated slipstream immersed area.
- Flight path angle mainly dependent on mission, but climbing to reduce stall tendency or descending to reduce power.
- Thrust line offset several degrees above the wing chord ( $\downarrow$  negative)
- Two propulsors for lower thrust and power at a given disc loading.
- Engines located inboard from the wing tips ( $X/R_p = 1.0$ ), immersing as much wing area as possible.
- Taper ratio approaching 1.0 to reduce power requirements near hover.

##### TILT-ROTOR AIRCRAFT

- Airfoil sections producing high lift coefficients at low wing incidence in addition to reduced negative lift coefficients.
- Upward fuselage rotation to generate increased wing and body drag forces.

- Low disc loading to minimize downwash and installed power requirements.
- High wing loading to reduce download on wing surfaces.
- Higher aspect ratio to reduce thrust and power requirements; limited by structural restrictions.
- Descending flight path to reduce thrust and power or horizontal approach to eliminate added velocity due to forward weight component.
- High fixed wing incidence to provide sufficient lift in transition, but limited by drag generation in cruise.
- Taper ratio less than 1.0 to produce small power reduction.
- Two propulsors, each located at wing tip ( $X/R_p = 0.0$ ).

Comparison of the two aircraft indicated that the majority of variations in transition characteristics were caused by differences in flow angles, velocities and immersed wing areas. In general, these were direct results of choice of disc loading and the ability or inability of the wing to tilt with the rotors. Results were heavily dependent on input aerodynamic characteristics of the airfoil sections employed, and relative magnitudes of the parameter variations would be expected to change somewhat with alternate airfoils.

Use of the parametric curves in specific design studies will provide numerical transition data as well as an indication of desirable and undesirable factors of a proposed configuration. Relative effects of parameter variation may be determined and an effective trade-off analysis made.

APPENDIX  
 DERIVATIVES USED IN NEWTON SOLUTION OF EQUILIBRIUM FORCE  
 SUMMATIONS (EQUATIONS [1] AND [2])

$$\begin{aligned}
 \frac{\partial R_1}{\partial T_p} = S_I q_s & \left[ -C_{L_s} \sin \beta \frac{d\beta}{dT_p} + \cos \beta \frac{dC_{L_s}}{dT_p} - C_{D_s} \cos \beta \frac{d\beta}{dT_p} \right. \\
 & \left. - \sin \beta \frac{dC_{D_s}}{dT_p} \right] + S_q C_{L_q} \frac{dq}{dT_p} + N_p \sin(\theta + \delta) \\
 & + N_p S_N q_s \left[ \cos \beta \frac{dC_{L_N}}{dT_p} - C_{L_N} \sin \beta \frac{d\beta}{dT_p} - \sin \beta \frac{dC_{D_N}}{dT_p} \right. \\
 & \left. + C_{D_N} \cos \beta \frac{d\beta}{dT_p} + C_{L_F} S_F \frac{dq}{dT_p} \right] \quad [A-1]
 \end{aligned}$$

$$\begin{aligned}
 \frac{\partial R}{\partial q_s} = S_I (C_{L_s} \cos \beta + S_I q_s & \left[ -C_{L_s} \sin \beta \frac{d\beta}{dq_s} + \cos \beta \frac{dC_{L_s}}{dq_s} \right. \\
 & \left. - C_{D_s} \cos \beta \frac{d\beta}{dq_s} - \sin \beta \frac{dC_{D_s}}{dq_s} \right] - S_I C_{D_s} \sin \beta + S_q C_{L_q} \frac{dq}{dq_s} \\
 & + N_p S_N (C_{L_N} \cos \beta - C_{D_N} \sin \beta + q_s \left( \cos \beta \frac{dC_{L_N}}{dq_s} - C_{L_N} \sin \beta \frac{d\beta}{dq_s} \right. \\
 & \left. - \sin \beta \frac{dC_{D_N}}{dq_s} - C_{D_N} \cos \beta \frac{d\beta}{dq_s} \right) + C_{L_F} S_F \frac{dq}{dq_s} \quad [A-2]
 \end{aligned}$$

$$\begin{aligned}
\frac{\partial R_2}{\partial T_p} = S_I q_s & \left[ -C_{L_s} \cos \beta \frac{d\beta}{dT_p} - \sin \beta \frac{dC_{L_s}}{dT_p} + C_{D_s} \sin \beta \frac{d\beta}{dT_p} \right. \\
& \left. - \cos \beta \frac{dC_{D_s}}{dT_p} \right] - S_q C_{D_q} \frac{dq}{dT_p} + N_p \cos(\theta + \delta) - f_F \frac{dq}{dT_p} \\
& + N_p S_N q_s \left[ -C_{L_N} \cos \beta \frac{d\beta}{dT_p} - \sin \beta \frac{dC_{L_N}}{dT_p} + C_{D_N} \sin \beta \frac{d\beta}{dT_p} \right. \\
& \left. - \cos \beta \frac{dC_{D_N}}{dT_p} \right] - C_{D_F} S_F \frac{dq}{dT_p} \quad [A-3]
\end{aligned}$$

$$\begin{aligned}
\frac{\partial P_2}{\partial q_s} = S_I q_s & \left[ -C_{L_s} \cos \beta \frac{d\beta}{dq_s} - \sin \beta \frac{dC_{L_s}}{dq_s} + C_{D_s} \sin \beta \frac{d\beta}{dq_s} \right. \\
& \left. - \cos \beta \frac{dC_{D_s}}{dq_s} \right] - S_I C_{L_s} \sin \beta - S_I C_{D_s} \cos \beta - S_q C_{D_q} \frac{dq}{dq_s} - f_F \frac{dq}{dq_s} \\
& + N_p S_N \left[ -C_{L_N} \sin \beta - C_{D_N} \cos \beta + q_s \left( -C_{L_N} \cos \beta \frac{d\beta}{dq_s} \right. \right. \\
& \left. \left. - \sin \beta \frac{dC_{L_N}}{dq_s} + C_{D_N} \sin \beta \frac{d\beta}{dq_s} - \cos \beta \frac{dC_{D_N}}{dq_s} \right) \right] - C_{D_F} S_F \frac{dq}{dq_s} \quad [A-4]
\end{aligned}$$

$$\frac{d\beta}{dT_p} = \frac{\sin(\theta+\delta)}{S_p q_s \cos \beta} \quad [A-5]$$

$$\frac{dC_{L_s}}{dT_p} = \frac{dC_{L_s}}{d\alpha_s} \frac{d\alpha_s}{dT_p} \quad [A-6]$$

where

$$\frac{d\alpha_s}{dT_p} = - \frac{d\beta}{dT_p} \quad [A-7]$$

and

$$\frac{dC_{L_s}}{d\alpha_s} = \frac{C_{L_1} - C_{L_s}}{\alpha_1 - \alpha_s} \quad [A-8]$$

$$\frac{dC_{L_N}}{dT_p} = \frac{dC_{L_N}}{d\beta} \frac{d\beta}{dT_p} \quad [A-9]$$

where

$$\frac{dC_{L_N}}{d\beta} = C_{D_B} \left( \sin^3 \alpha_N - 2 \sin \alpha_N \cos^2 \alpha_N \right) \quad [A-10]$$

$$\frac{dC_{D_s}}{dT_p} = \frac{dC_{D_s}}{d\alpha_s} \frac{d\alpha_s}{dT_p} \quad [A-11]$$

where

$$\frac{dC_{D_s}}{d\alpha_s} = \frac{C_{D_1} - C_{D_s}}{\alpha_1 - \alpha_s} \quad [A-12]$$

$$\frac{dC_{D_N}}{dT_p} = \frac{dC_{D_N}}{d\beta} \frac{d\beta}{dT_p} \quad [A-13]$$

where

$$\frac{dC_{D_N}}{d\beta} = -3 C_{D_B} \sin^2 \alpha_N \cos \alpha_N \quad [A-14]$$

$$\frac{dq_s}{dT_p} = -q_s \sin \beta \frac{d\beta}{dT_p} - \frac{\cos(\theta+\delta)}{S_p} \quad [A-15]$$

$$\frac{d\beta}{dq_s} = \frac{-T_p \sin(\theta+\delta)}{B q_s^2 S_p} \quad [A-16]$$

where

$$B = \sqrt{1 - \left[ \frac{T_p \sin(\theta+\delta)}{S_p q_s} \right]^2} \quad [A-17]$$

$$\frac{dC_{L_s}}{dq_s} = \frac{dC_{L_s}}{d\alpha_s} \frac{d\alpha_s}{dq_s} \quad [A-18]$$

where

$$\frac{d\alpha_s}{dq_s} = - \frac{d\beta}{dq_s} \quad [A-19]$$

$$\frac{dC_{D_s}}{dq_s} = \frac{dC_{D_s}}{d\alpha_s} \frac{d\alpha_s}{dq_s} \quad [A-20]$$

$$\frac{dC_{L_N}}{dq_s} = \frac{dC_{L_N}}{d\beta} \frac{d\beta}{dq_s} \quad [A-21]$$

$$\frac{dC_{D_N}}{dq_s} = \frac{dC_{D_N}}{d\beta} \frac{d\beta}{dq_s} \quad [A-22]$$

$$\frac{dq}{dq_s} = \cos \beta - q_s \sin \beta \frac{d\beta}{dq_s} \quad [A-23]$$

Equations [A-1] through [A-23] are used in a modified Newton-Raphson's solution of the simultaneous nonlinear equations:

$$\frac{\partial R_1}{\partial T_p} dT_p + \frac{\partial R_1}{\partial q_s} dq_s = -dR_1 \quad [A-24]$$

$$\frac{\partial R_2}{\partial T_p} dT_p + \frac{\partial R_2}{\partial q_s} dq_s = -dR_2 \quad [A-25]$$

for  $dT_p$  and  $dq_s$  in the solution of Equations [1] and [2] in the text, see Appendix A of Reference 1.

#### REFERENCES

1. Levin, Stuart M. The Light Intratheater Transport. Space/Aeronautics (N.Y.), v. 50, Oct 1968, p. 44-53, incl. illus.
2. Kirkpatrick, Douglas G. Methodology for Design and Evaluation of a Twin Rigid-Rotor V/STOL Aircraft. Wash., Mar 1968. 77 p. incl. illus. (Naval Ship Research and Development Center. Rpt. 2764. Aero Rpt. 1149) (Thesis (M.S.) Maryland Univ.) (DDC AD 835 583)
3. Stuart, Joseph III. Tilt Wing Propelloplane Design Requirements. American Helicopter Society. Journal (N.Y.), v. 2, Apr 1957, p. 10-19.
4. Hoerner, Sighard F. Fluid-Dynamic Drag. [Midland Park, N. J.] 1965. 1 v.
5. Ortega, James M. and Werner C. Rheinboldt. On Discretization and Differentiation of Operators With Application to Newton's Method. Langley, Va., May 1965. 22 p. (National Aeronautics & Space Adm. CR-63634) (Maryland Univ. Computer Science Ctr. TR-65-16. Contract [i.e. Grant] NSG-398)
6. Beppu, G. and H. C. Curtiss, Jr. An Analytical Study of Factors Influencing the Longitudinal Stability of Tilt-Wing VTOL Aircraft. Fort Eustis, Va., Jul 1966. 90 p. incl. illus. (Army. Aviation Materiel Labs. Tech Rpt. 66-53) (Princeton Univ. Dept. of Aerospace and Mechanical Sciences. Rpt. 756. Contract DA-44-177-AMC-8 (T))
7. Brasseur, Gary W. A Preliminary Investigation to Study the Effect of Flat Spoilers on the Aerodynamic Characteristics of Wings at Angles of Attack From  $0^\circ$  to  $90^\circ$ . Wash., Apr 1966. 29 p. incl. illus. (Naval Ship Research and Development Center. Rpt. 2214. Aerp Rpt. 1113) (DDC AD 636 750)
8. Fink, Marvin P. Aerodynamic Data on Large Semispan Tilting Wing With 0.5-Diameter Chord, Single-Slotted Flap, and Single Propeller 0.08 Chord Below Wing. Wash., Jul 1967. 200 p. incl. illus. (National Aeronautics and Space Adm. Tech Note D-4030)

9. Reader, Kenneth R. and Richard D. Murphy. Powered Model Investigation of the Effects of Gated Spoilers on the Aerodynamic Characteristics of Wings at Angles of Attack From  $0^{\circ}$  to  $90^{\circ}$ . Wash., Apr 1967. 53 p. incl. illus. (Naval Ship Research and Development Center. Rpt. 2406. Aero Rpt. 1132) DDC AD 655 248)
10. Strand, Torstein, E. S. Levinsky and M. H. Y. Wei. Unified Performance Theory for V/STOL Aircraft in Equilibrium Level Flight. San Diego, Calif., May 1966. 122 l. incl. illus. (Air Vehicle Corp. Rpt. 350. Contract Nonr 4926(00))
11. Lichten, R. L. Some Performance and Operating Characteristics of Convertiplanes. American Helicopter Society. Journal (N.Y.), v. 3, Apr 1958, p. 13-24.
12. Guerrieri, Mario A. and Joseph Stuart III. A Simplified Theoretical Investigation of a Wing-Propeller Combination Through a Range of Angles of Attack From  $0^{\circ}$  to  $90^{\circ}$  and a Comparison With Experimental Results. Palo Alto, Calif., Oct 1955. [19] l. incl. illus. (Hiller Aircraft Corp. Engineering Rpt. 461.3. Contract Nonr 1657(00))

TABLE 1  
Ideal Hover Quantities  
W=30,000 lb.

$\frac{DL}{q_s H}$	$V_{S_H}$	$V_{P_H}$	$THP_H$
5.0	64.85	32.42	1768.57
10.0	91.71	45.85	2501.14
15.0	112.32	56.16	3063.26
20.0	129.70	64.85	3537.14
25.0	145.00	72.50	3954.65
30.0	158.84	79.42	4332.10
35.0	171.57	85.79	4679.20
40.0	183.42	91.71	5002.28
45.0	194.54	97.27	5305.72
50.0	205.07	102.53	5592.71
55.0	215.08	107.54	5865.69
60.0	224.64	112.32	6126.51
65.0	233.81	116.91	6376.68
70.0	242.64	121.32	6617.39
75.0	251.15	125.58	6849.65
80.0	259.39	129.70	7074.29
85.0	267.37	133.69	7292.00
90.0	275.13	137.56	7503.41
95.0	282.66	141.33	7709.03
100.0	290.01	145.00	7909.29

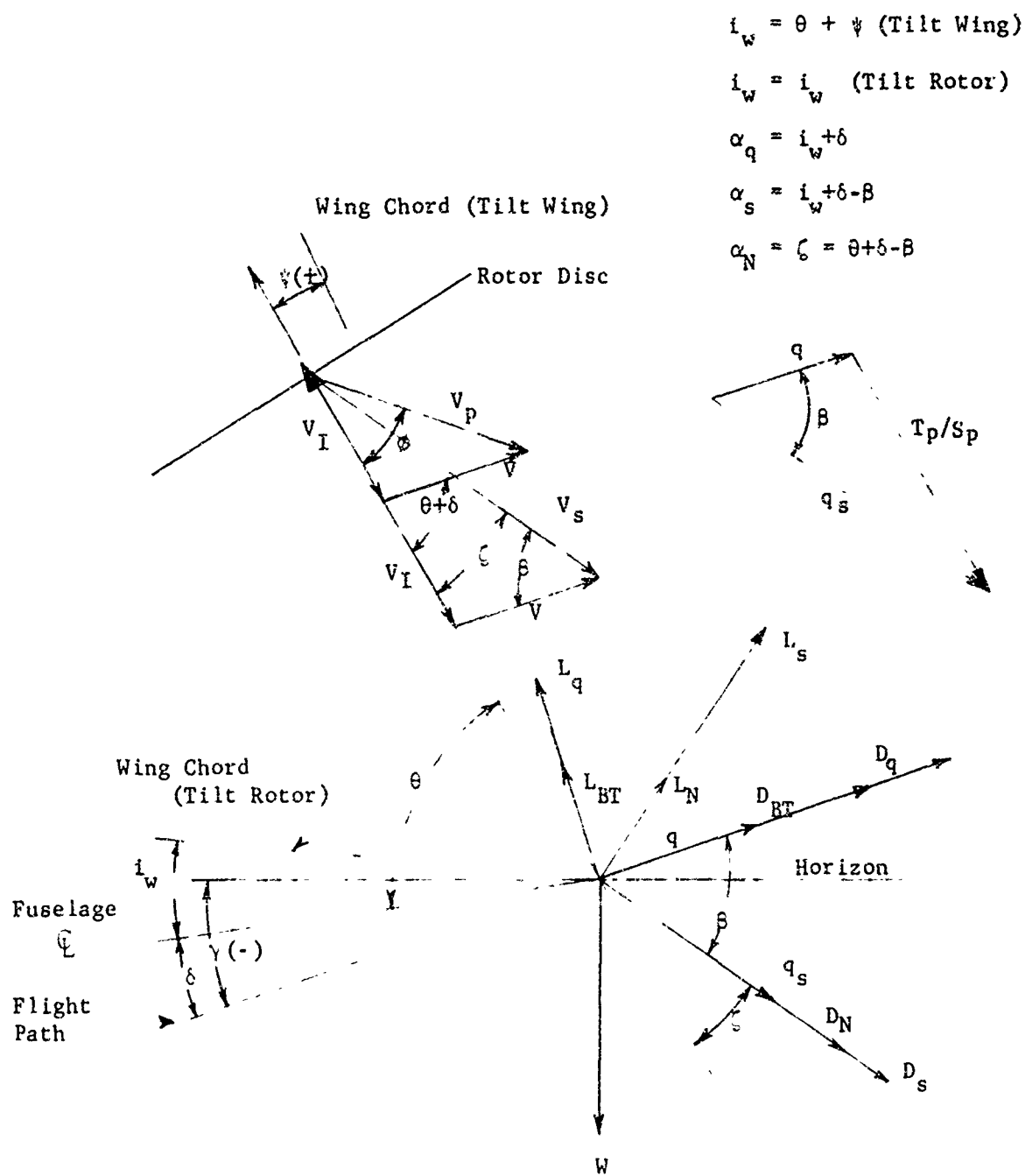
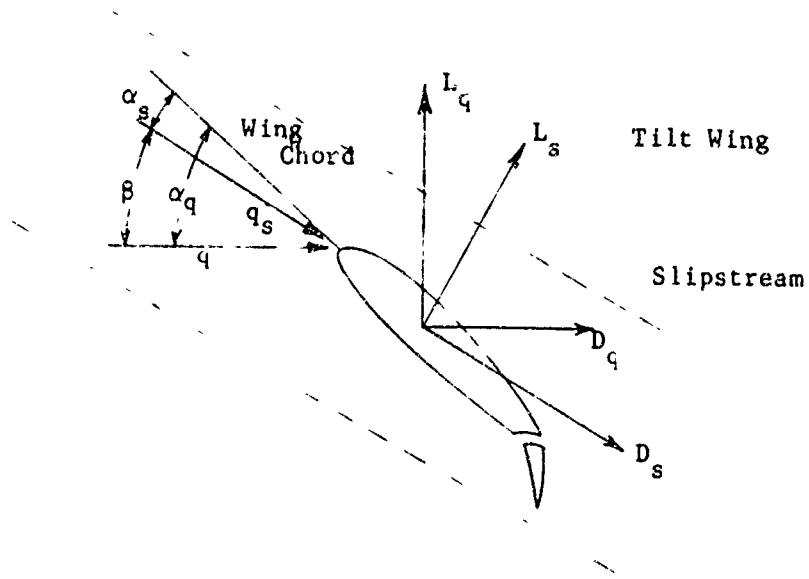


Figure 1 - Velocity, Force, and Pressure Geometries  
 (a) Body, Wing, and Rotor



$$\begin{aligned} \Sigma F_{w_h} &= -D_q - D_s \cos \beta - L_s \sin \beta \\ \Sigma F_{w_v} &= L_q - D_s \sin \beta + L_s \cos \beta \end{aligned}$$

$+F_v$   
 $+F_h$

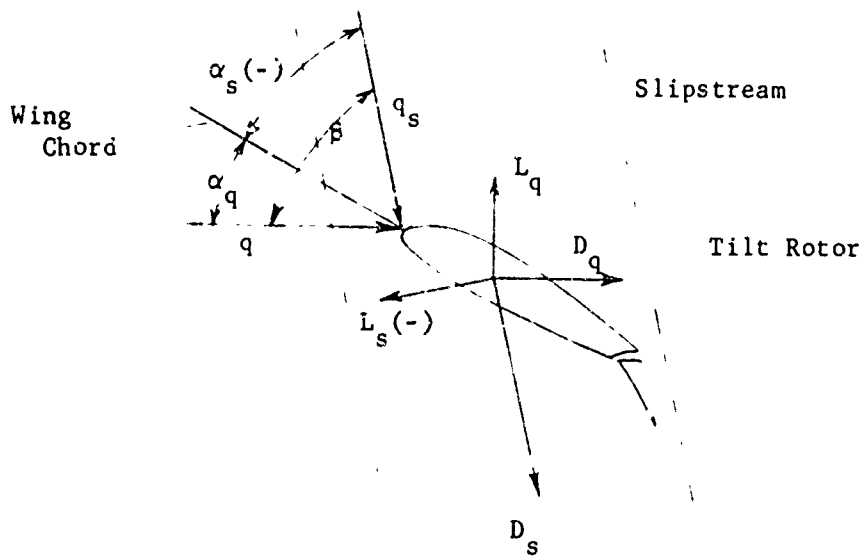


Figure 1 - (Concluded)

(b) Wing Only

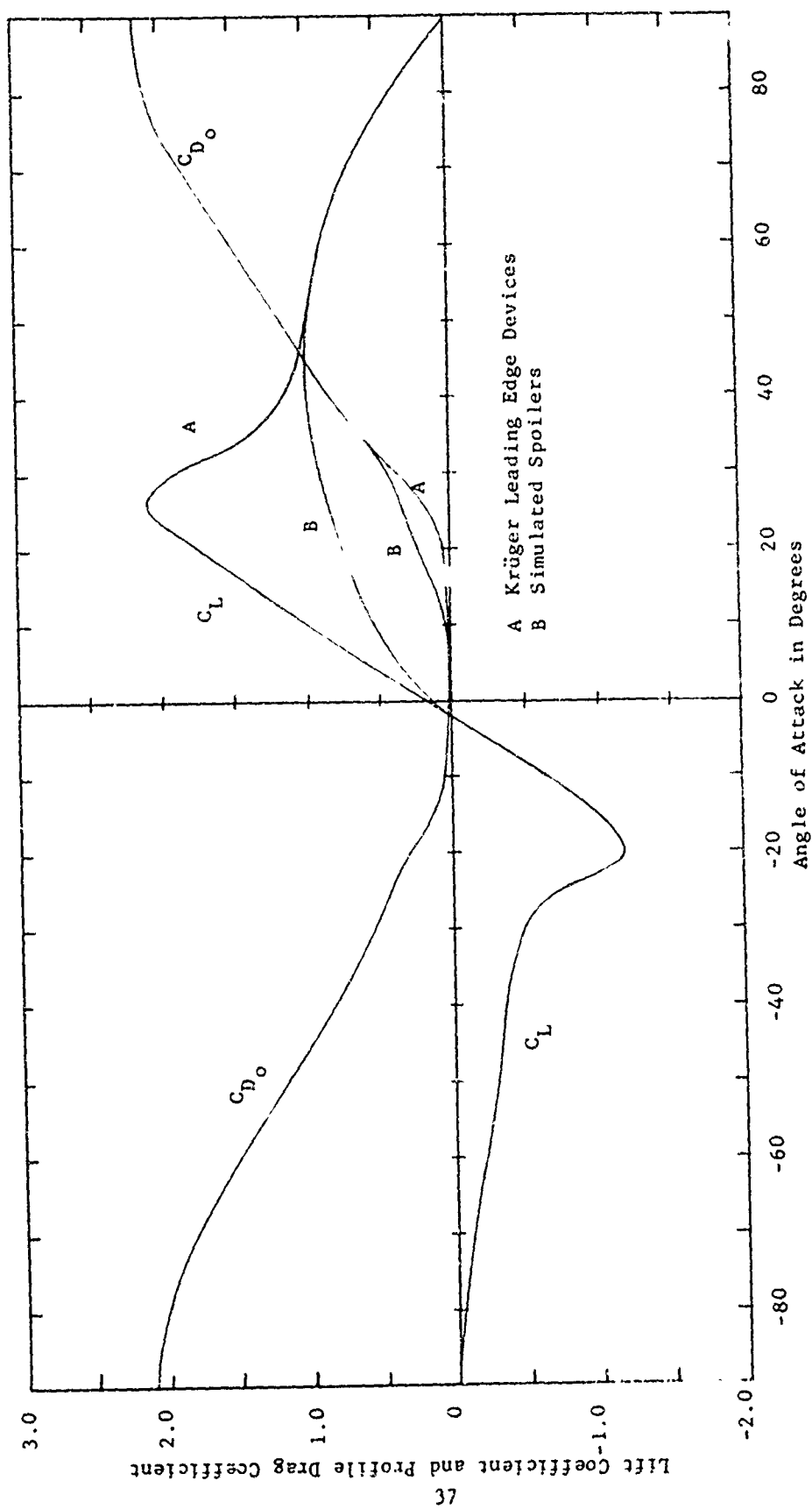


Figure 2 - Airfoil Characteristics  
 (a) NACA 63<sub>3</sub>-418 Airfoil

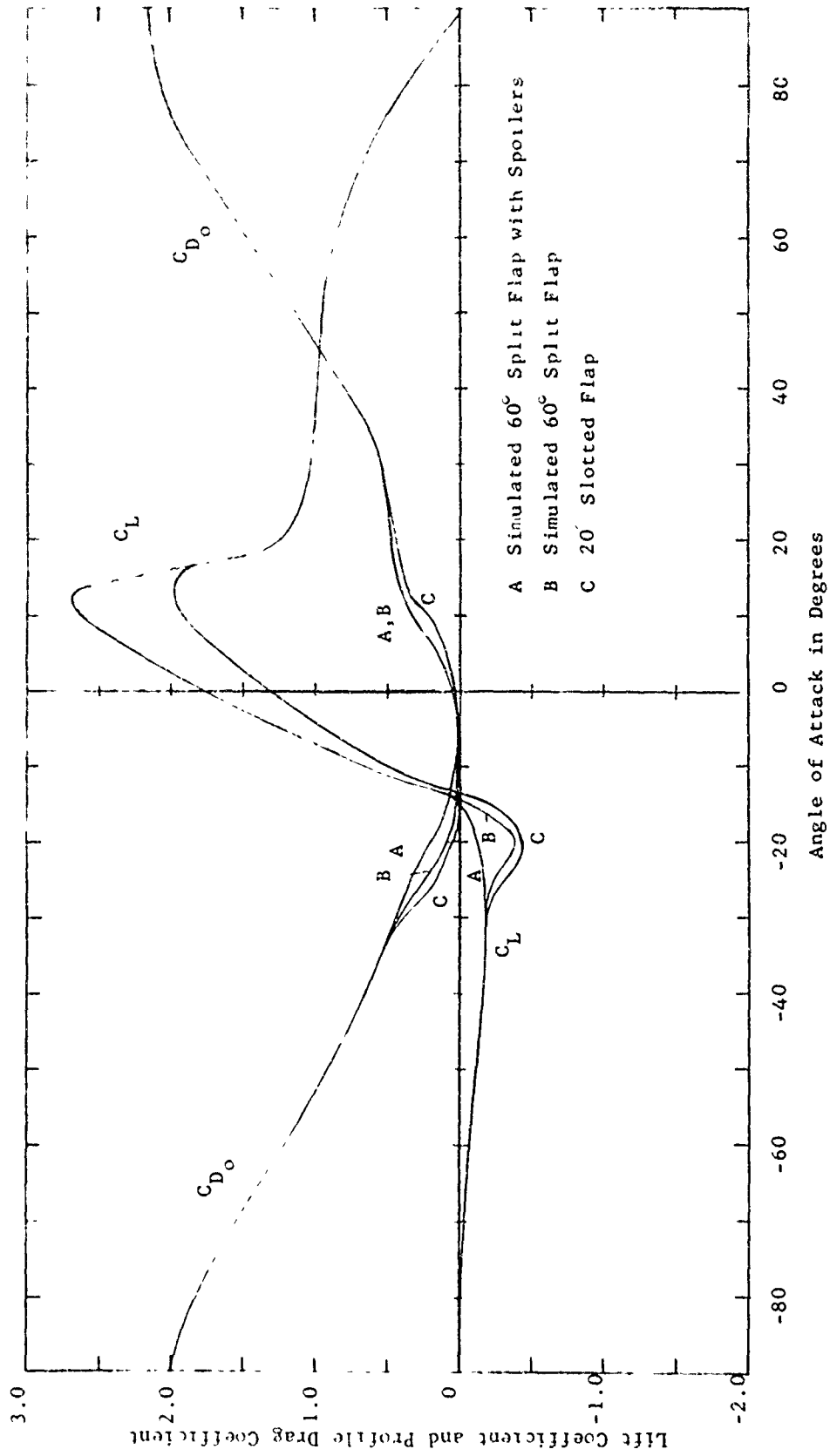


Figure 2 (Concluded)

(b) NACA 4415 Airfoil

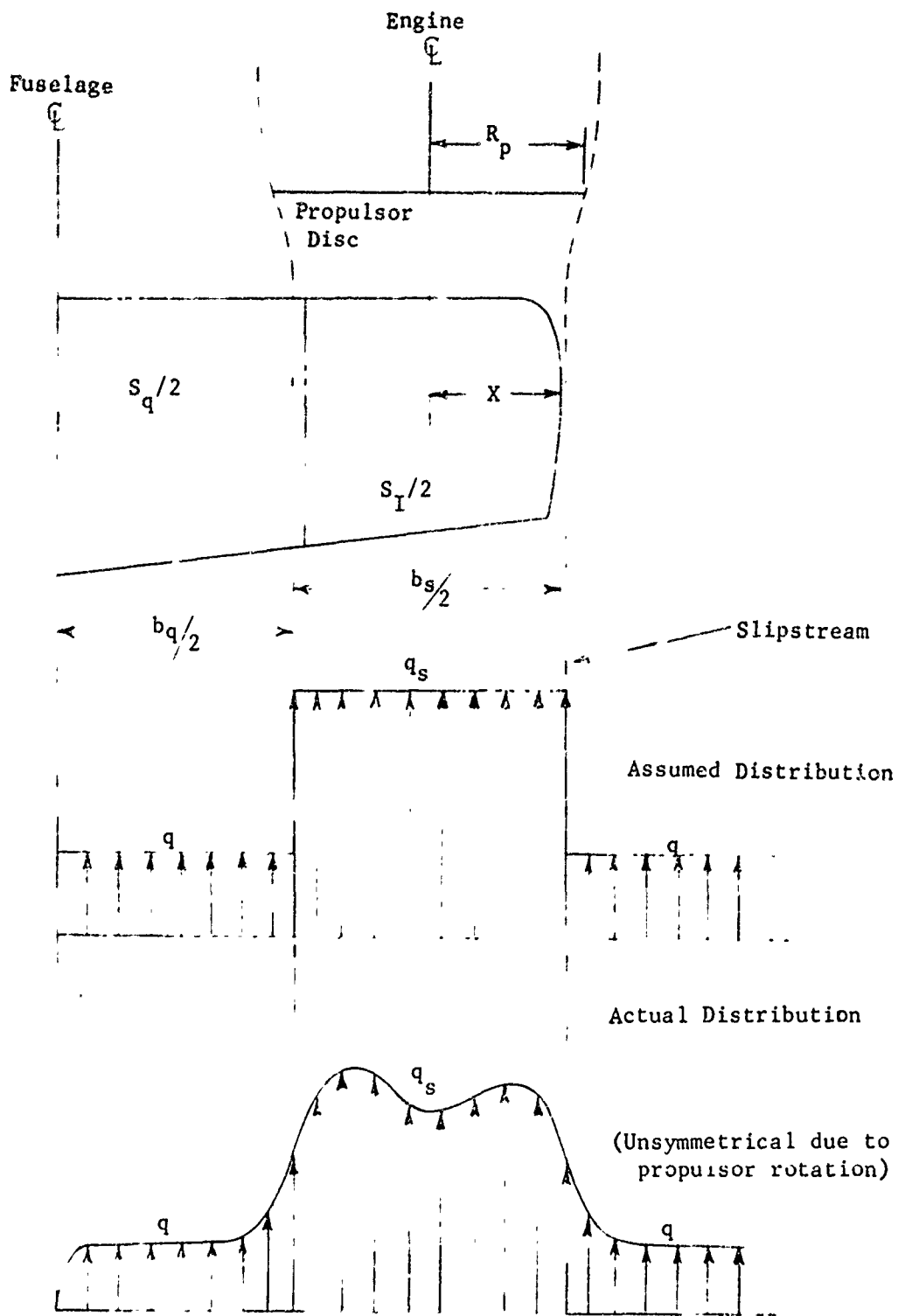


Figure 3 - Dynamic Pressure Distributions

\_\_\_\_\_ Experimental  
 - - - - -  $S_{I_C} = S_I$ , Curve A  
 - - - - -  $S_{I_C} = 1.3 S_I$ , Curve B

$THP_H = 1618.9$

$V_{s_H} = 169.6 \text{ ft/sec}$

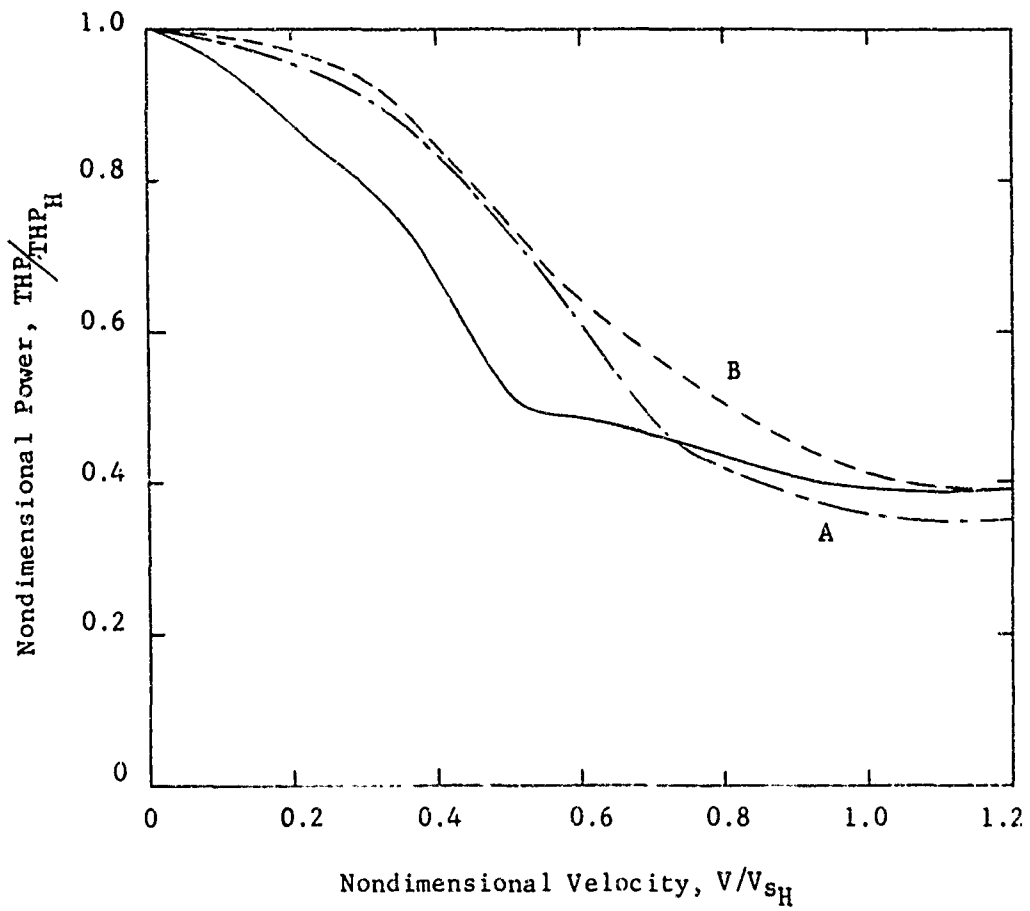


Figure 4 - Experimental and Calculated Data for Canadair CL-84

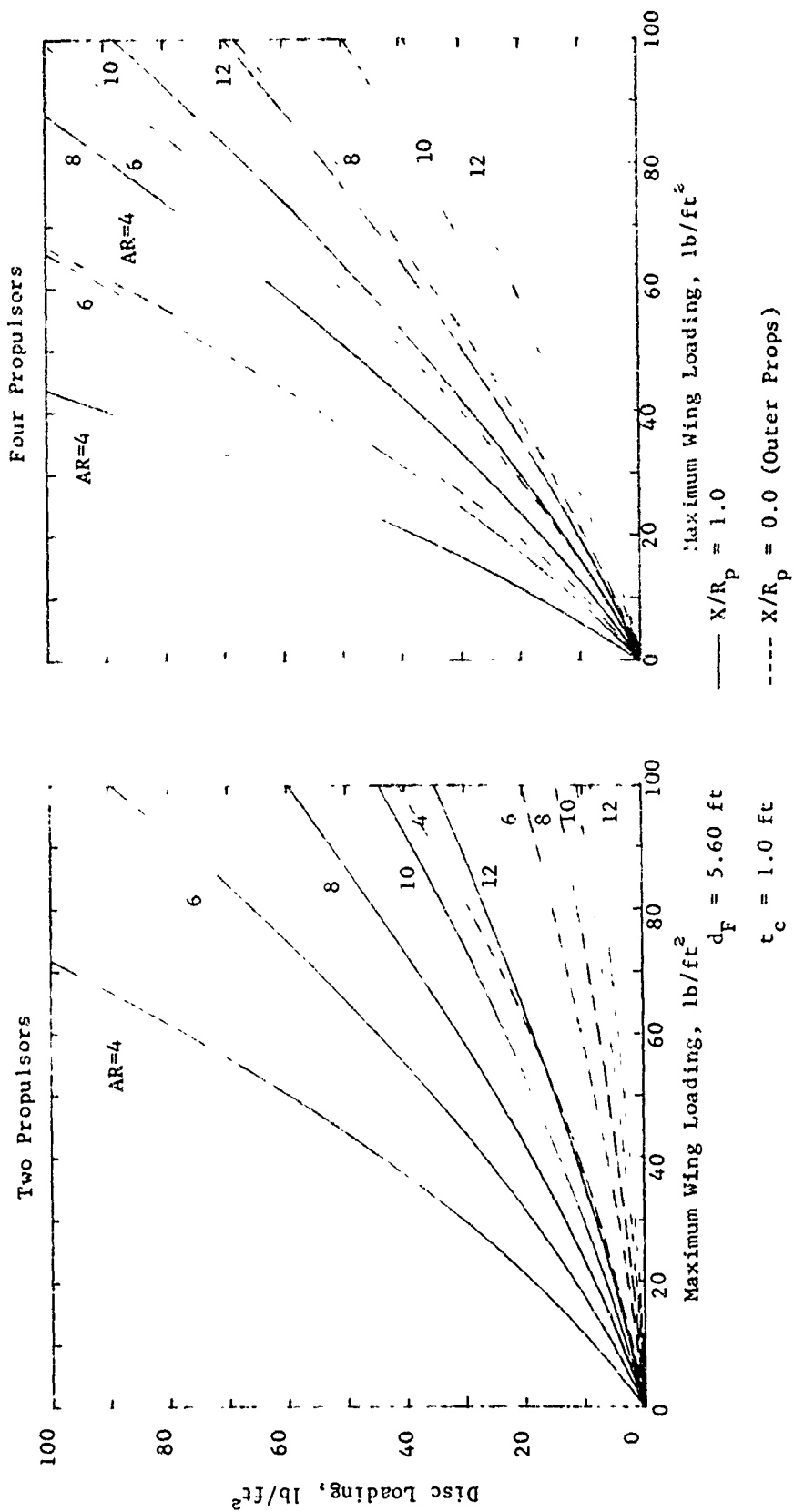


Figure 5 - Design Limitations Based on Fuselage-Propulsor Interference  
Gross Weight ~ 10,000 Pounds

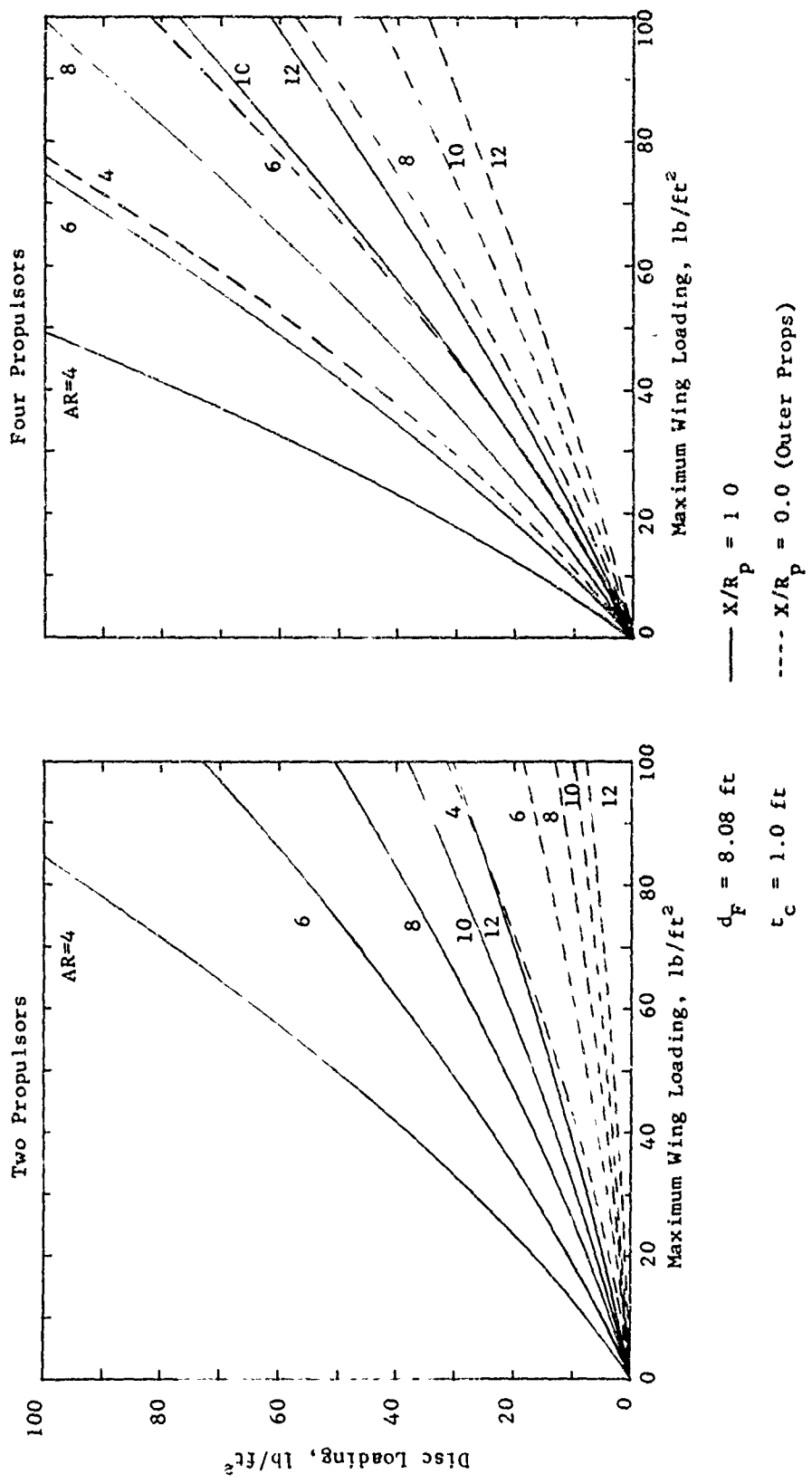


Figure 6 - Design Limitations Based on Fuselage-Propulsor Interference  
Gross Weight = 30,000 Pounds

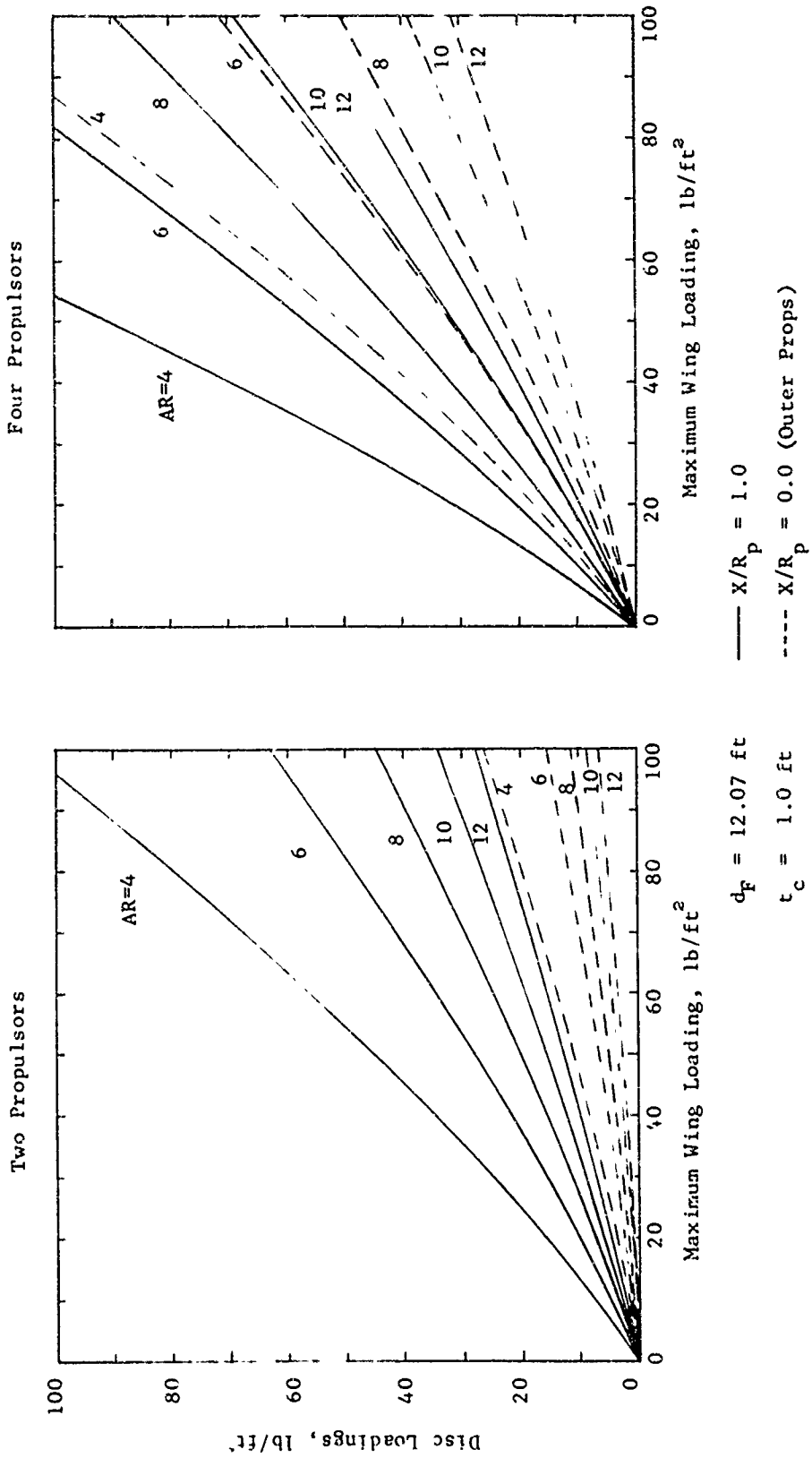


Figure 7 - Design Limitations Based on Fuselage-Propulsor Interference

Gross Weight = 100,000 Pounds

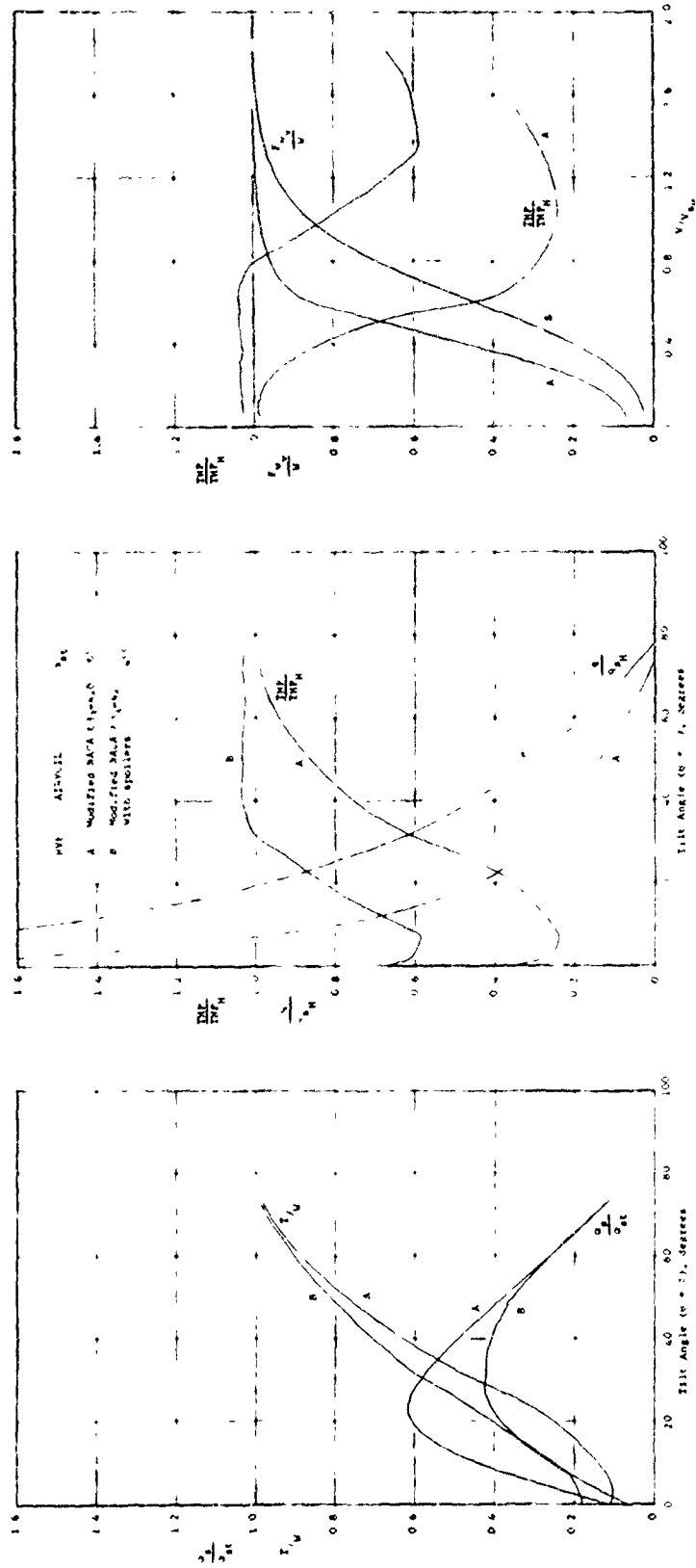


Figure 8 - Effects of Airfoil Variation on Tilt-Wing Configuration  
 (DL = 50 lb/ft<sup>2</sup> W/S = 50 lb/ft<sup>2</sup> AR = 8.0)

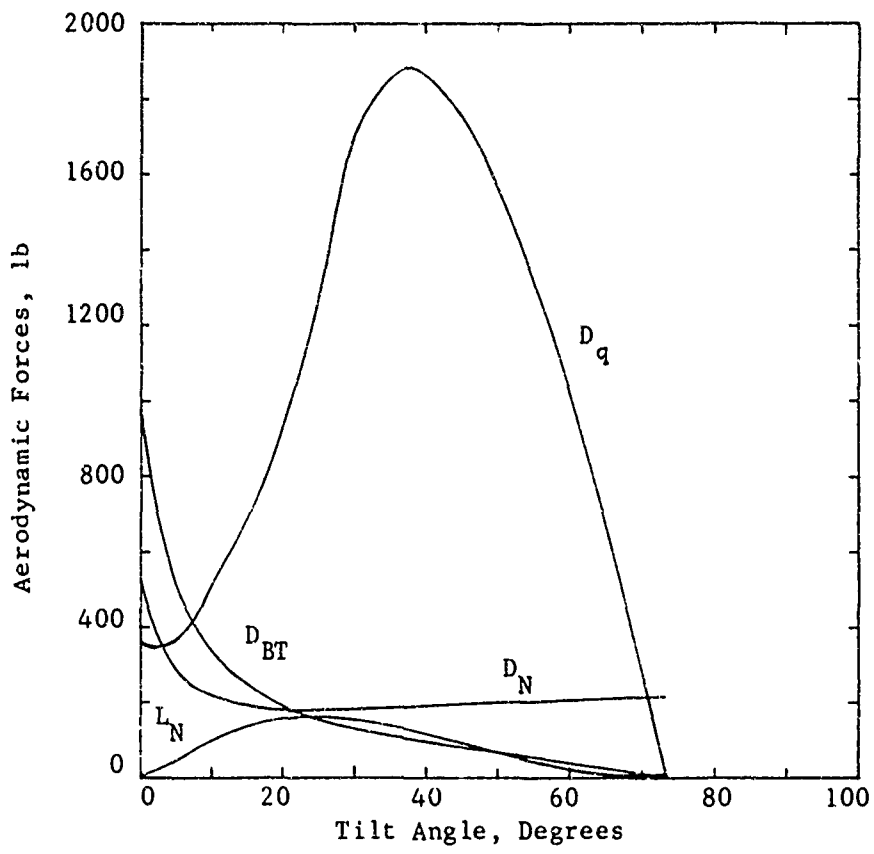
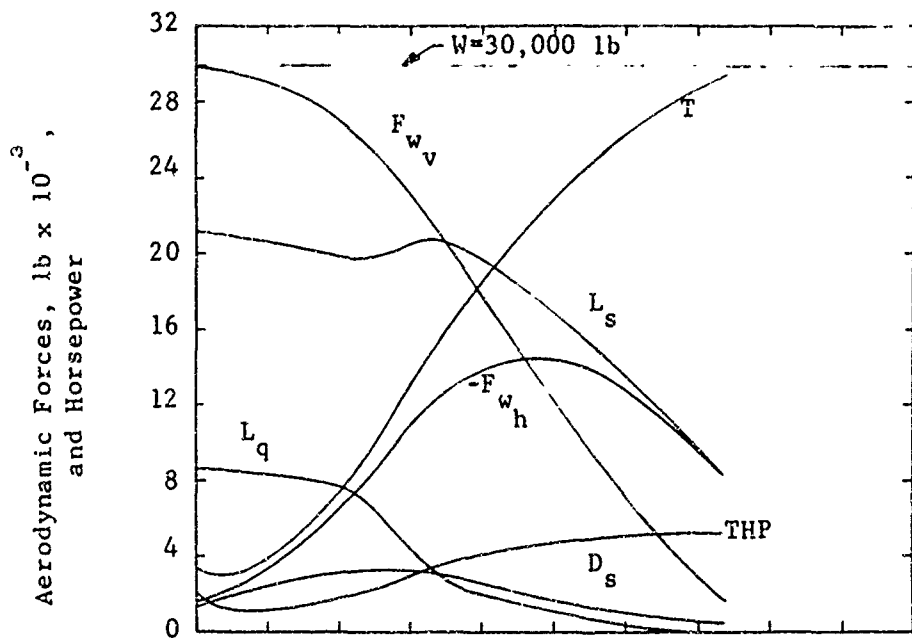


Figure 9 - Transition Data for Baseline\* Tilt-Wing Configuration  
 (a) Aerodynamic Forces and Horsepower  
 \* (see p. 13 for baseline design parameter)

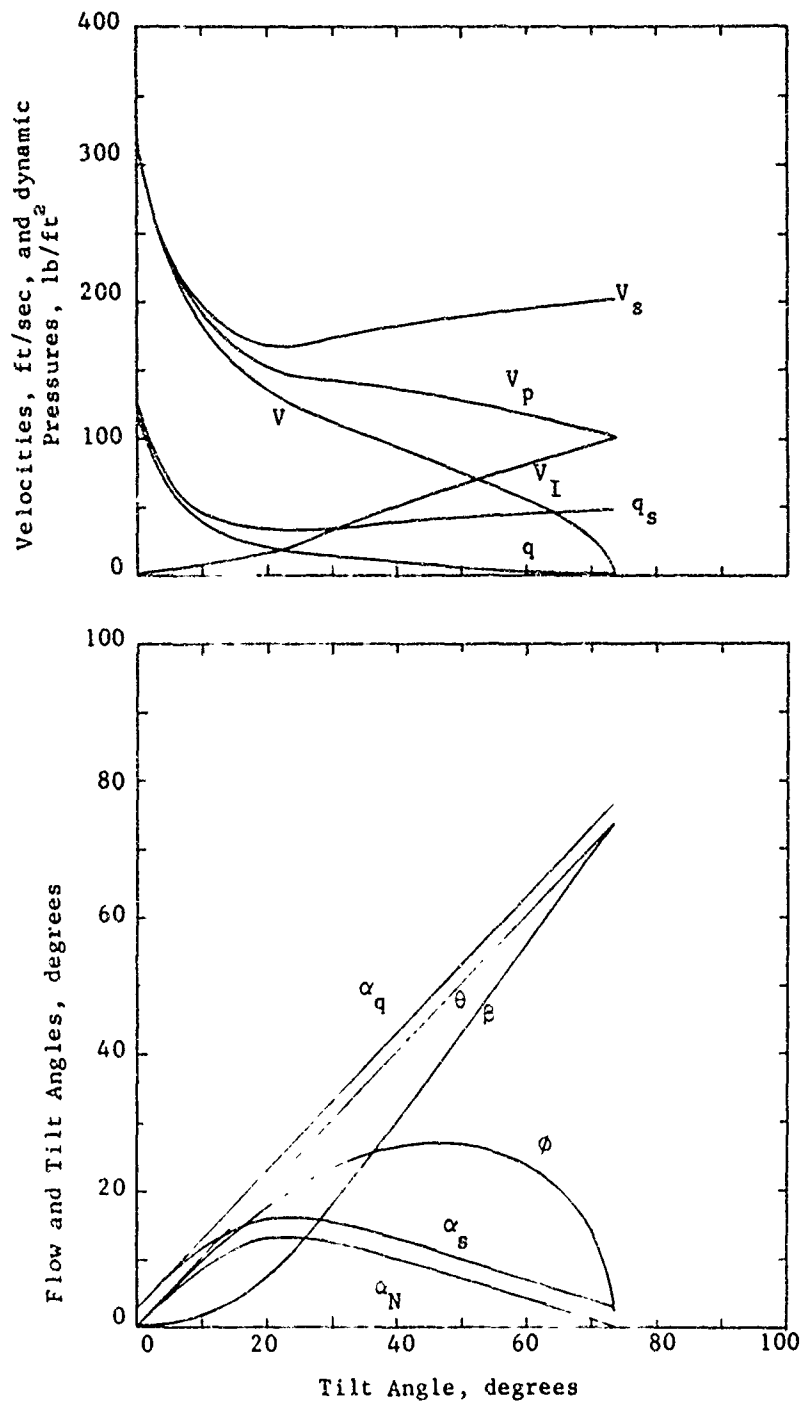


Figure 9 - (Concluded)

(b) Angles, Velocities and Dynamic Pressures

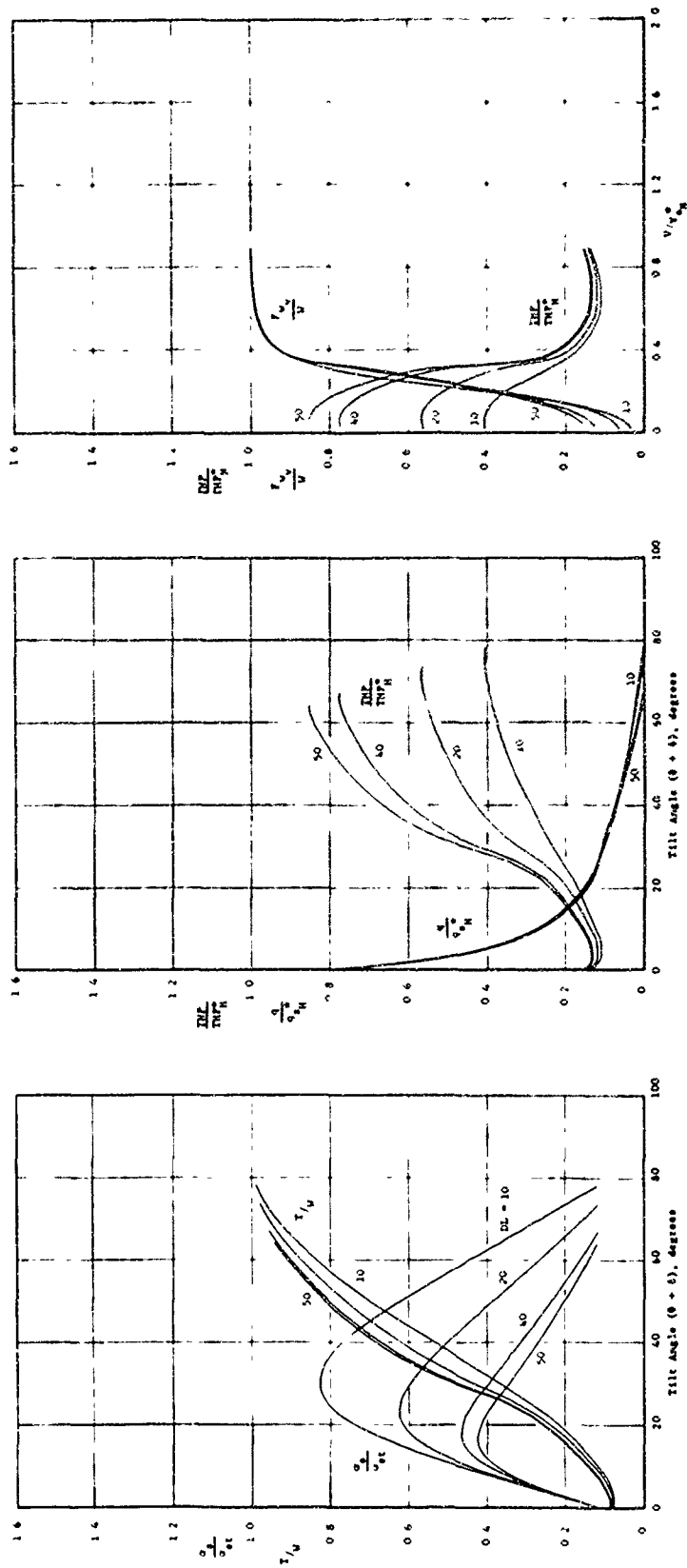


Figure 10 - Effects of Variation in Disc Loading on Baseline Tilt-Wing Configuration  
 (a) Wing Loading = 20 lb/ft<sup>2</sup>, Disc Loading = 10 → 50 lb/ft<sup>2</sup>  
 ( $q_{S_H}^* = 60$  lb/ft<sup>2</sup>)

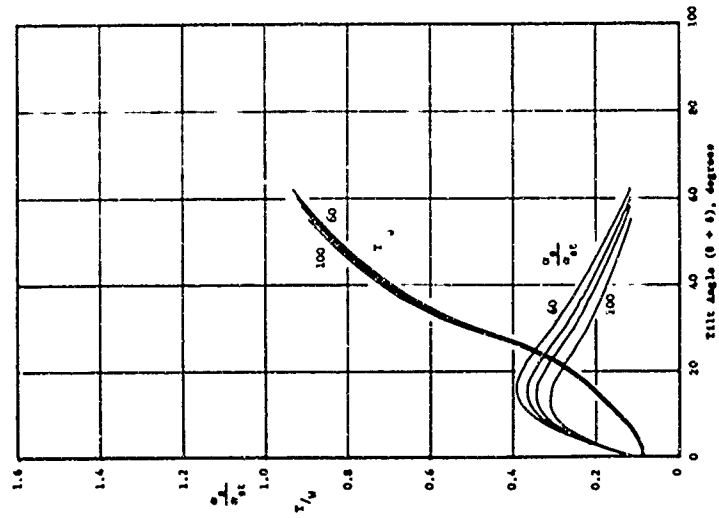
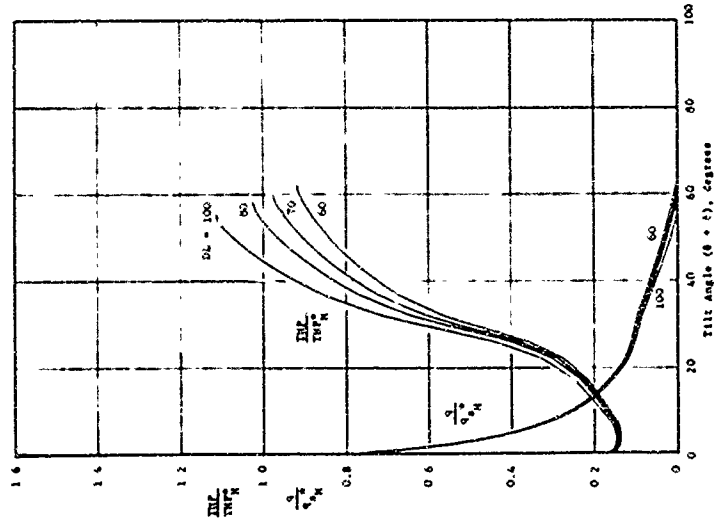
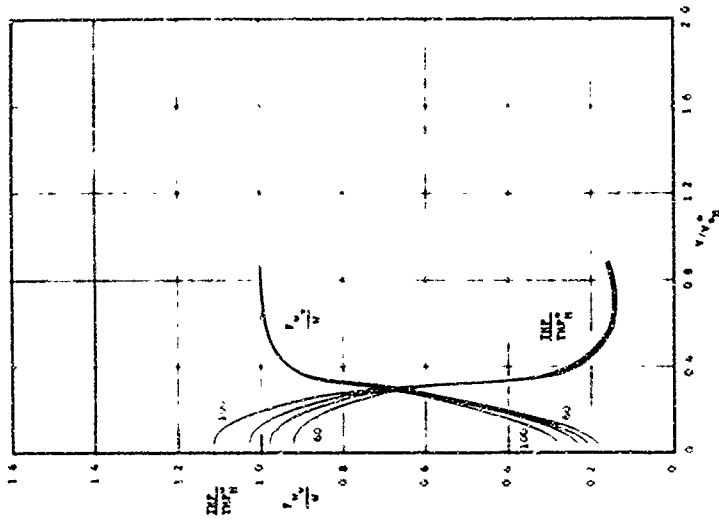


Figure 10 - (Continued)  
 (b) Wing Loading = 20 lb/ft<sup>2</sup>, Disc Loading = 60 → 100 lb/ft<sup>2</sup>  
 (q<sub>sH</sub>\* = 60 lb/ft<sup>2</sup>)

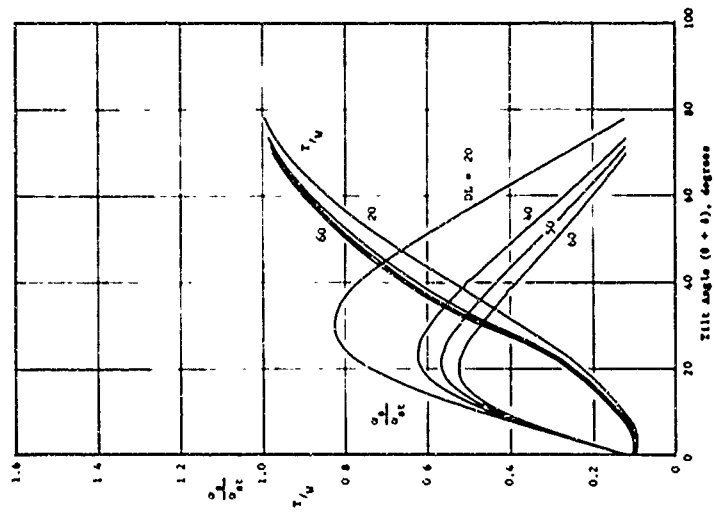
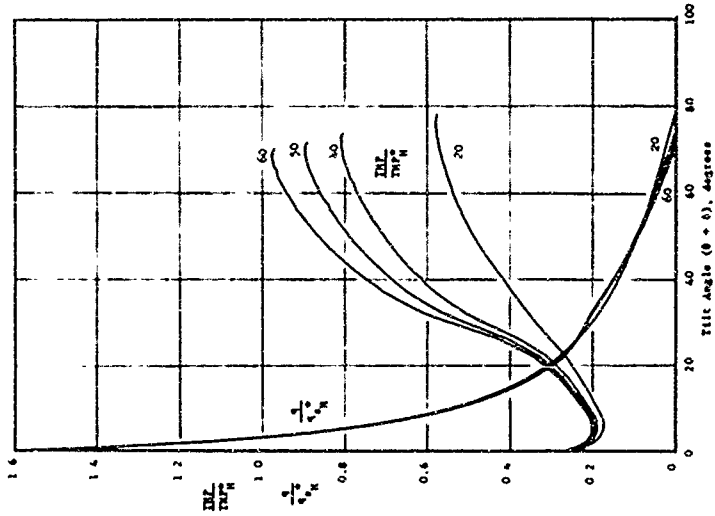
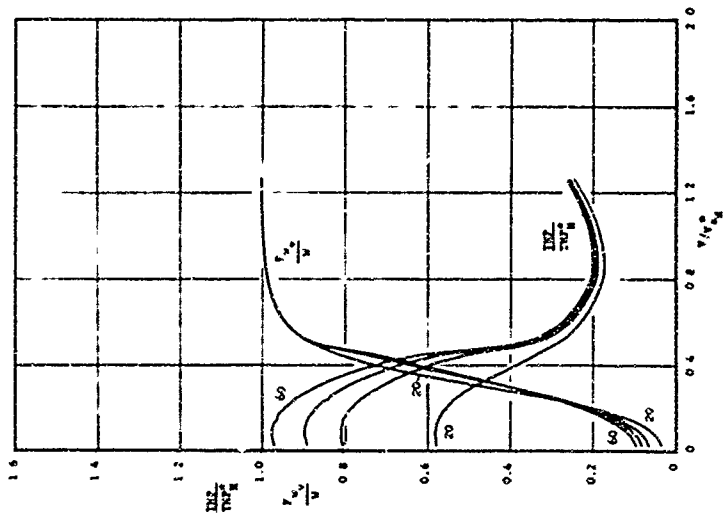


Figure 10 - (Continued)  
 (c) Wing Loading = 40 lb/ft<sup>2</sup>, Disc Loading = 20 → 60 lb/ft<sup>2</sup>  
 ( $q_{SH}^* = 60$  lb/ft<sup>2</sup>)

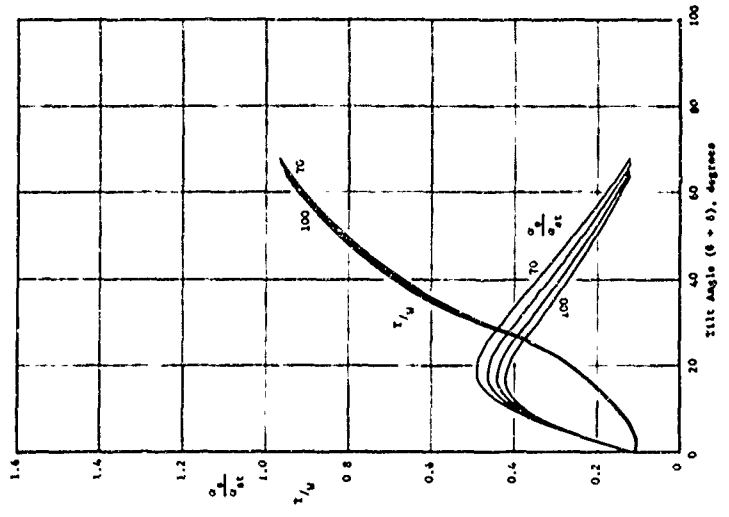
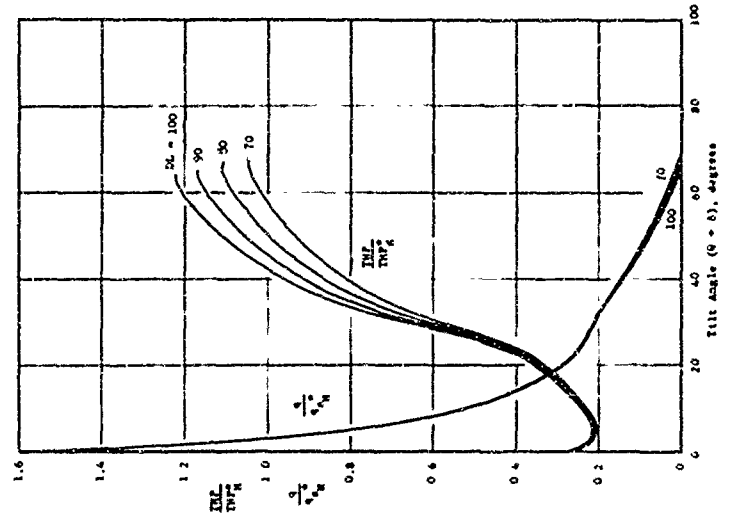
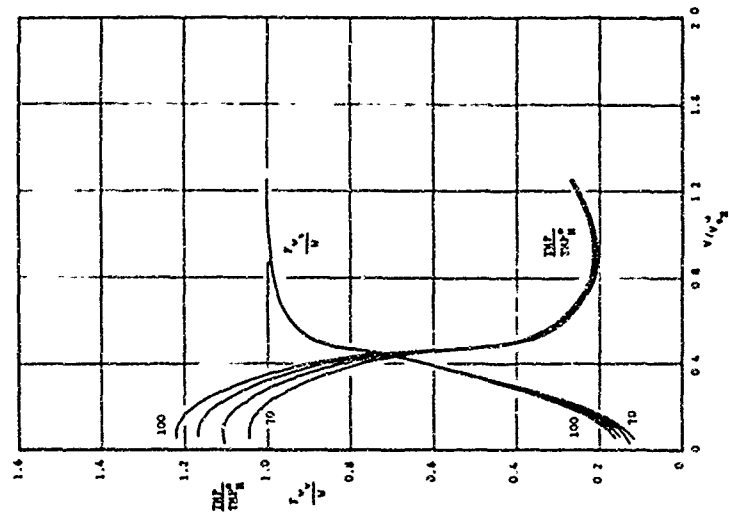


Figure 10 - (Continued)  
 (d) Wing Loading = 40 lb/ft<sup>2</sup>, Disc Loading = 70 to 100 lb/ft<sup>2</sup>  
 ( $q_{SH}^* = 60$  lb/ft<sup>2</sup>)

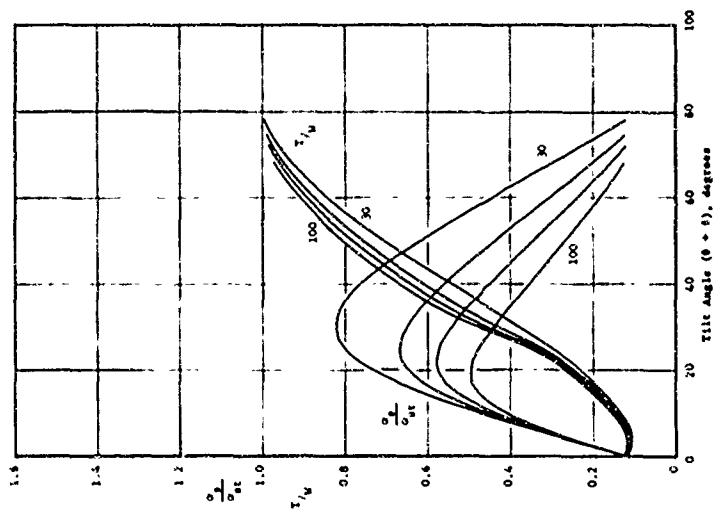
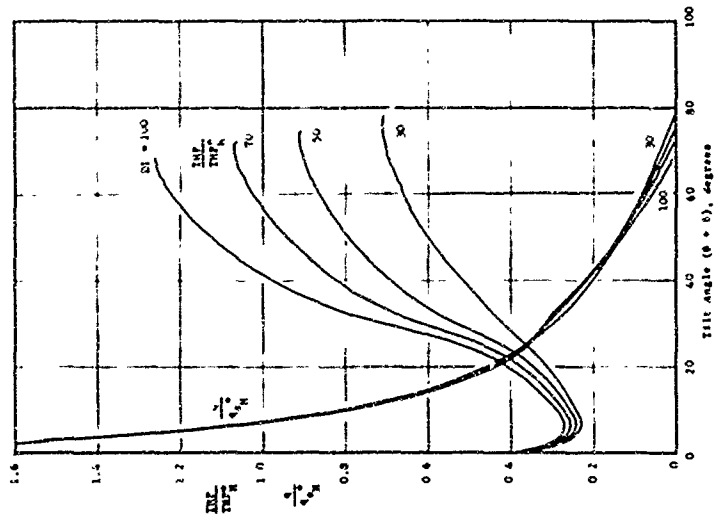
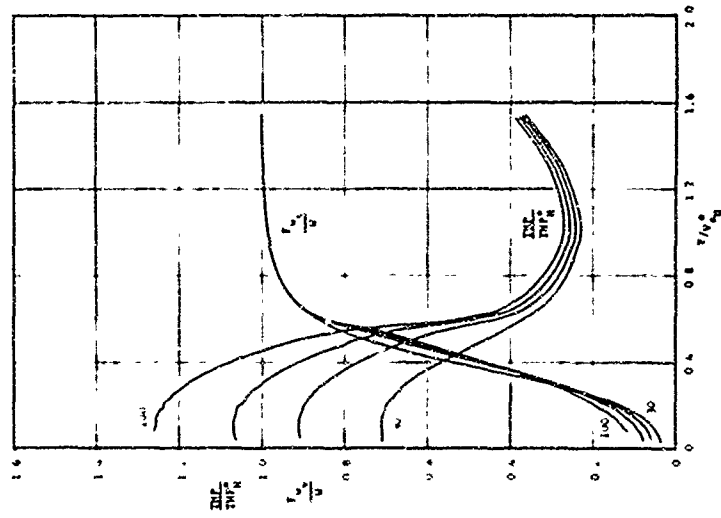


Figure 10 - (Continued)  
 (e) Wing Loading = 60 lb/ft<sup>2</sup>  
 ( $q_{SH}^* = 60 \text{ lb/ft}^2$ )

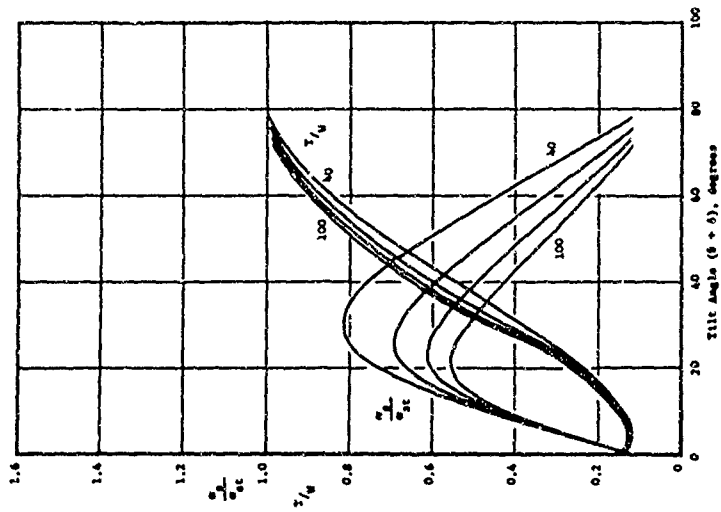
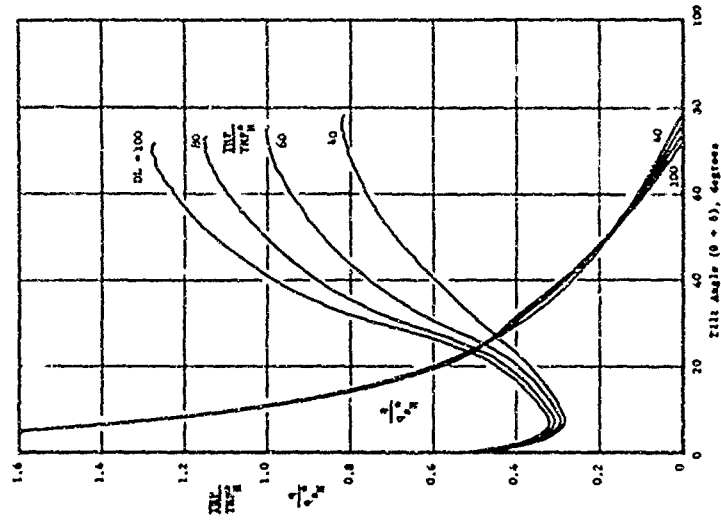
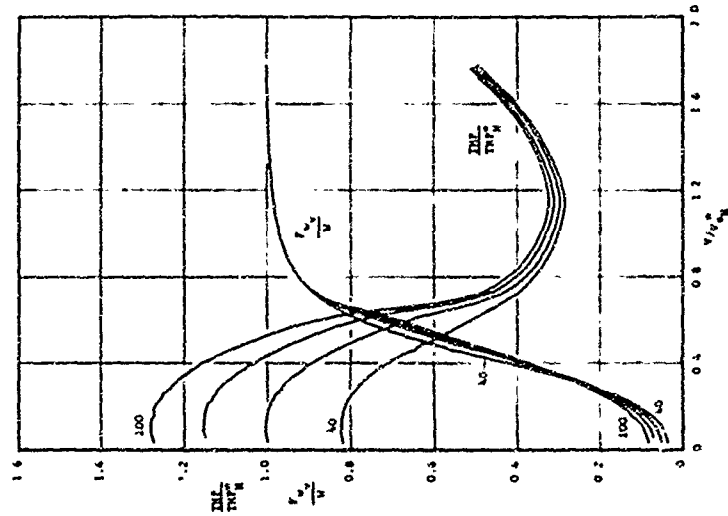


Figure 10 - (Continued)  
 (f) Wing Loading = 80 lb/ft<sup>2</sup>  
 ( $q_{SH}^* = 60$  lb/ft<sup>2</sup>)

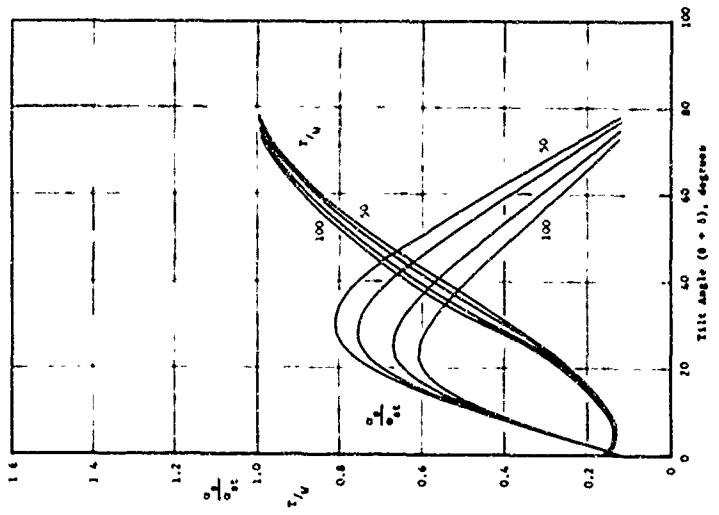
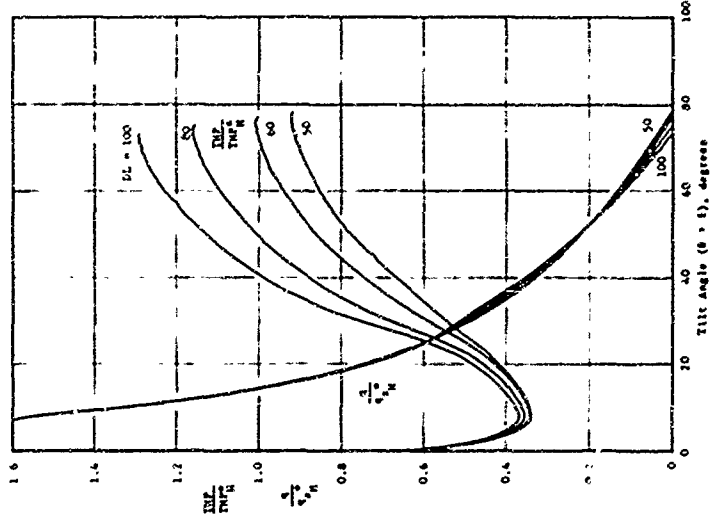
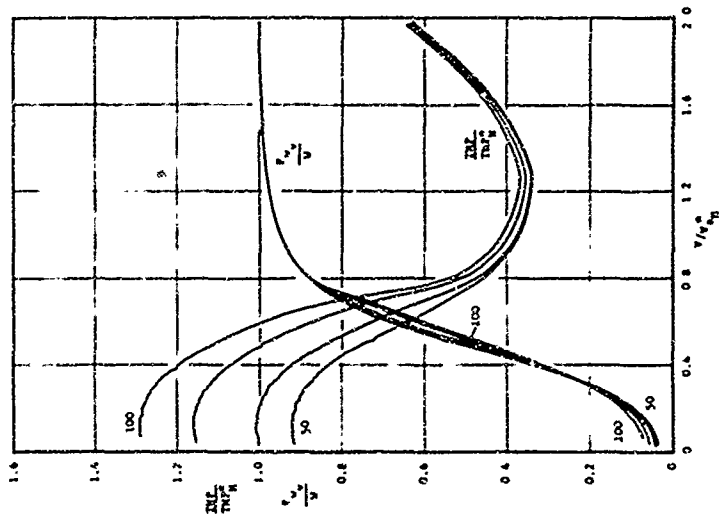
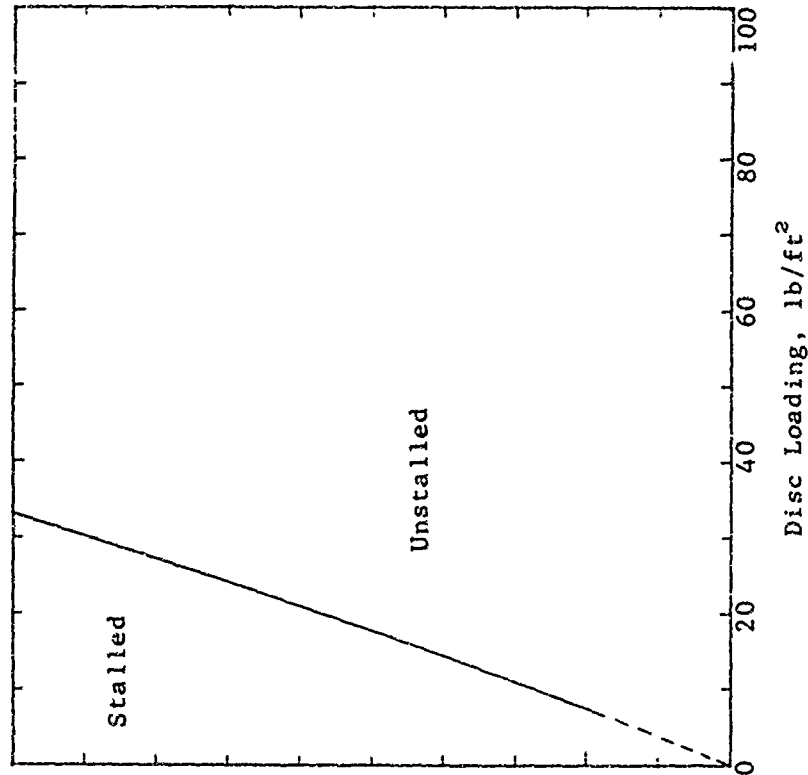
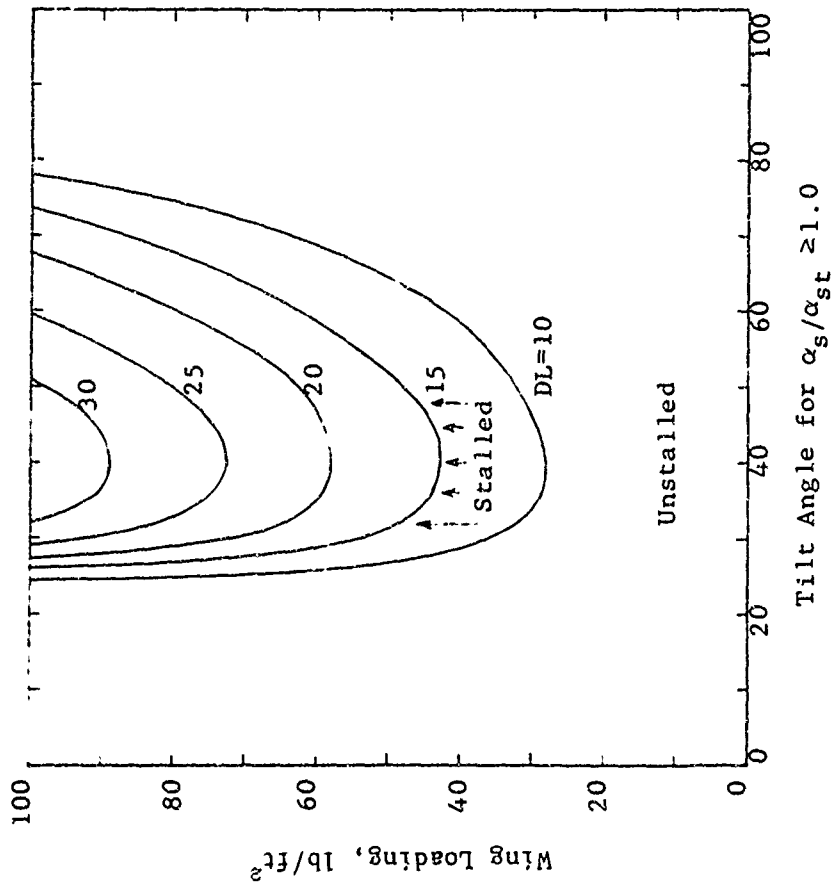


Figure 10 - (Concluded)  
 (g) Wing Loading = 100 lb/ft<sup>2</sup>  
 ( $q_{SH}^* = 60$  lb/ft<sup>2</sup>)



AR=8.0     $N_p=2$      $\delta=0$   
 $\lambda=0.9$      $\gamma=0$

Figure 11 - Effects of Low Disc Loadings on Wing Stall For Lightly Immersed Tilting Wings ( $X/R_p = 0.0$ )

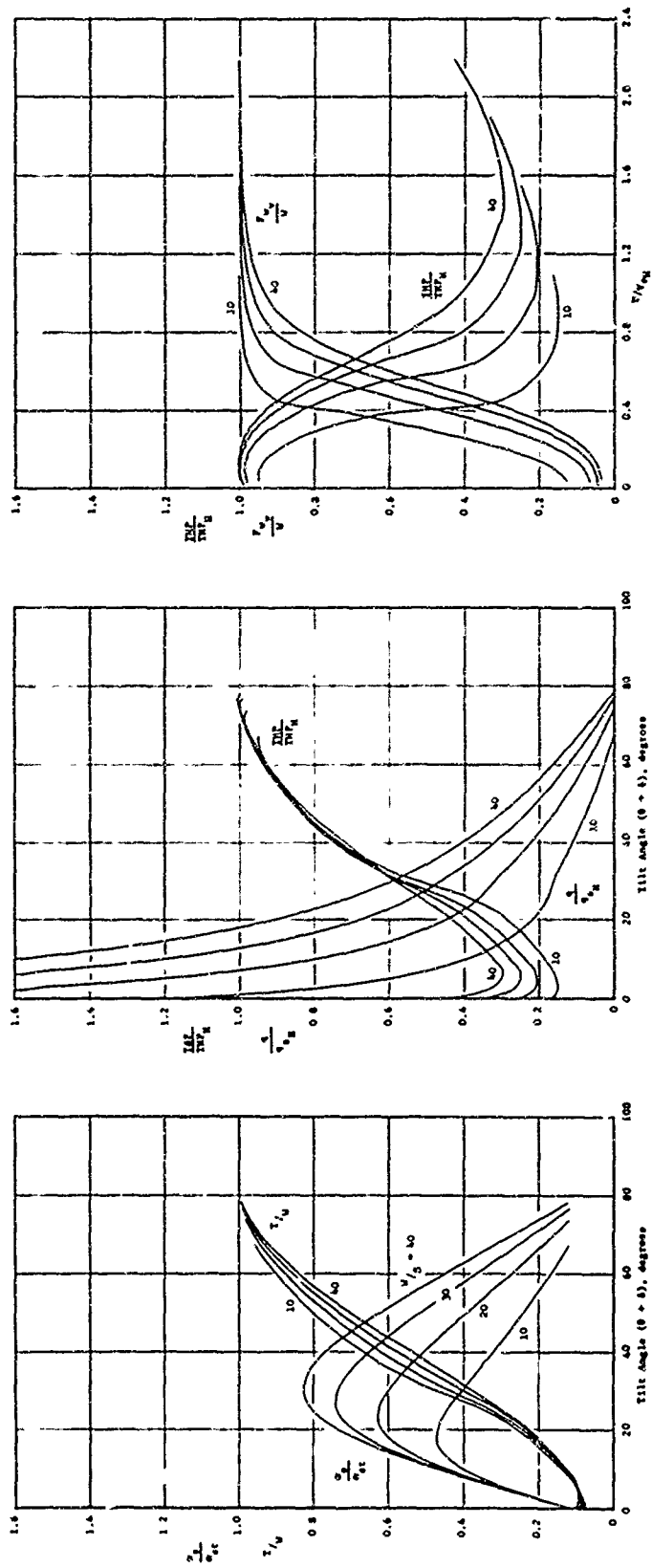


Figure 12 - Effects of Variation in Wing Loading on Baseline Tilt-Wing Configuration  
 (a) Disc Loading = 20 lb/ft<sup>2</sup>

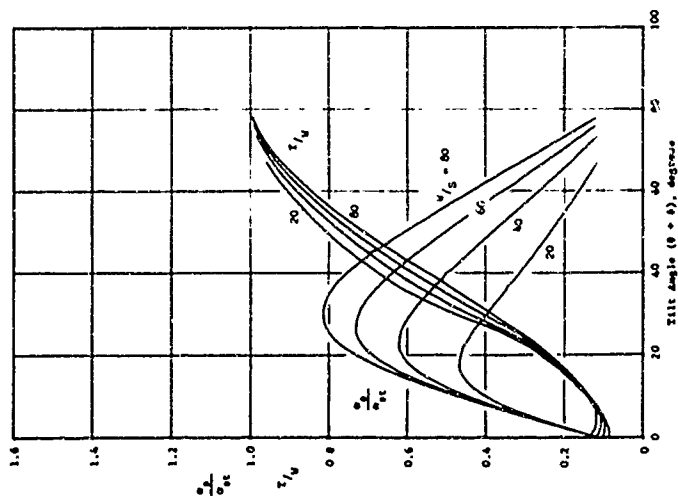
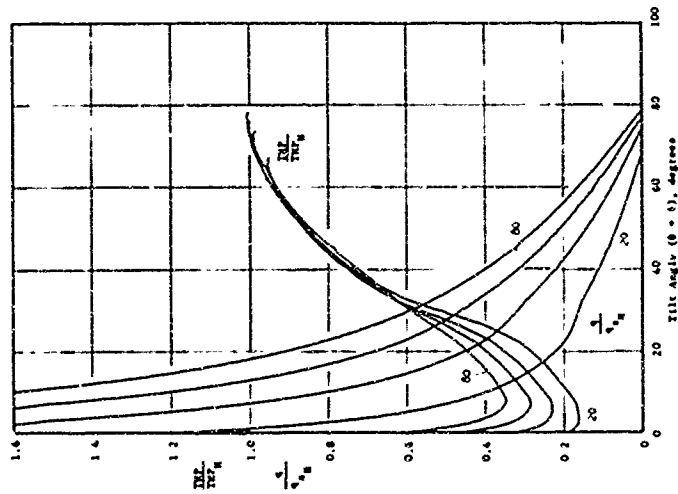
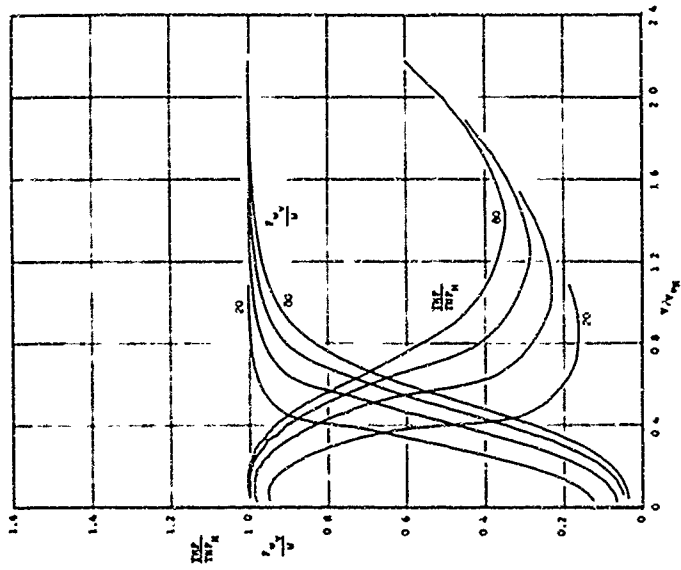


Figure 12 - (Continued)  
 (b) Disc Loading = 40 lb/ft<sup>2</sup>

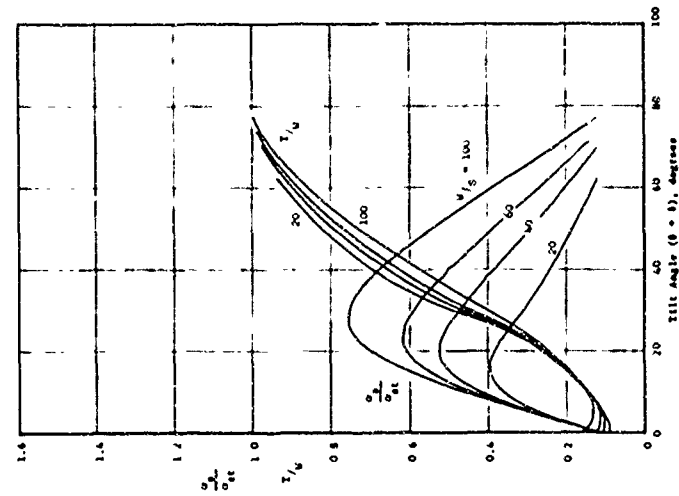
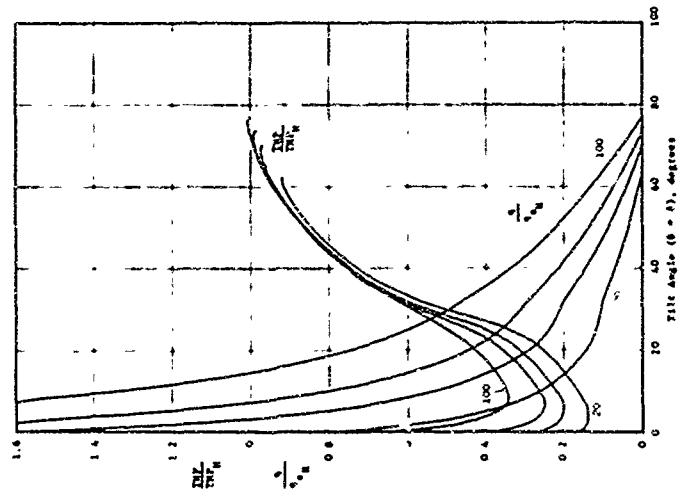
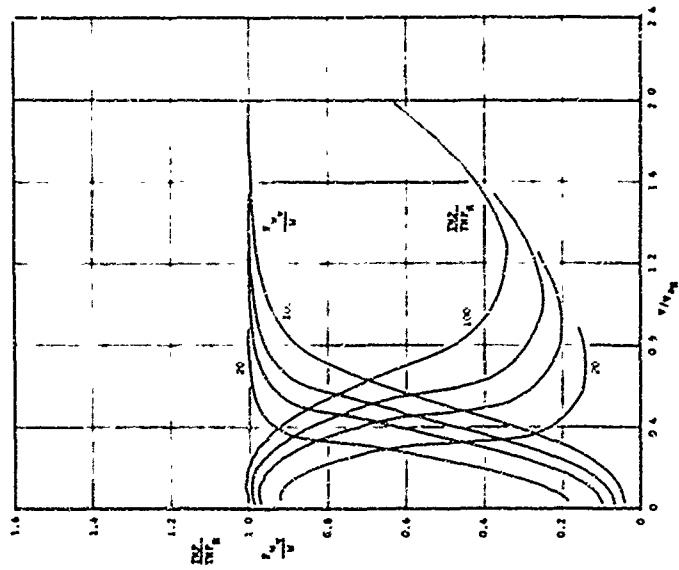


Figure 12 - (Continued)  
 (c) Disc Loading = 60 lb/ft<sup>2</sup>

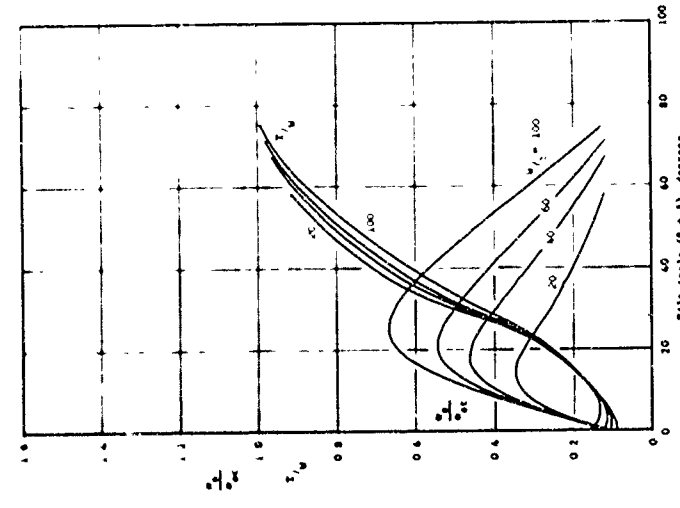
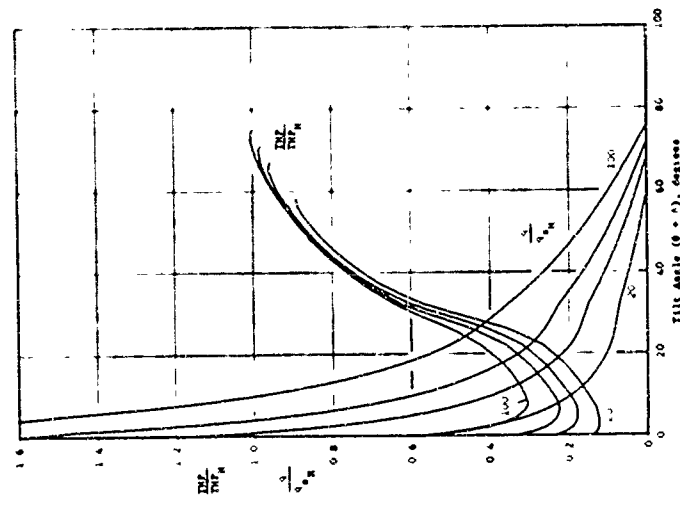
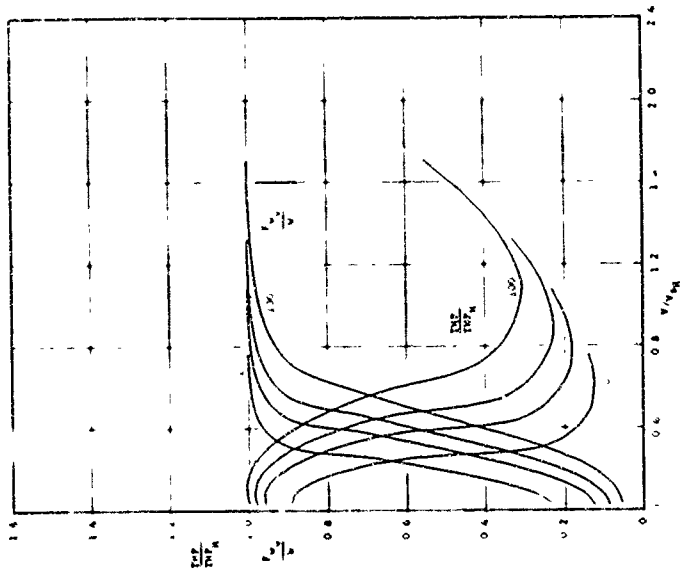


Figure 12 - (Continued)  
 (d) Disc Loading = 80 lb/ft<sup>2</sup>

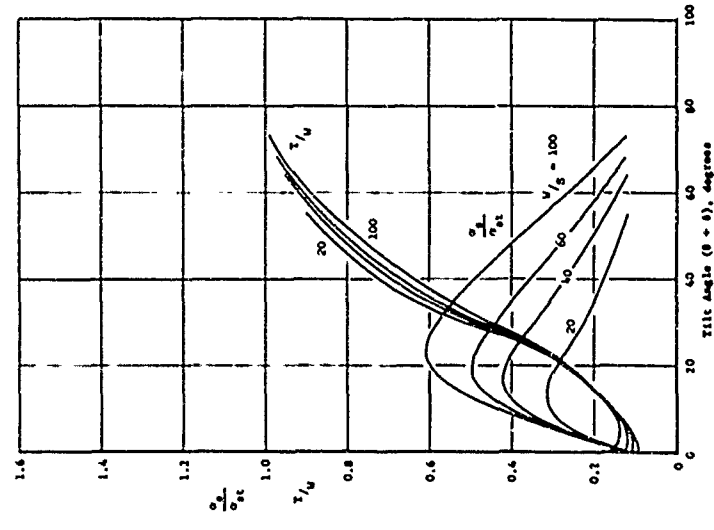
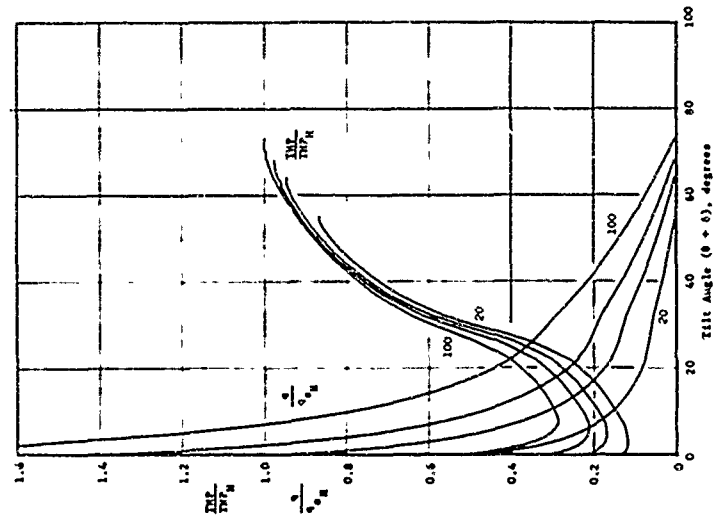
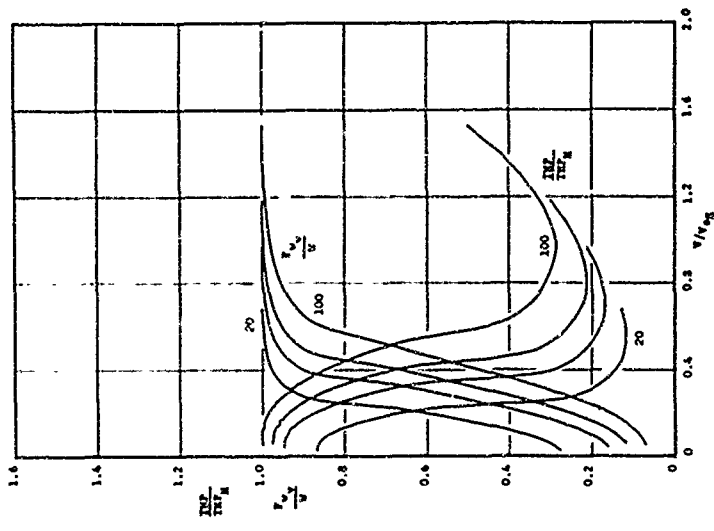


Figure 12 - (Concluded)  
 (e) Disc Loading = 100 lb/ft<sup>2</sup>

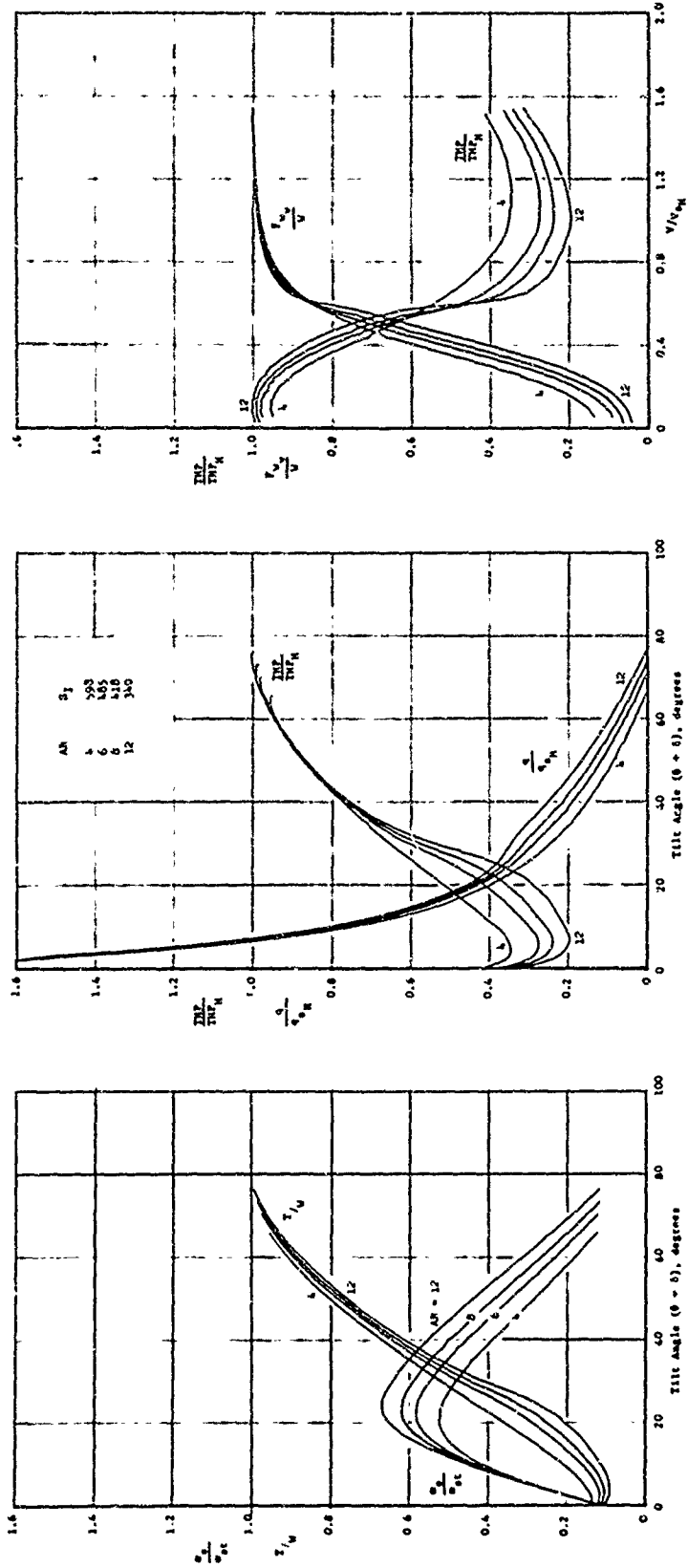


Figure 13 - Effects of Variation in Aspect Ratio on Baseline Tilt-Wing Configuration

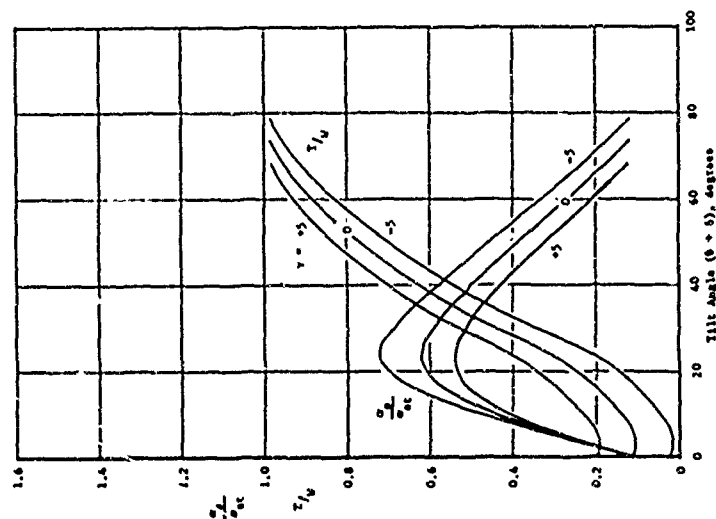
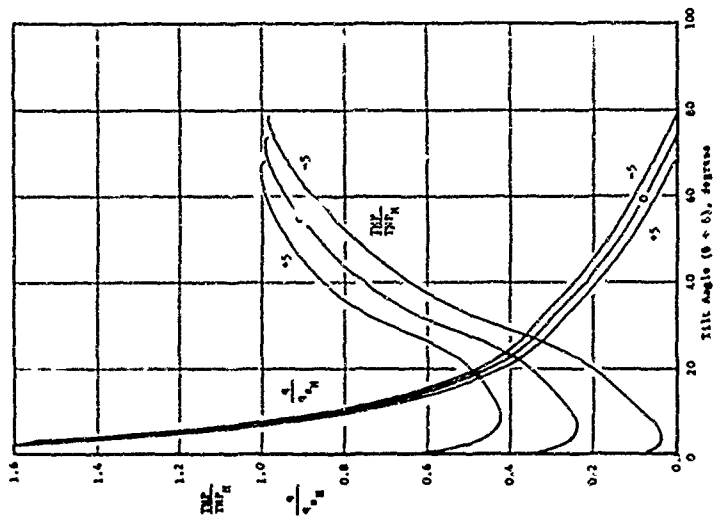
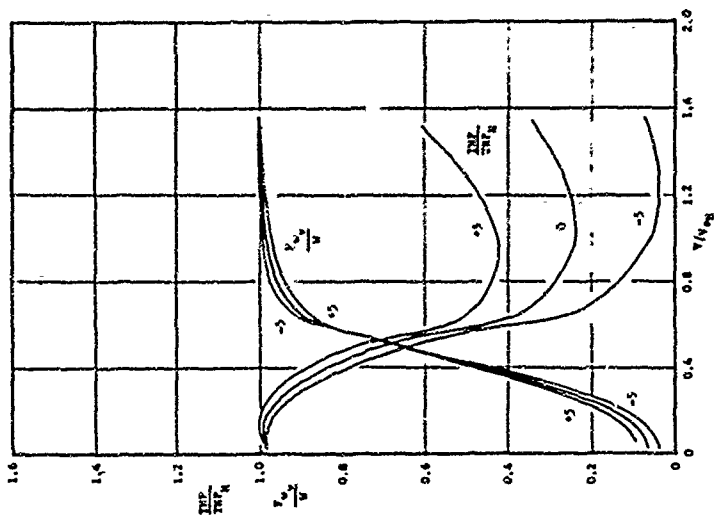


Figure 14 - Effects of Variation in Flight Path Angle on Baseline Tilt-Wing Configuration

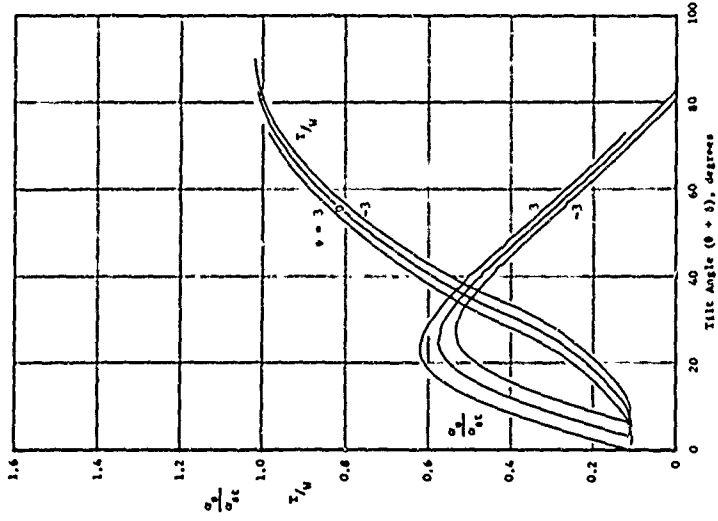
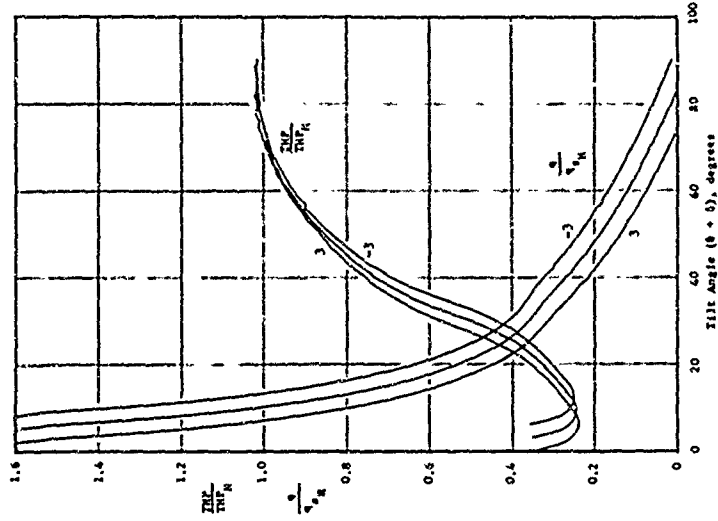
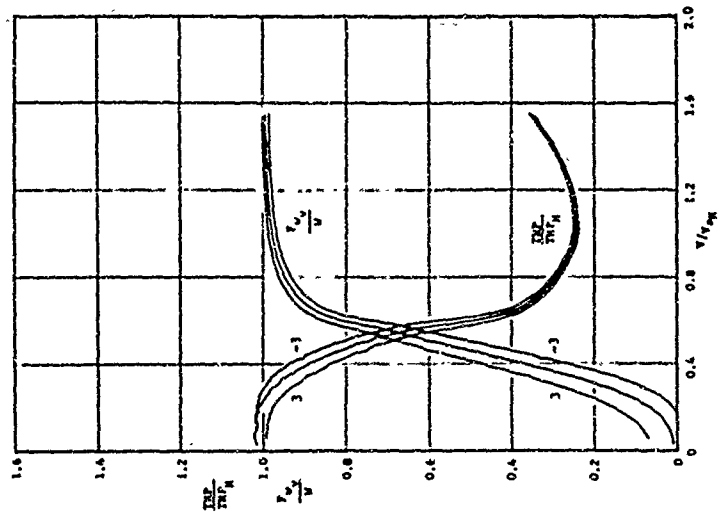


Figure 15 - Effects of Variation in Thrust Offset Angle on Baseline  
Tilt-Wing Configuration

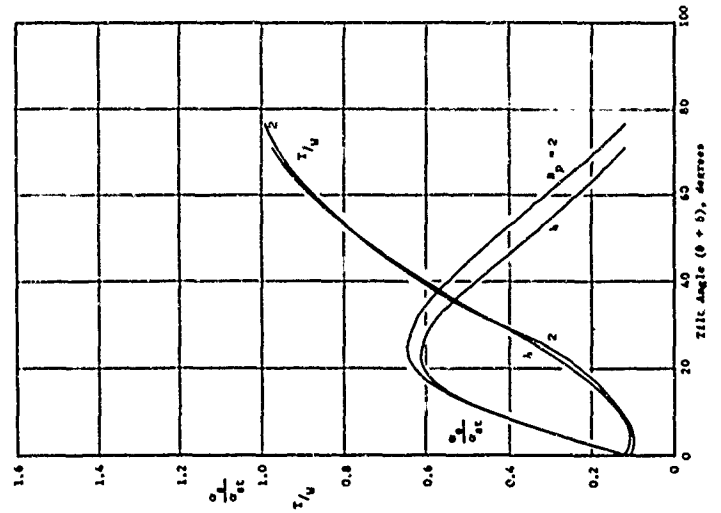
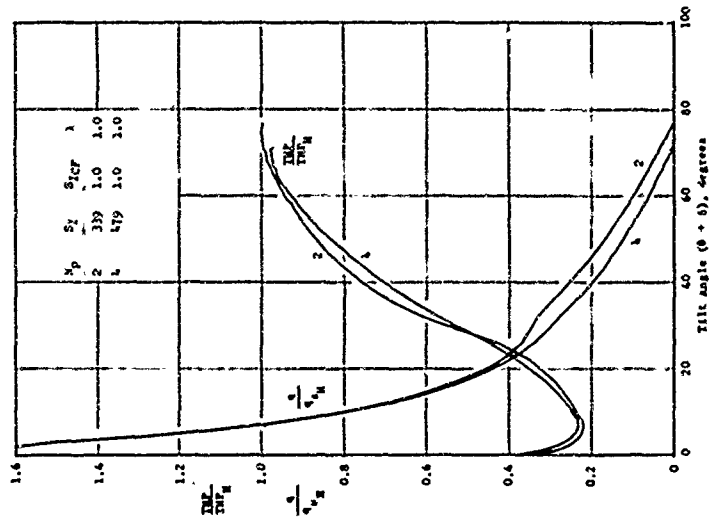
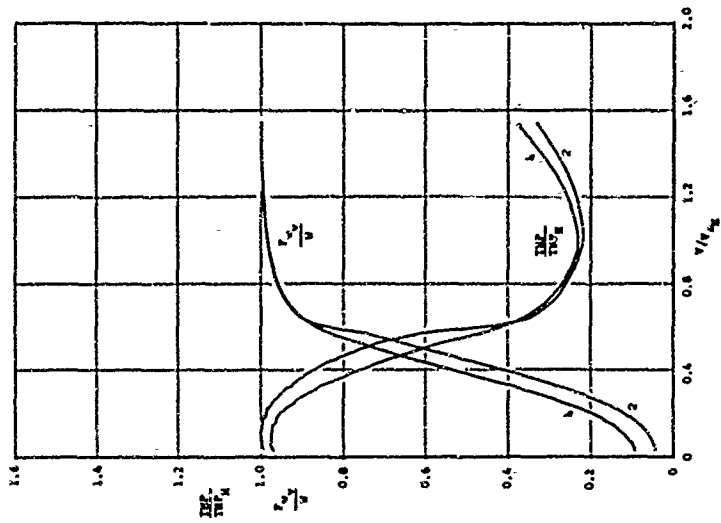


Figure 16 - Effects of Variation in Number of Engines on Baseline Tilt-Wing Configuration

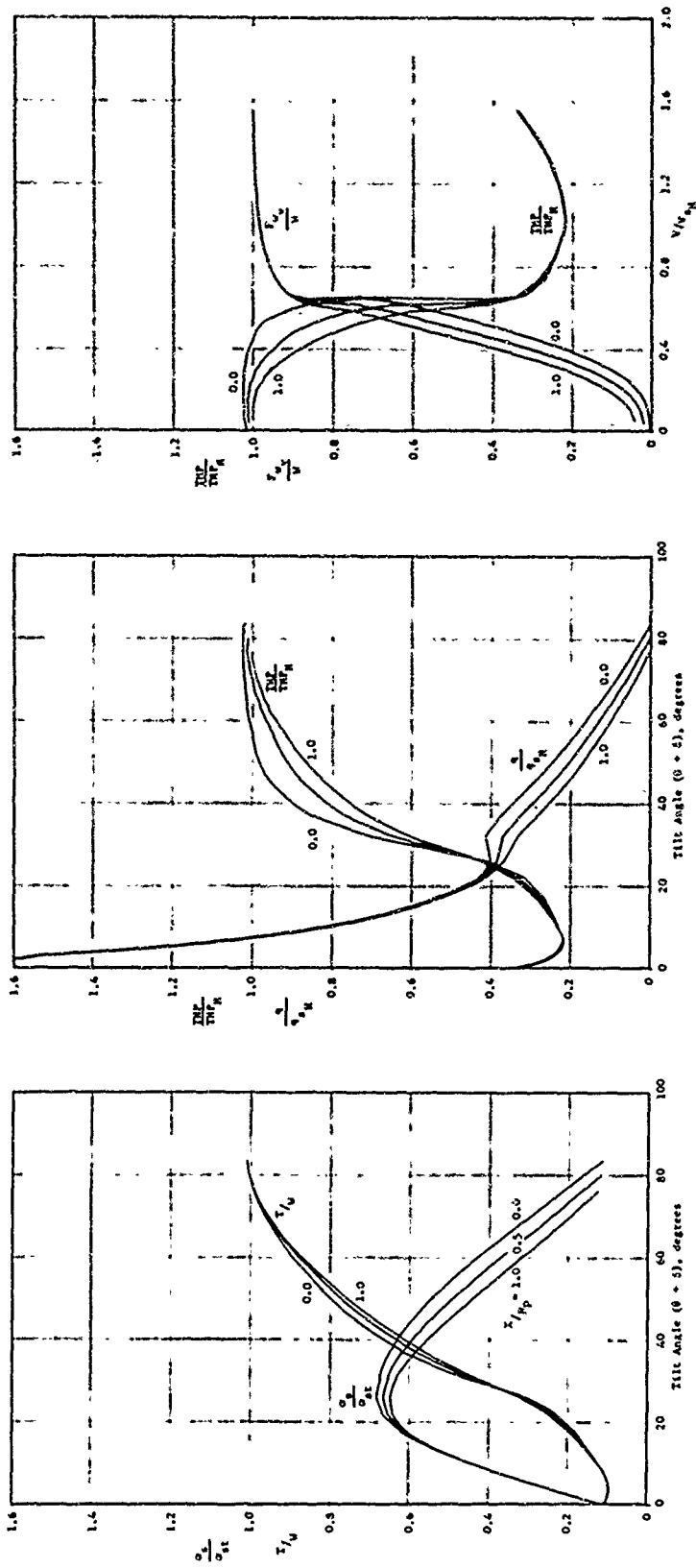


Figure 17 - Effects of Variation in Spanwise Engine Location on Baseline Tilt-Wing Configuration

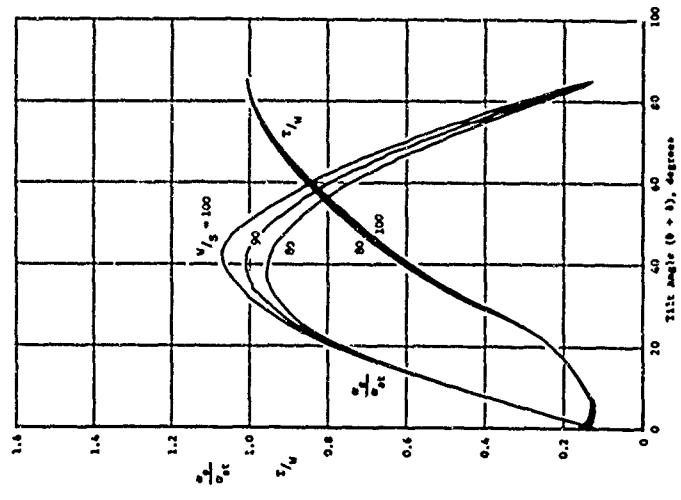
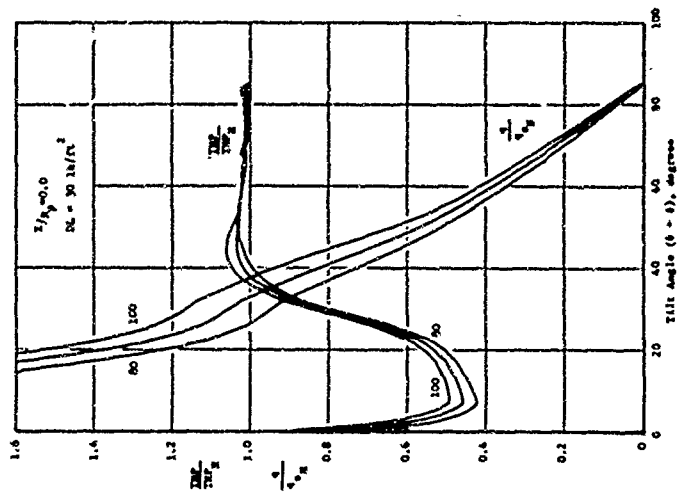
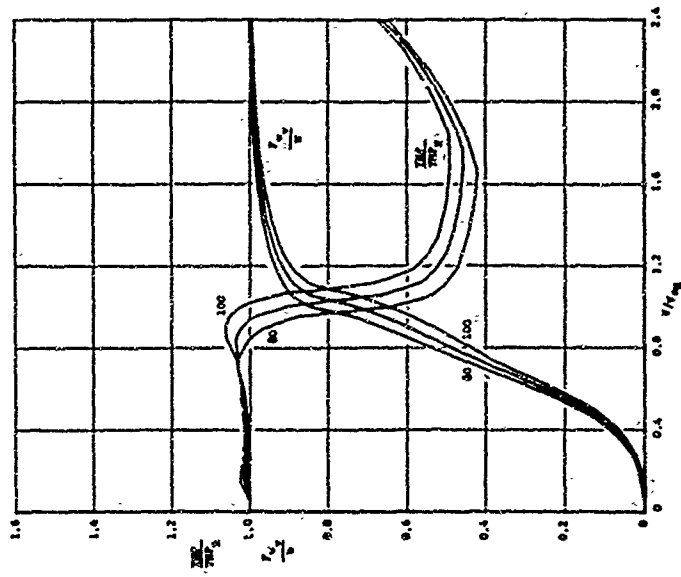


Figure 18 - Effects of Reduced Wing Immersion and High Wing Loading on Baseline Tilt-Wing Configuration

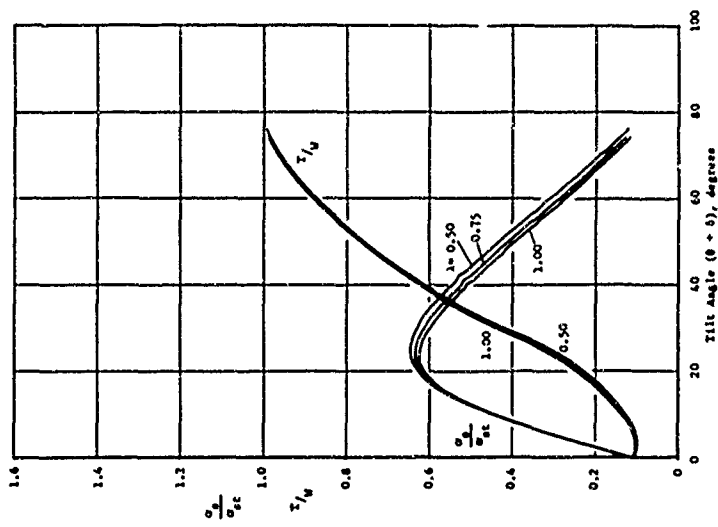
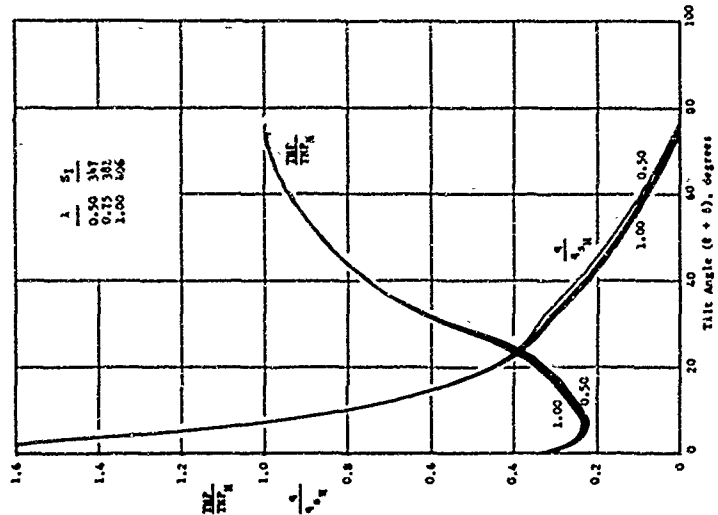
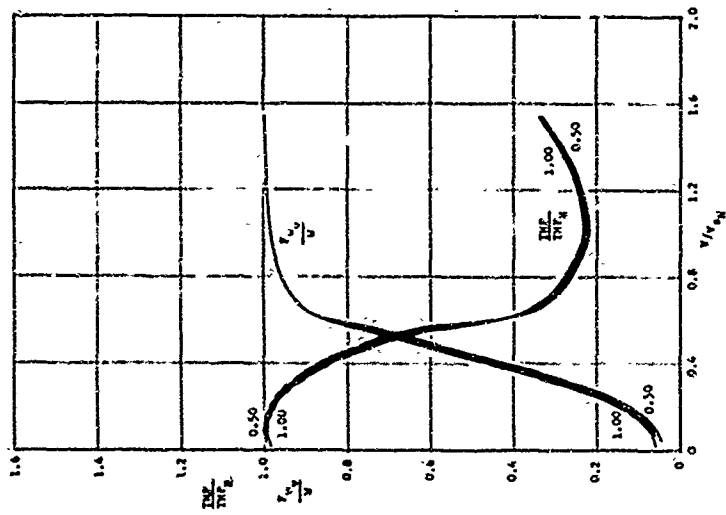


Figure 19 - Effects of Variation in Taper Ratio on Baseline Tilt-Wing Configuration

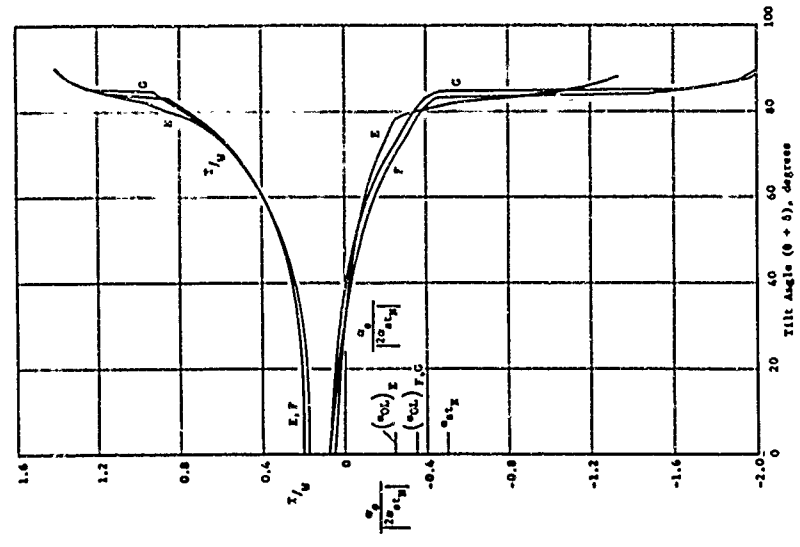
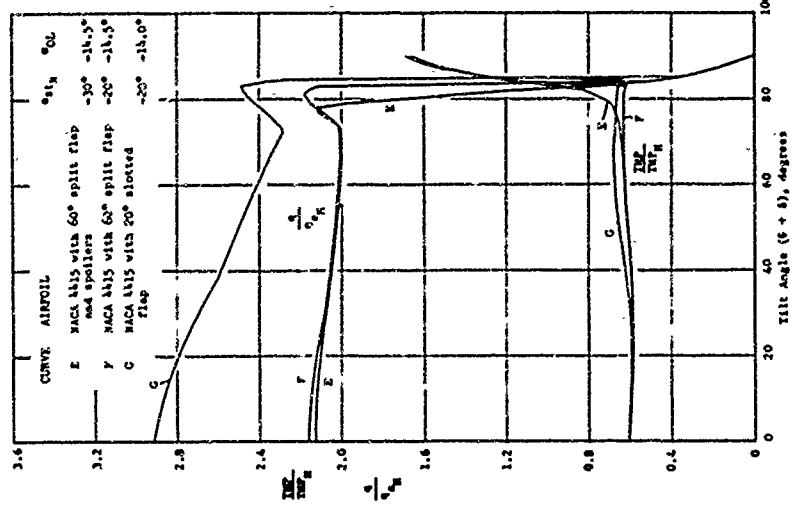
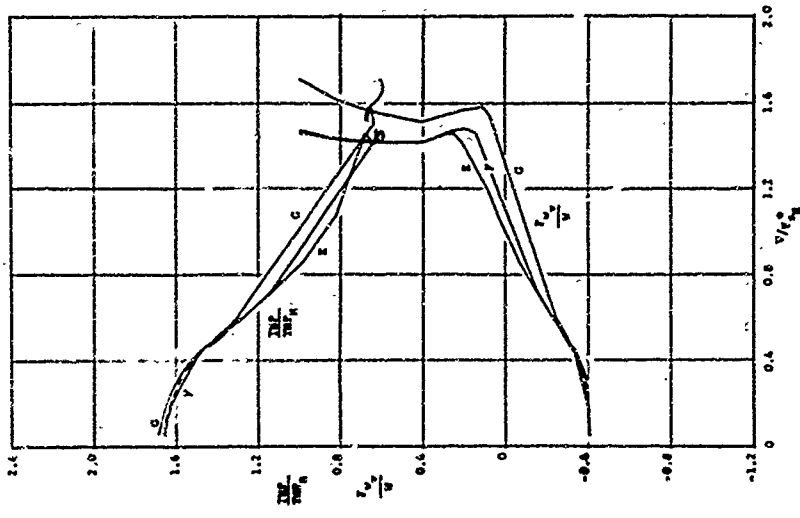


Figure 20 - Effects of Airfoil Variation on Tilt-Rotor Configuration  
 (DL = 15 lb/ft<sup>2</sup>, W/S = 70 lb/ft<sup>2</sup>, AR = 8.0,  $\delta = 0^\circ$ )

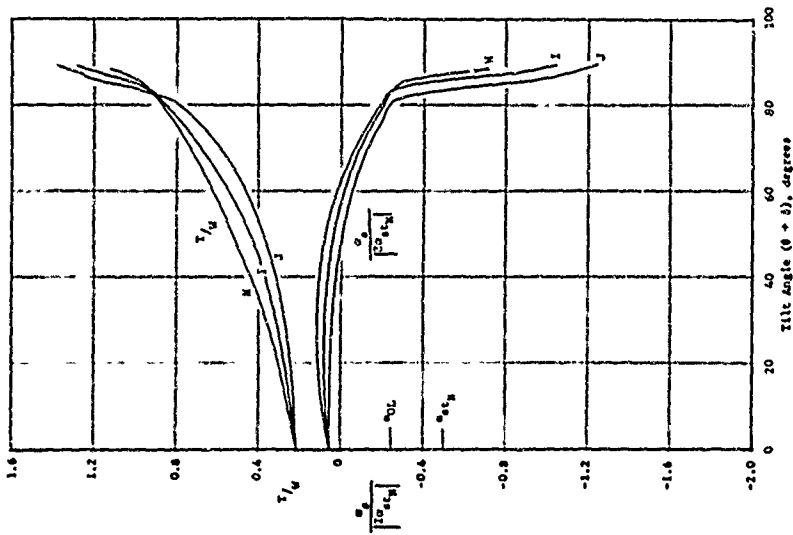
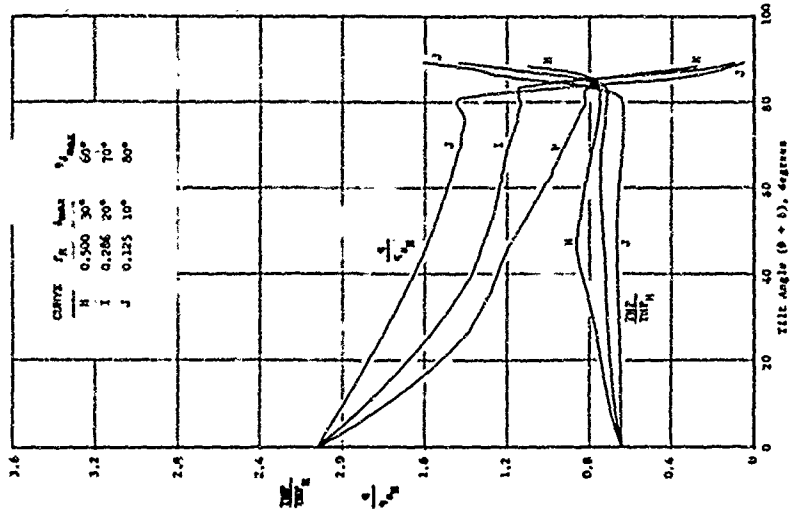
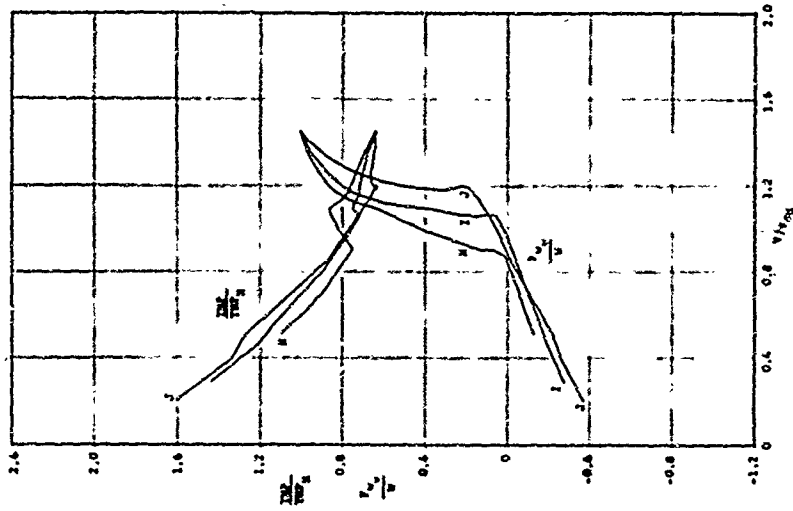


Figure 21 - Effects of Fuselage Rotation on Tilt-Rotor Configuration  
 (DL = 15 lb/ft<sup>2</sup>, W/S = 70 lb/ft<sup>2</sup>, J.R. = 8.0)

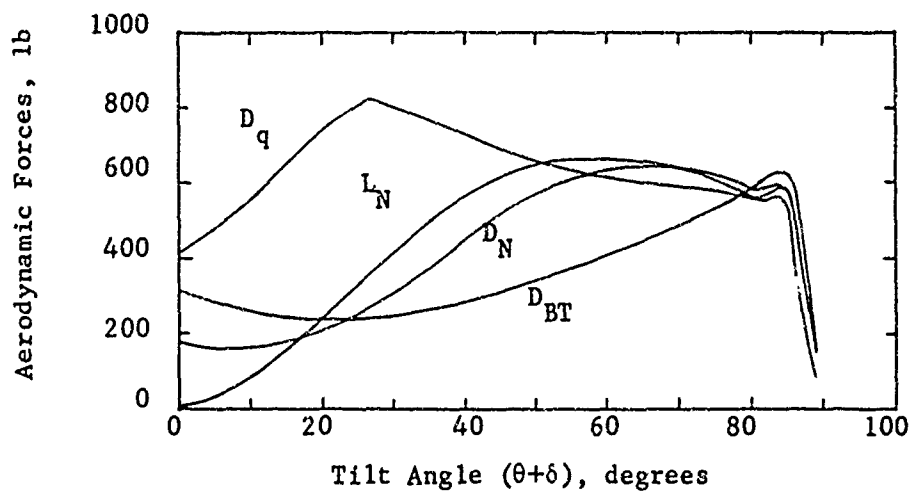
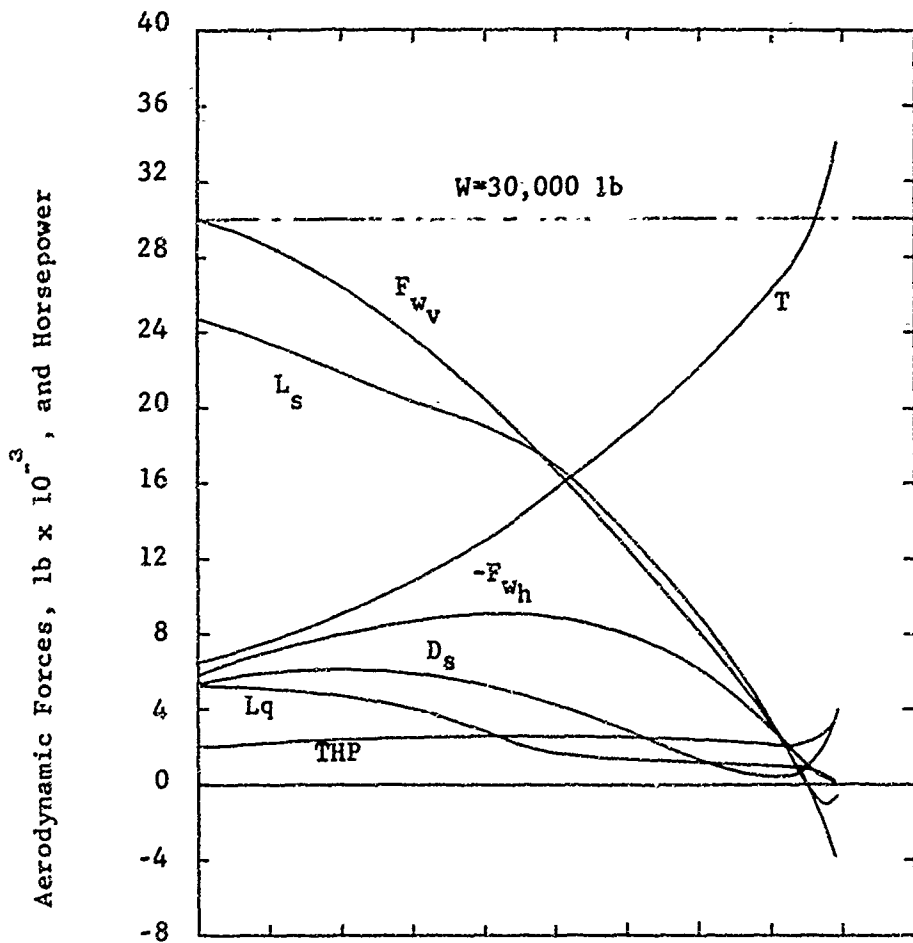
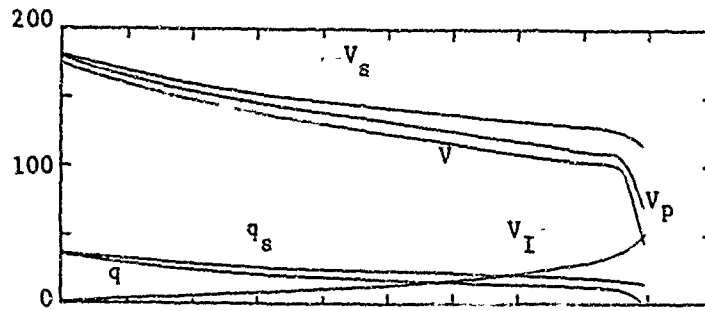


Figure 22 - Transition Data for Baseline\* Tilt-Rotor Configuration

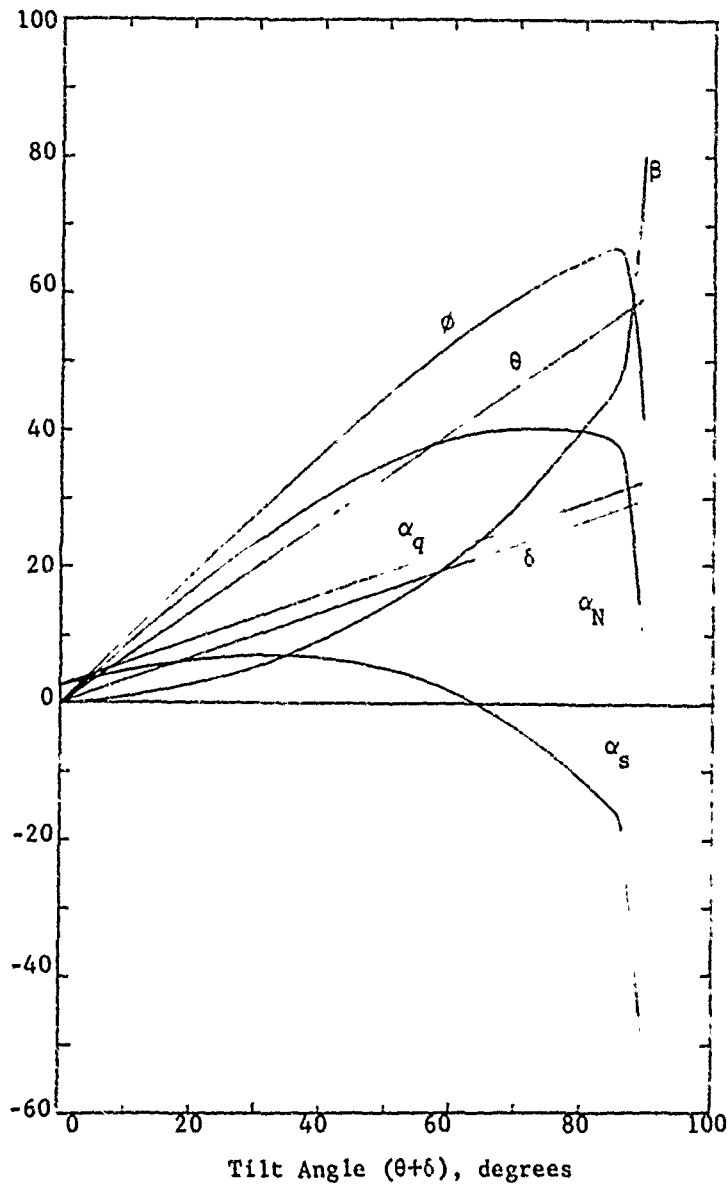
(a) Aerodynamic Forces and Horsepower

\* (see p. 20 for baseline design parameters)

Velocities, ft/sec, and  
Dynamic Pressures, lb/ft<sup>2</sup>



Tilt, Flow, and Body Rotation Angles, degrees



Tilt Angle ( $\theta + \delta$ ), degrees

Figure 22 - (Concluded)

(b) Angles, Velocities, and Dynamic Pressures

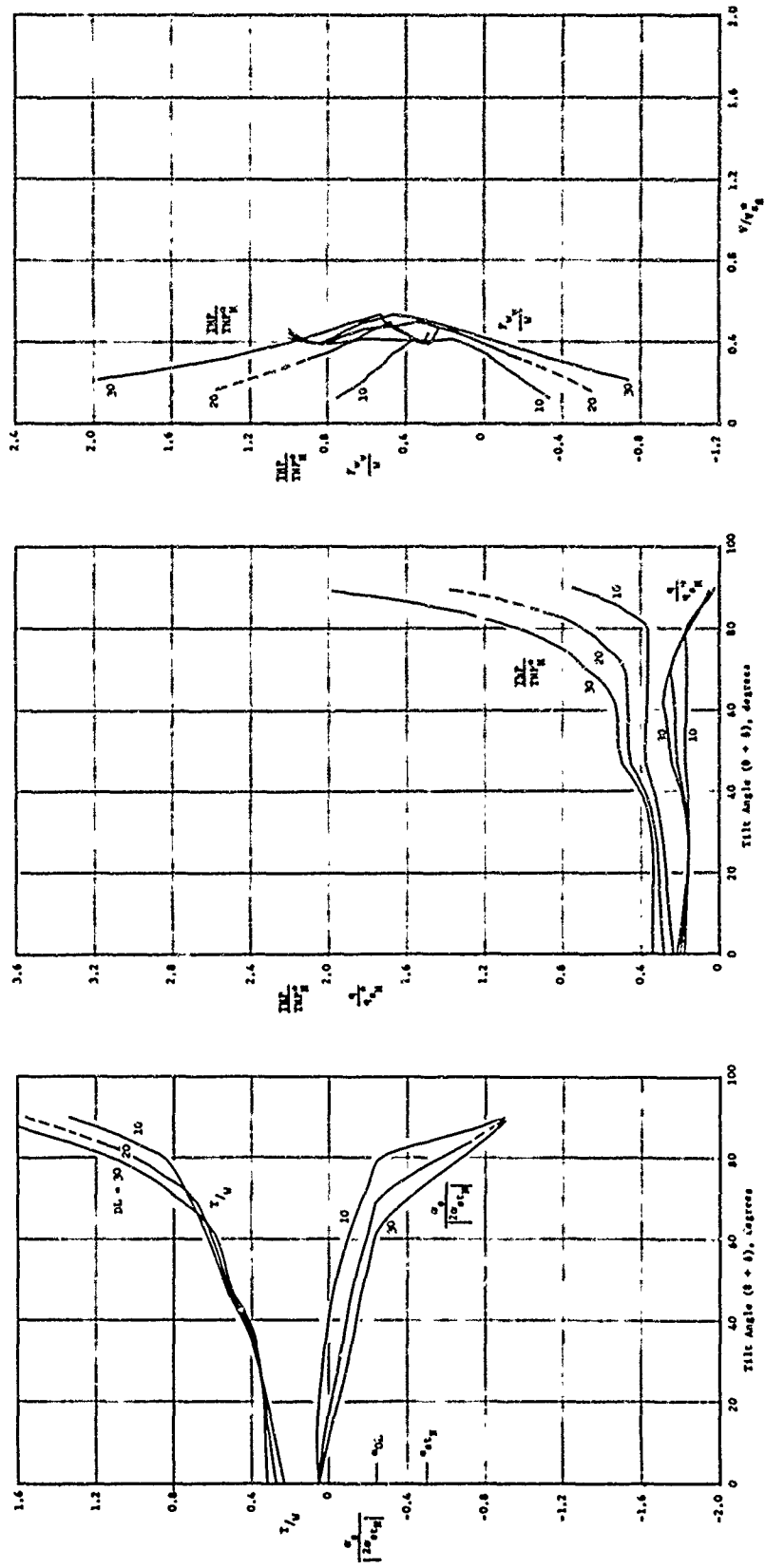


Figure 23 - Effects of Variation in Disc Loading on Baseline Tilt-Rotor Configuration

(a) Wing Loading = 20 lb/ft<sup>2</sup>  
 ( $q_{SH}^* = 40$  lb/ft<sup>2</sup>)

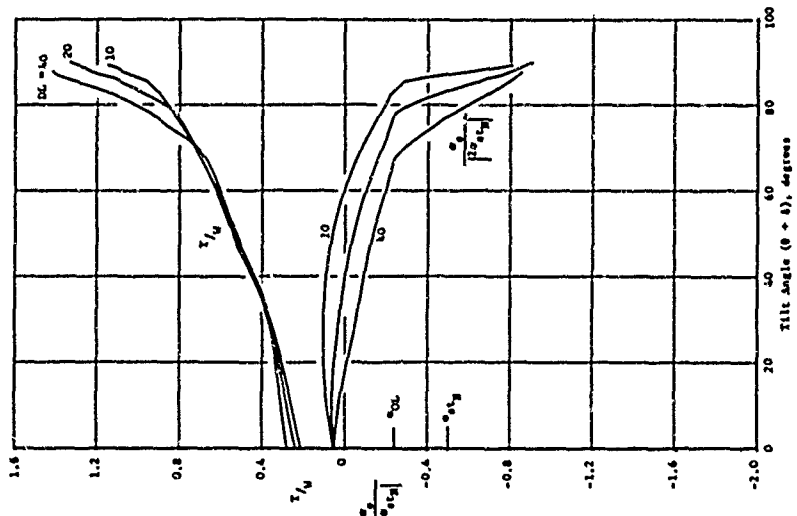
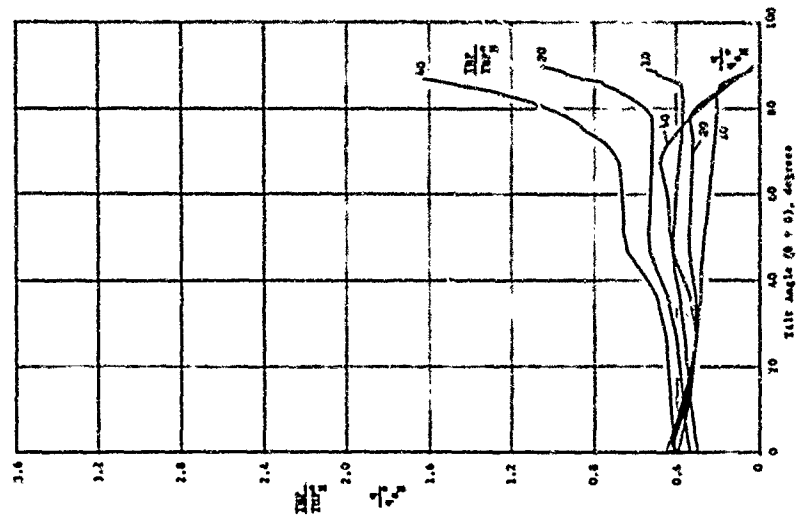
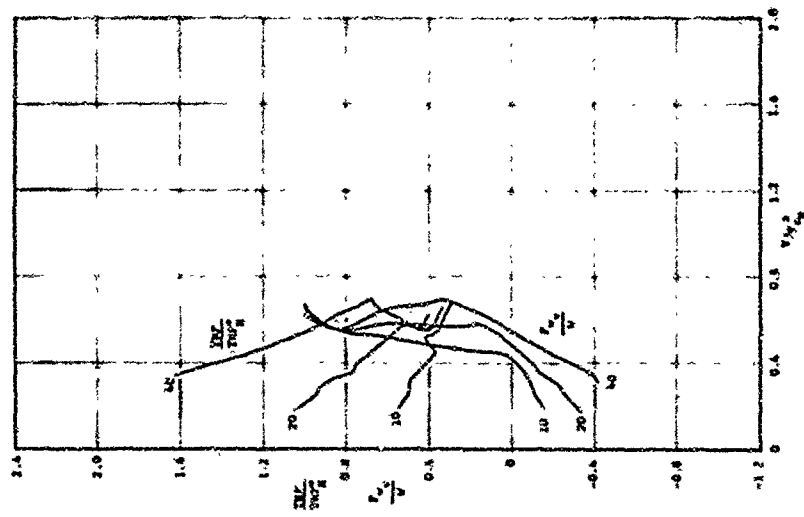


Figure 23 - (Continued)  
 (b) Wing Loading = 40 lb/ft<sup>2</sup>  
 ( $q_{SH}^* = 40 \text{ lb/ft}^2$ )

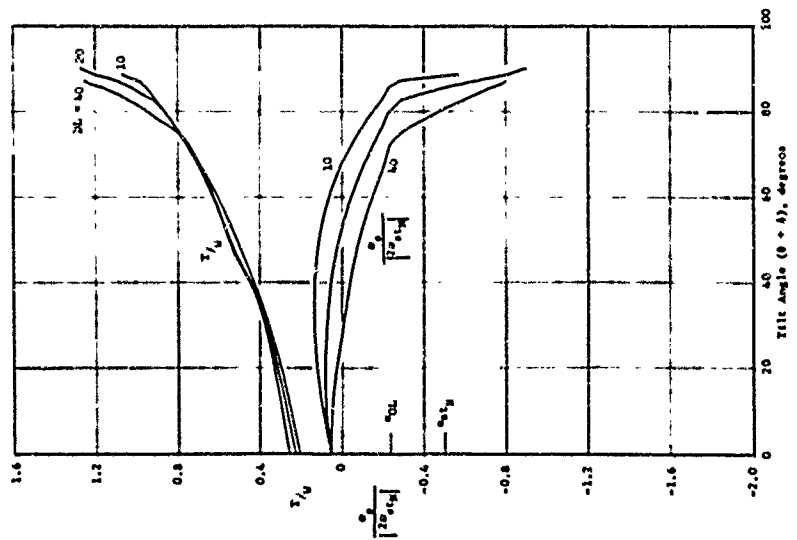
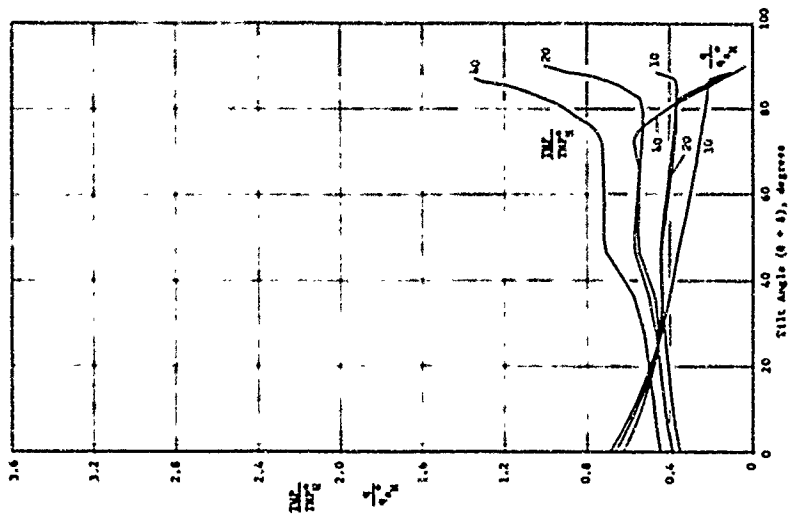
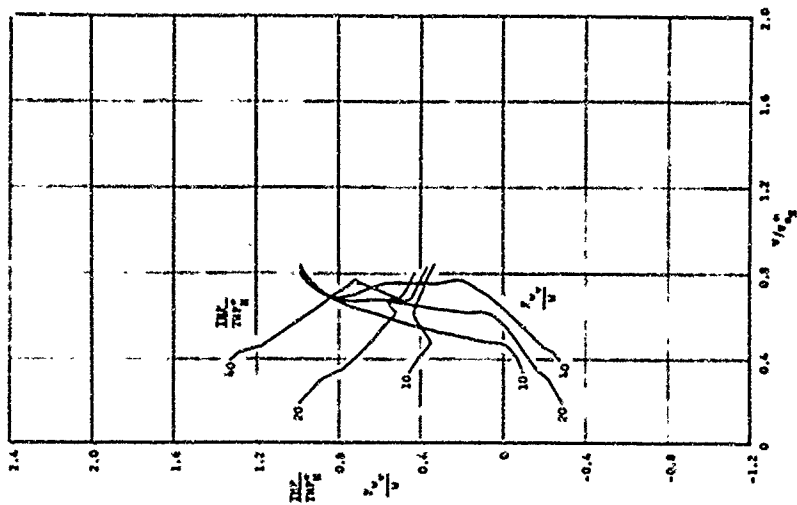


Figure 23 - (Continued)  
(c) Wing Loading = 60 lb/ft<sup>2</sup>  
( $q_{SH}^* = 40$  lb/ft<sup>2</sup>)

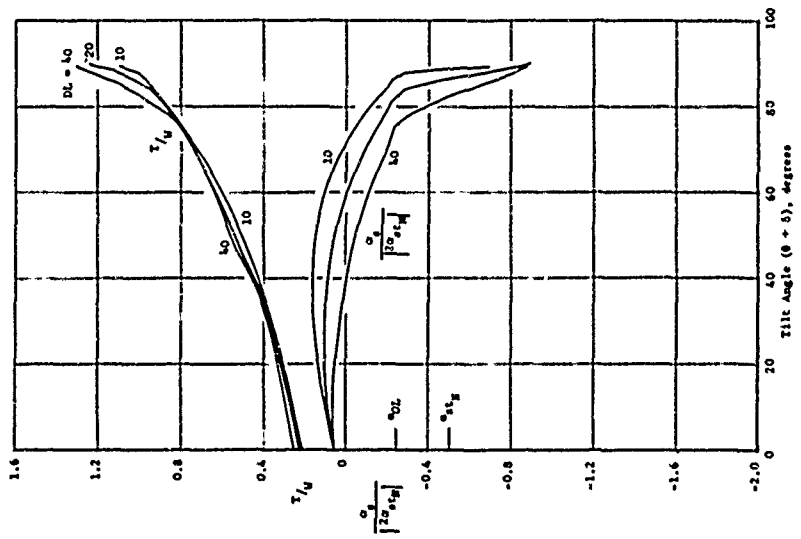
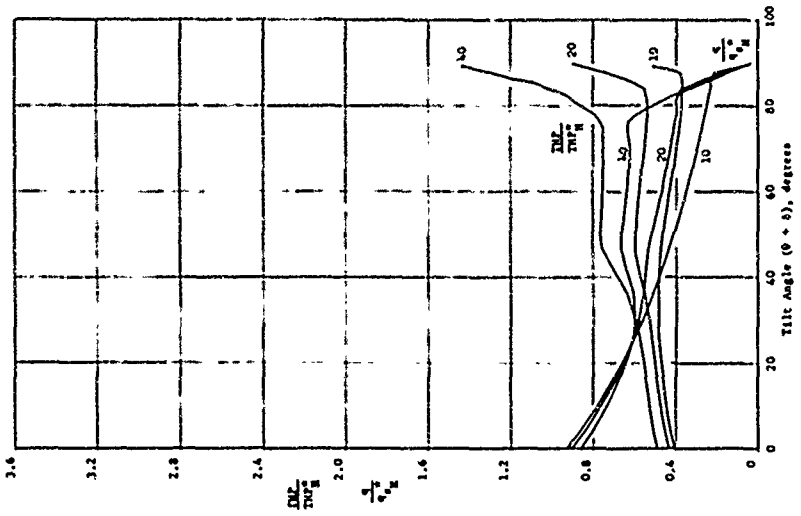
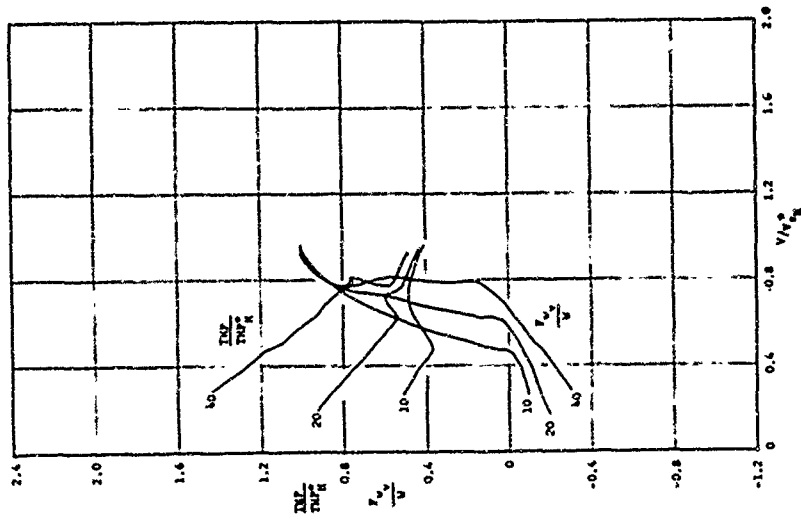


Figure 23 - (Continued)  
 (d) Wing Loading = 80 lb/ft<sup>2</sup>  
 ( $q_{st_H}^* = 40$  lb/ft<sup>2</sup>)

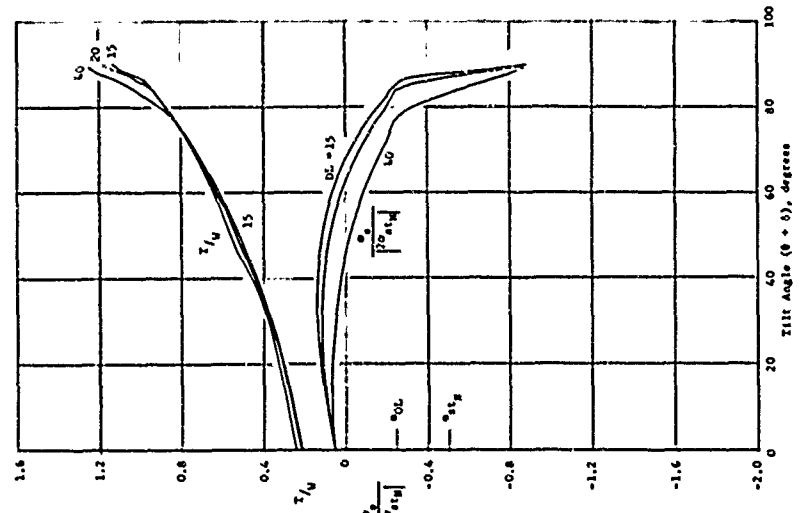
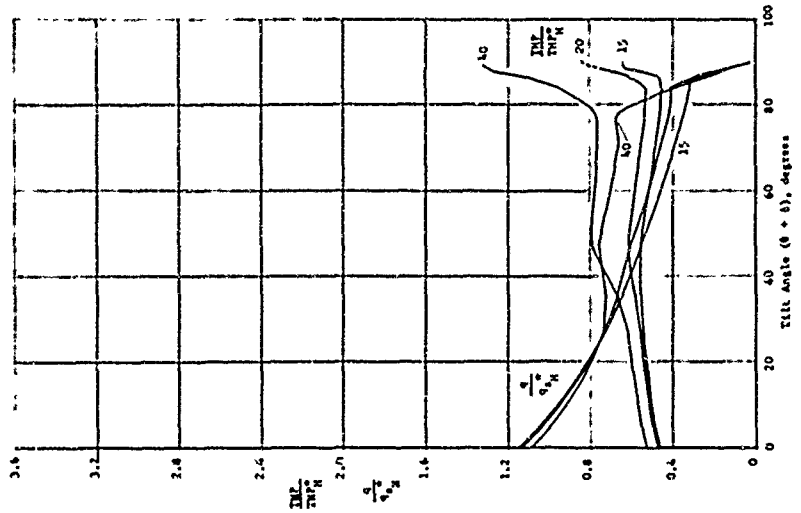
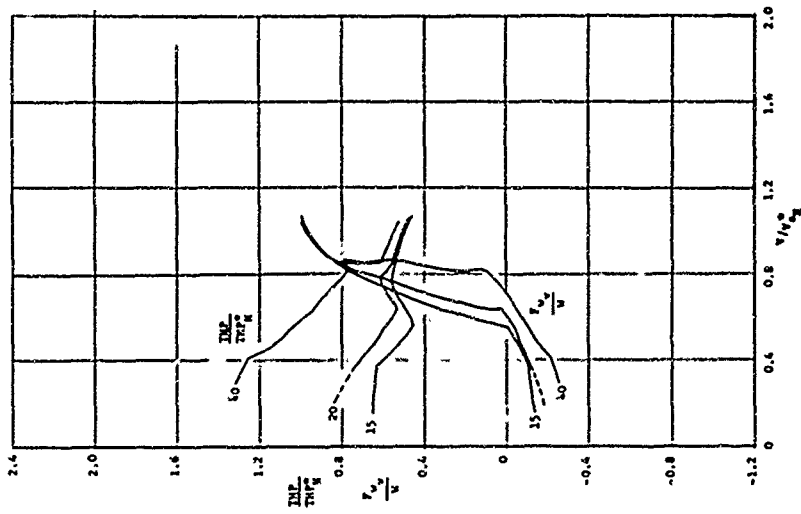


Figure 23 - (Concluded)  
 (e) Wing Loading = 100 lb/ft<sup>2</sup>  
 ( $q_{st}^* = 40$  lb/ft<sup>2</sup>)

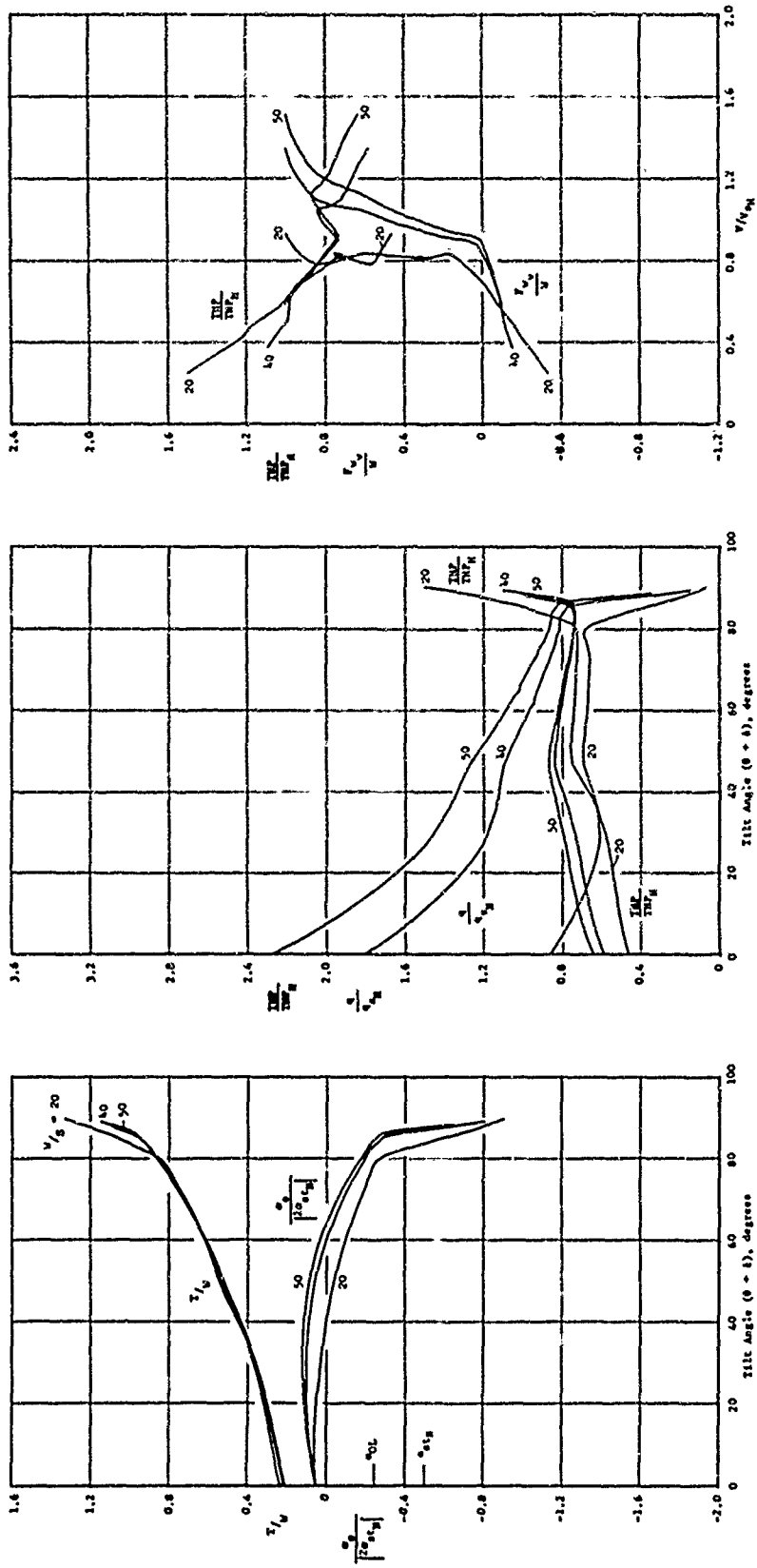


Figure 24 - Effects of Variation in Wing Loading on Baseline Tilt-Rotor Configuration  
 (a) Disc Loading = 10 lb/ft<sup>2</sup>, Wing Loading = 20 - 50 lb/ft<sup>2</sup>

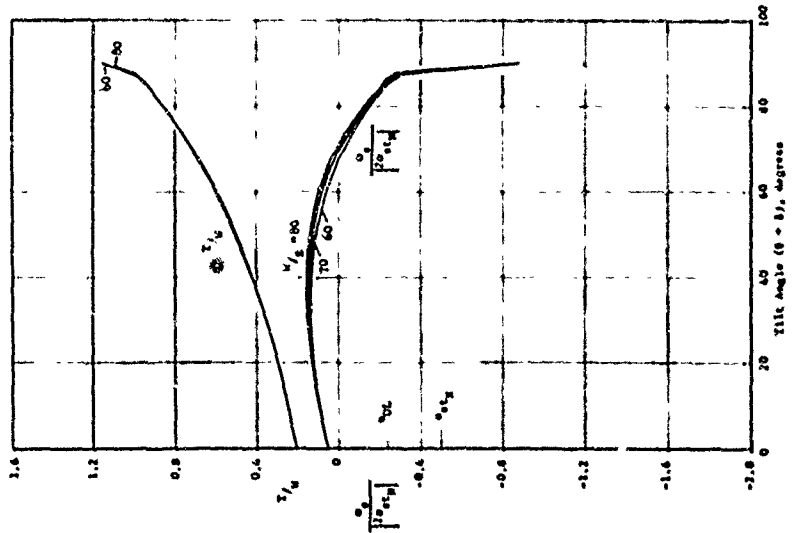
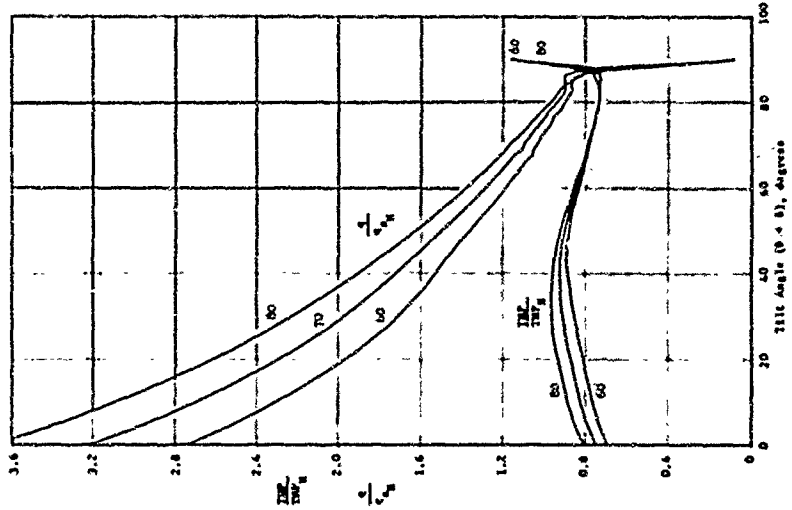
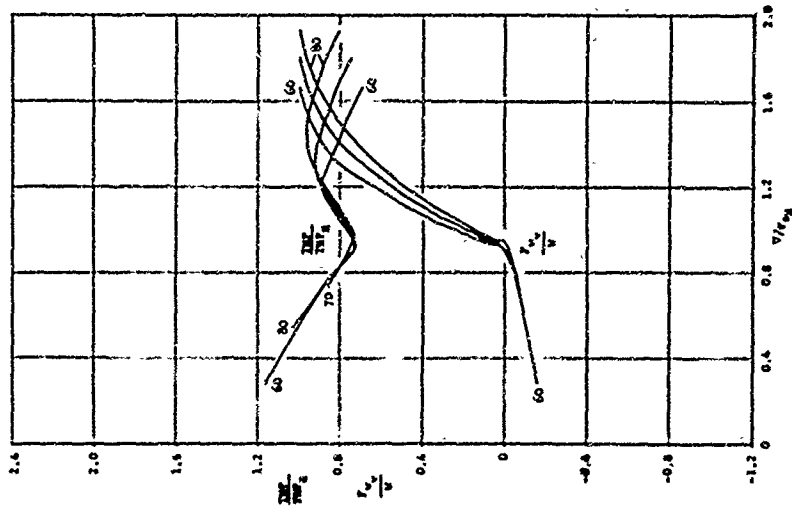


Figure 24 - (Continued)  
 (b) Disc Loading = 10 lb/ft<sup>2</sup>, Wing Loading = 60 - 80 lb/ft<sup>2</sup>

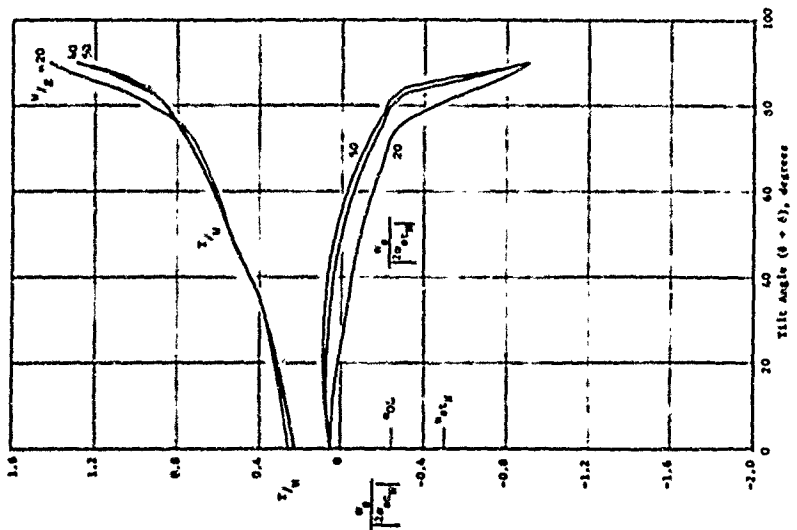
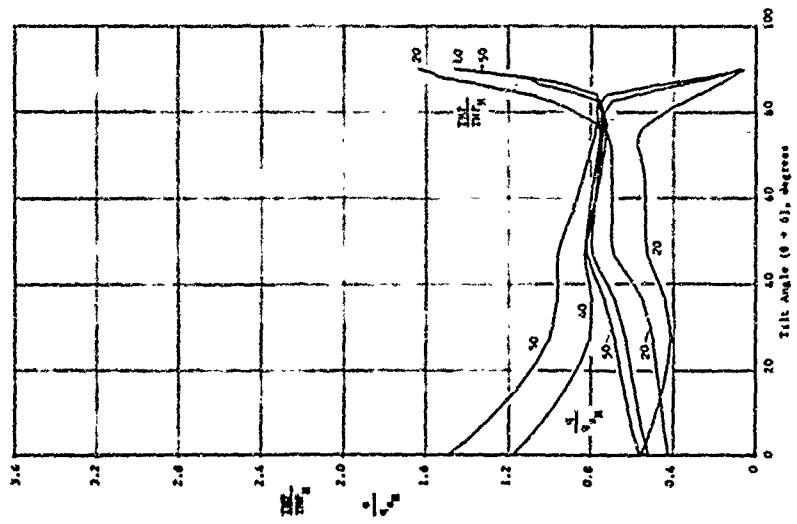
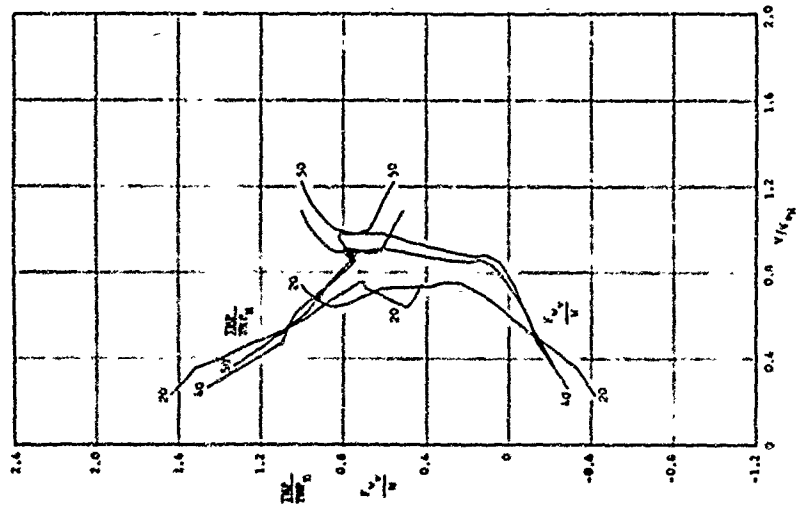


Figure 24 - (Continued)  
 (c) Disc Loading = 15 lb/ft<sup>2</sup>, Wing Loading = 20 - 50 lb/ft<sup>2</sup>

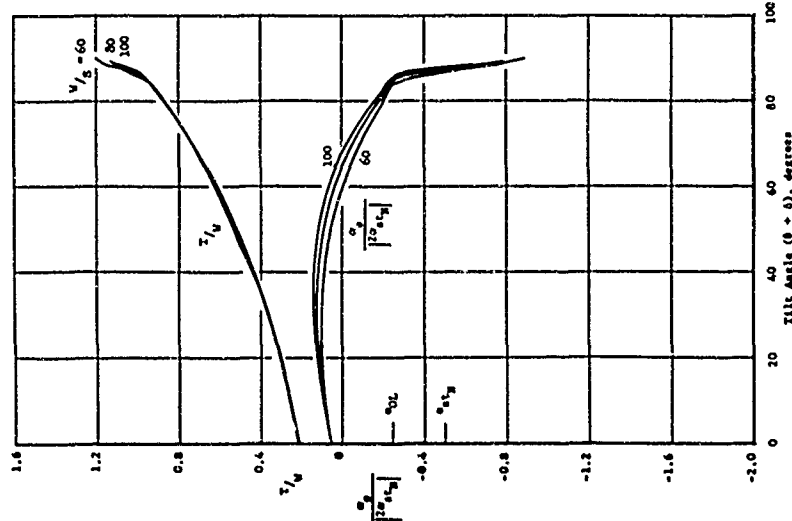
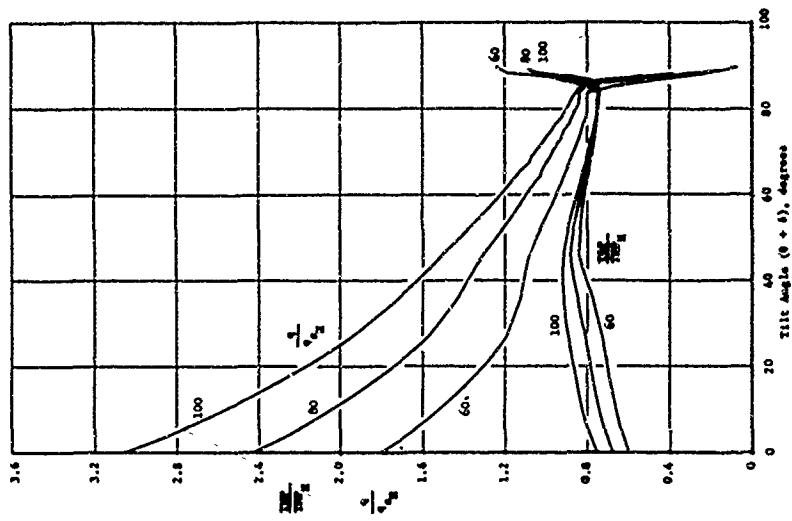
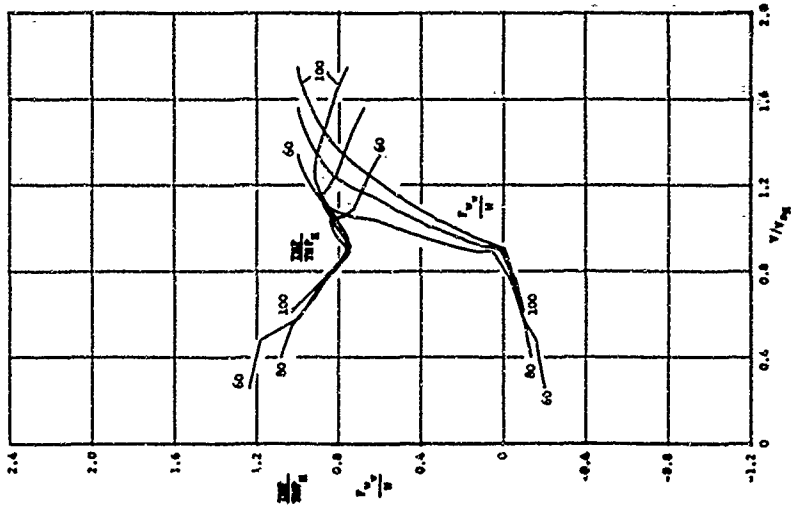


Figure 24 - (Continued)  
 (d) Disc Loading = 15 lb/ft<sup>2</sup>, Wing Loading = 60 ~ 100 lb/ft<sup>2</sup>

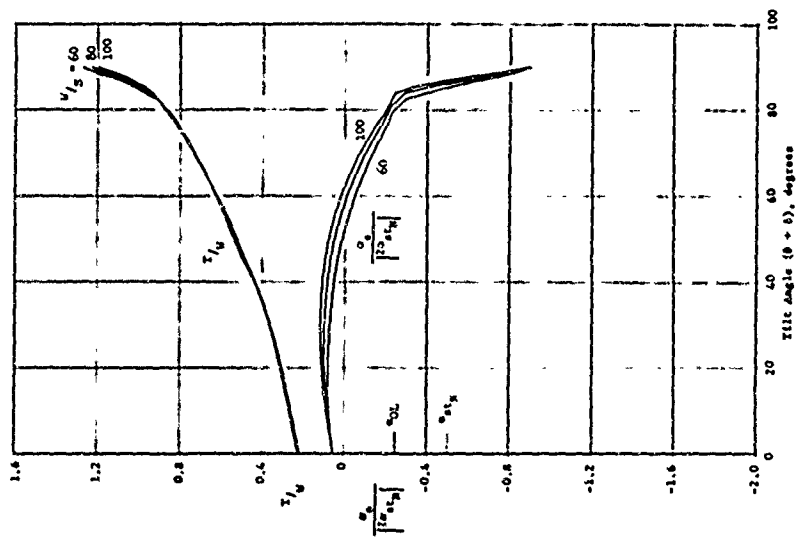
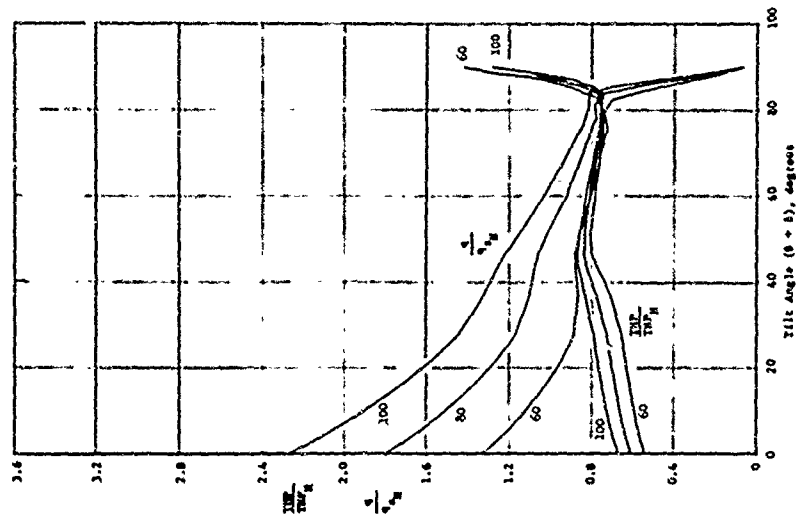
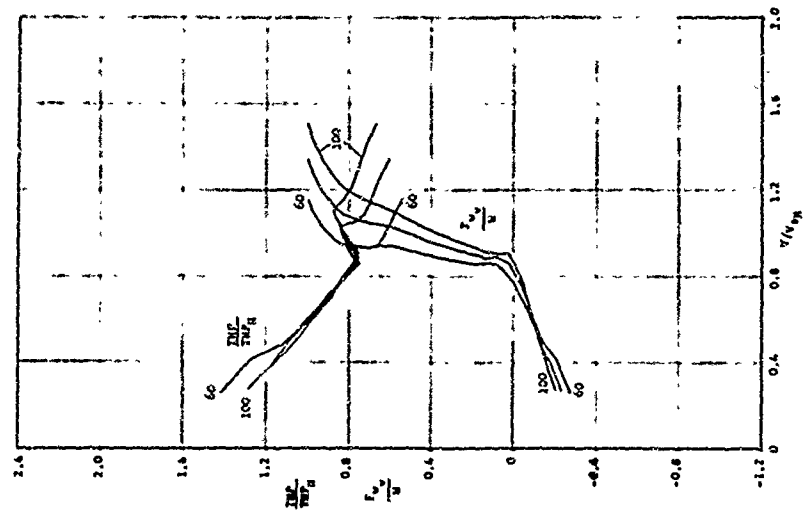


Figure 24 - (Continued)  
 (e) Disc Loading = 20 lb/ft<sup>2</sup>

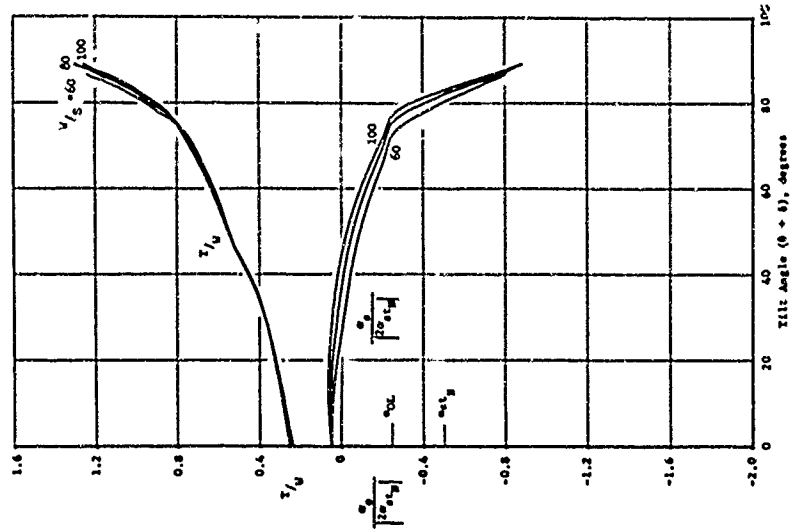
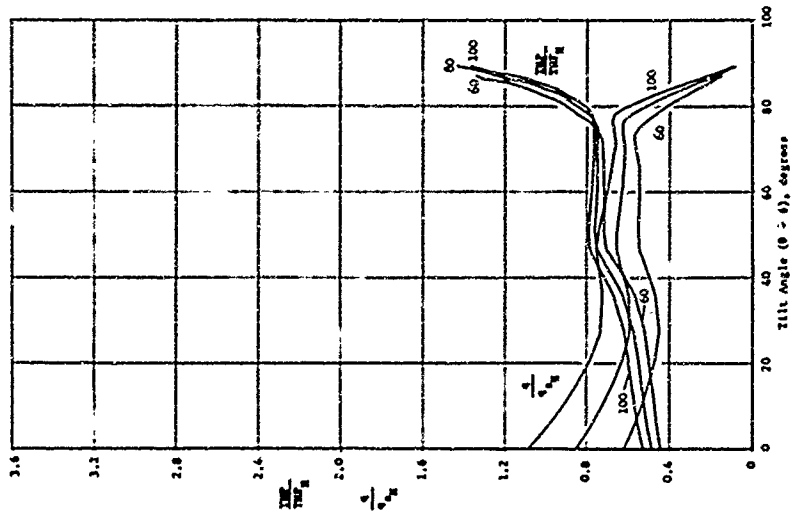
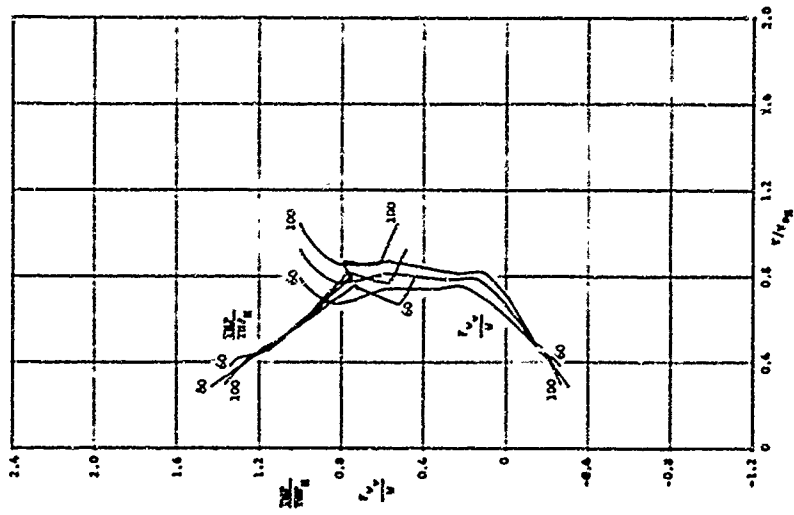


Figure 24 - (Concluded)  
 (F) Disc Loading = 40 lb/ft<sup>2</sup>

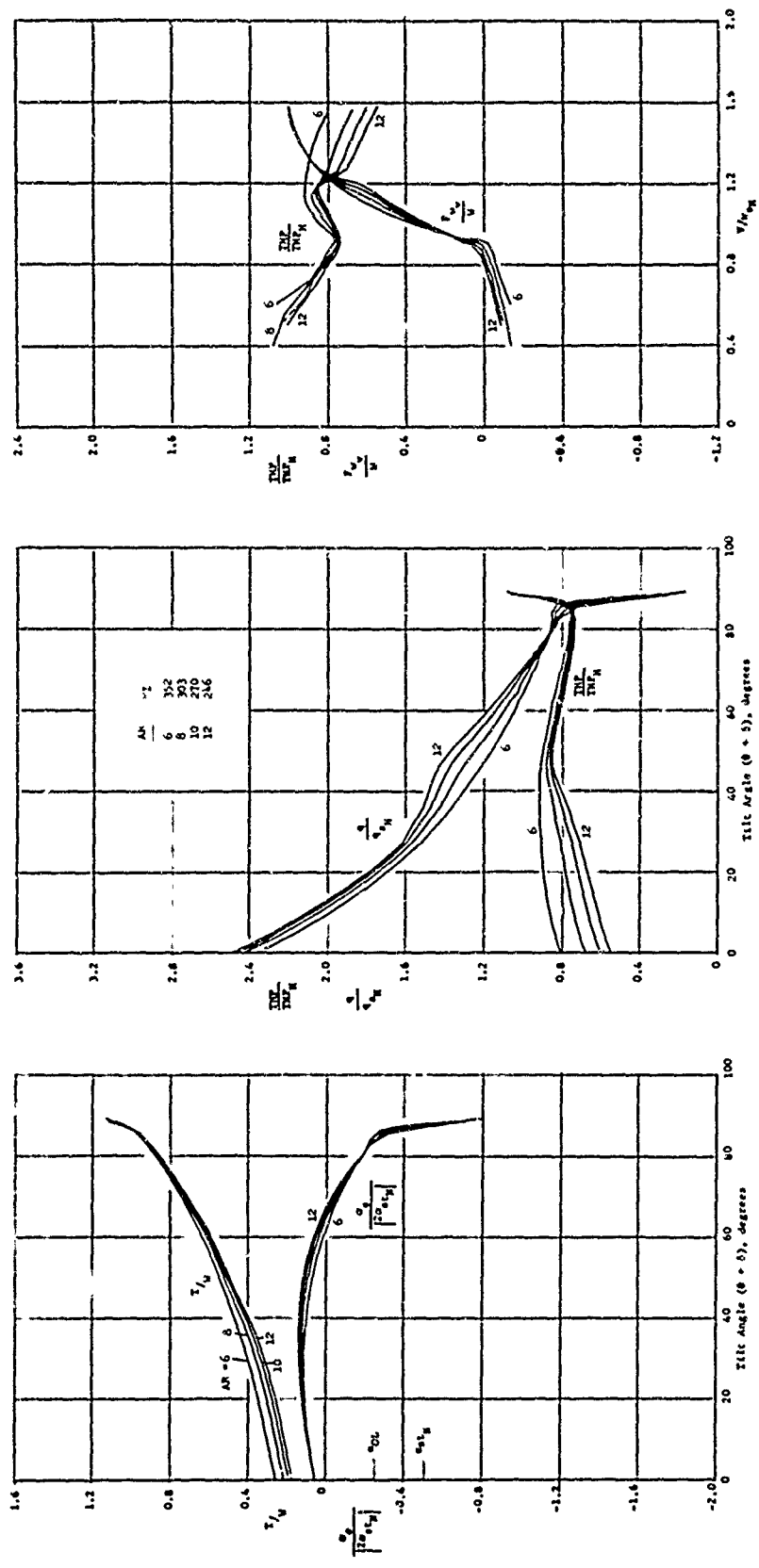


Figure 25 - Effects of Variation in Aspect Ratio on Baseline Tilt-Rotor Configuration

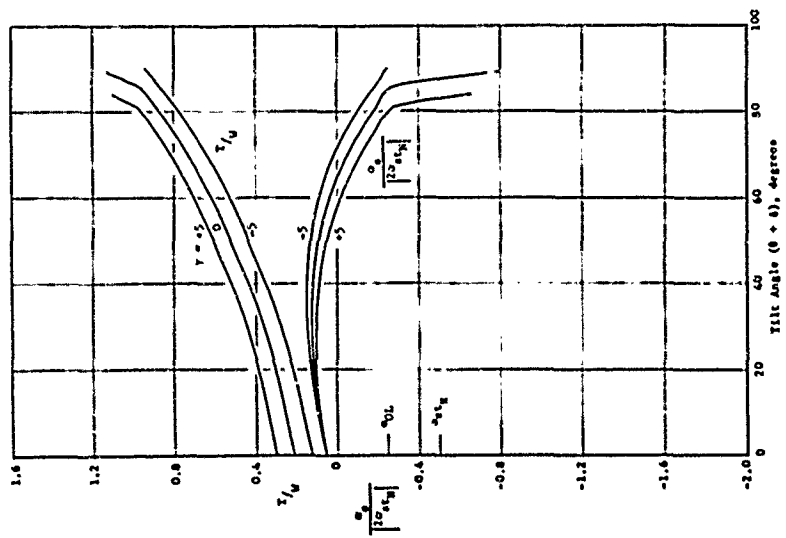
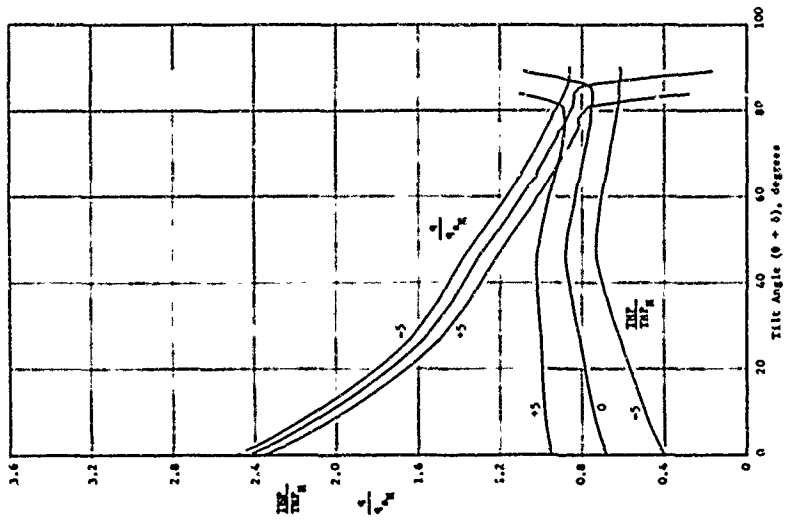
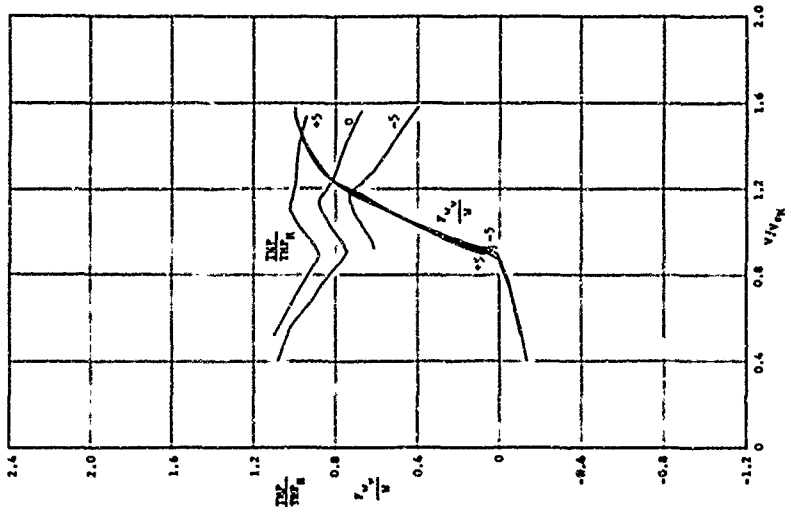


Figure 26 - Effects of Variation in Flight Path Angle on Baseline Tilt-Rotor Configuration

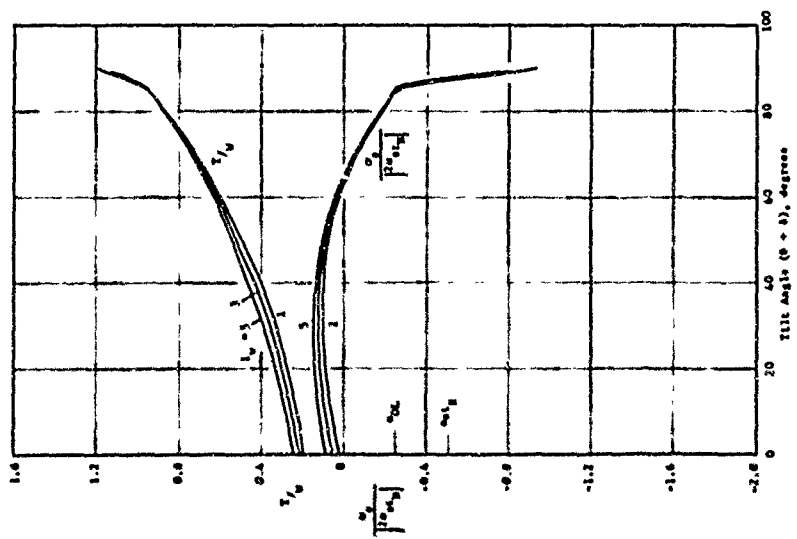
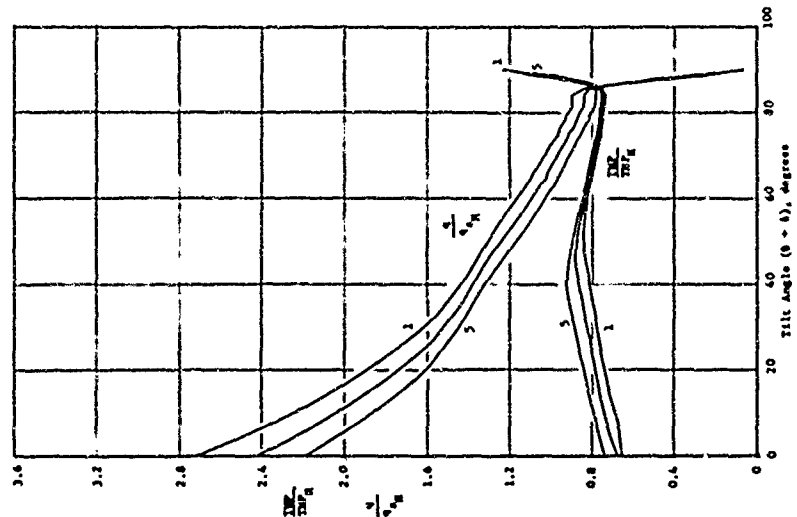
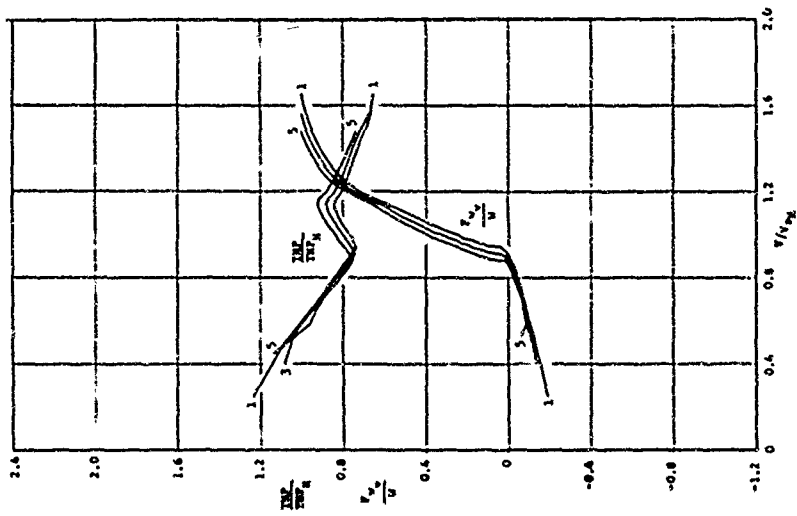


Figure 27 - Effects of Variation in Wing Incidence on Baseline Tilt-Rotor Configuration

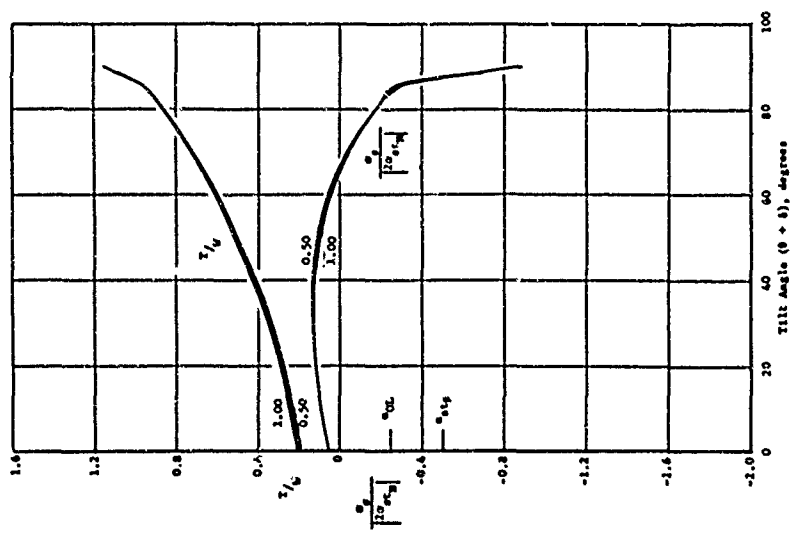
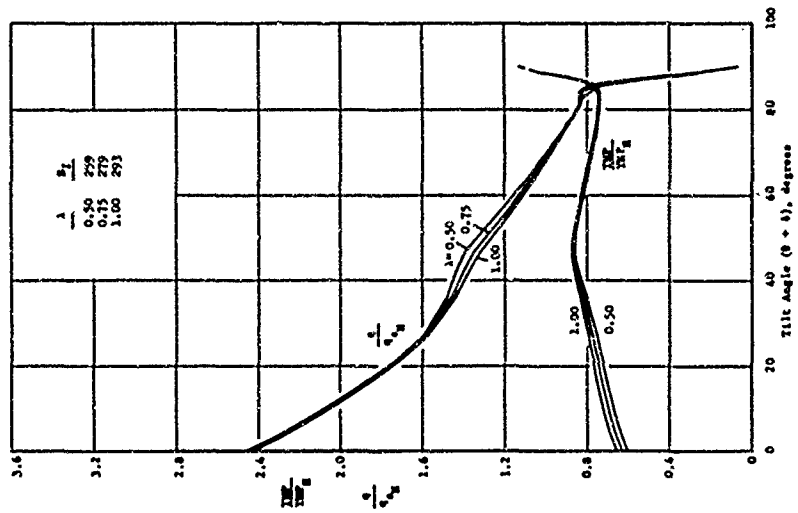
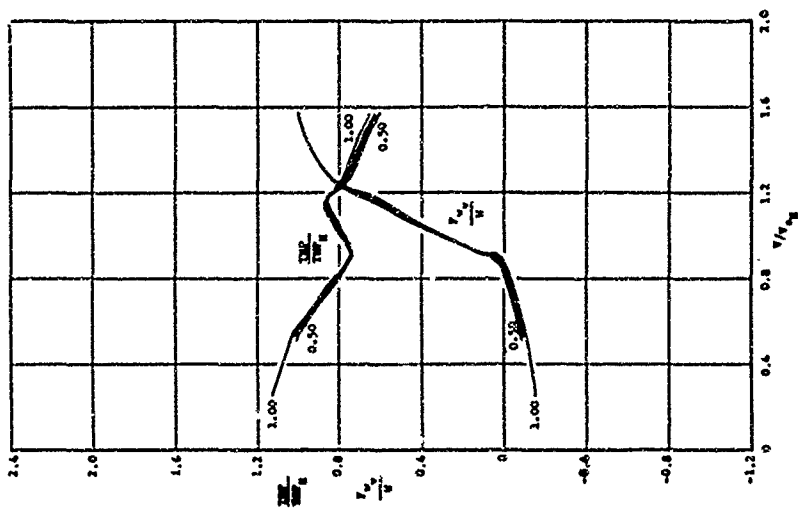


Figure 28 - Effects of Variation in Taper Ratio on Baseline Tilt-Rotor Configuration

Unclassified

Security Classification

DOCUMENT CONTROL DATA - R & D		
<i>(Security classification of title, body of abstract and indexing annotation must be entered when the overall report is classified)</i>		
1. ORIGINATING ACTIVITY (Corporate author) DEPARTMENT OF AERODYNAMICS Naval Ship Research and Development Center Washington, D. C. 20007		2a. REPORT SECURITY CLASSIFICATION Unclassified
		2b. GROUP
3. REPORT TITLE PARAMETRIC TRADE-OFF ANALYSIS FOR TILTING FREE PROPULSOR V/STOL AIRCRAFT IN EQUILIBRIUM TRANSITION		
4. DESCRIPTIVE NOTES (Type of report and inclusive dates)		
5. AUTHOR(S) (First name, middle initial, last name) Robert J. Englar and Douglas G. Kirkpatrick		
6. REPORT DATE July 1969	7a. TOTAL NO. OF PAGES 95	7b. NO. OF REFS 12
8a. CONTRACT OR GRANT NO.	9a. ORIGINATOR'S REPORT NUMBER(S) Report 3168	
b. PROJECT NO. WF 012 01 06 c. TASK 10106 d. NSRDC 635-659	9b. OTHER REPORT NO(S) (Any other numbers that may be assigned this report) Aero Report 1158	
10. DISTRIBUTION STATEMENT This document has been approved for public release and sale; its distribution is unlimited.		
11. SUPPLEMENTARY NOTES	12. SPONSORING MILITARY ACTIVITY Naval Air Systems Command Department of the Navy Washington, D. C. 20360	
13. ABSTRACT An analysis for tilting free propulsor Vertical/Short Take-Off and Landing (V/STOL) aircraft in equilibrium transition is presented. Families of curves are generated in terms of nondimensional flight parameters so that the effects of aerodynamic interactions and varying geometric configurations may be studied. For known values of the ideal hover quantities, the transition characteristics, including thrust and power requirements, may be determined for specific aircraft designs. Suggestions are presented as to those characteristics which should be incorporated into the design of a tilting free propulsor V/STOL aircraft. A comparison is then made between a tilt-wing and tilt-rotor aircraft, each employing the favorable characteristics prescribed by the tradeoff study.		

DD FORM 1 NOV 65 1473 (PAGE 1)

S/N 0101-807-6801

Unclassified

Security Classification

14 KEY WORDS	LINK A		LINK B		LINK C	
	ROLE	WT	ROLE	WT	ROLE	WT
V/STOL Aircraft						
Equilibrium Transition						
Trade-Off Analysis						
Tilt Wing V/STOL Aircraft						
Tilt Rotor V/STOL Aircraft						
V/STOL Aircraft Performance						
V/STOL Aircraft Design						
Transition aerodynamic characteristics						